AD-A071 474 OHIO STATE UNIV COLUMBUS ELECTROSCIENCE LAB F/G 20/14
SWEPT FREQUENCY SCATTERING MEASUREMENTS OF AIRCRAFT.(U)
MAY 79 K A SHUBERT, D L MOFFATT F19628-77-C-0125
UNCLASSIFIED ESL-784677-1 RADC-TR-79-110 NL

1 OF 2
AD A071474

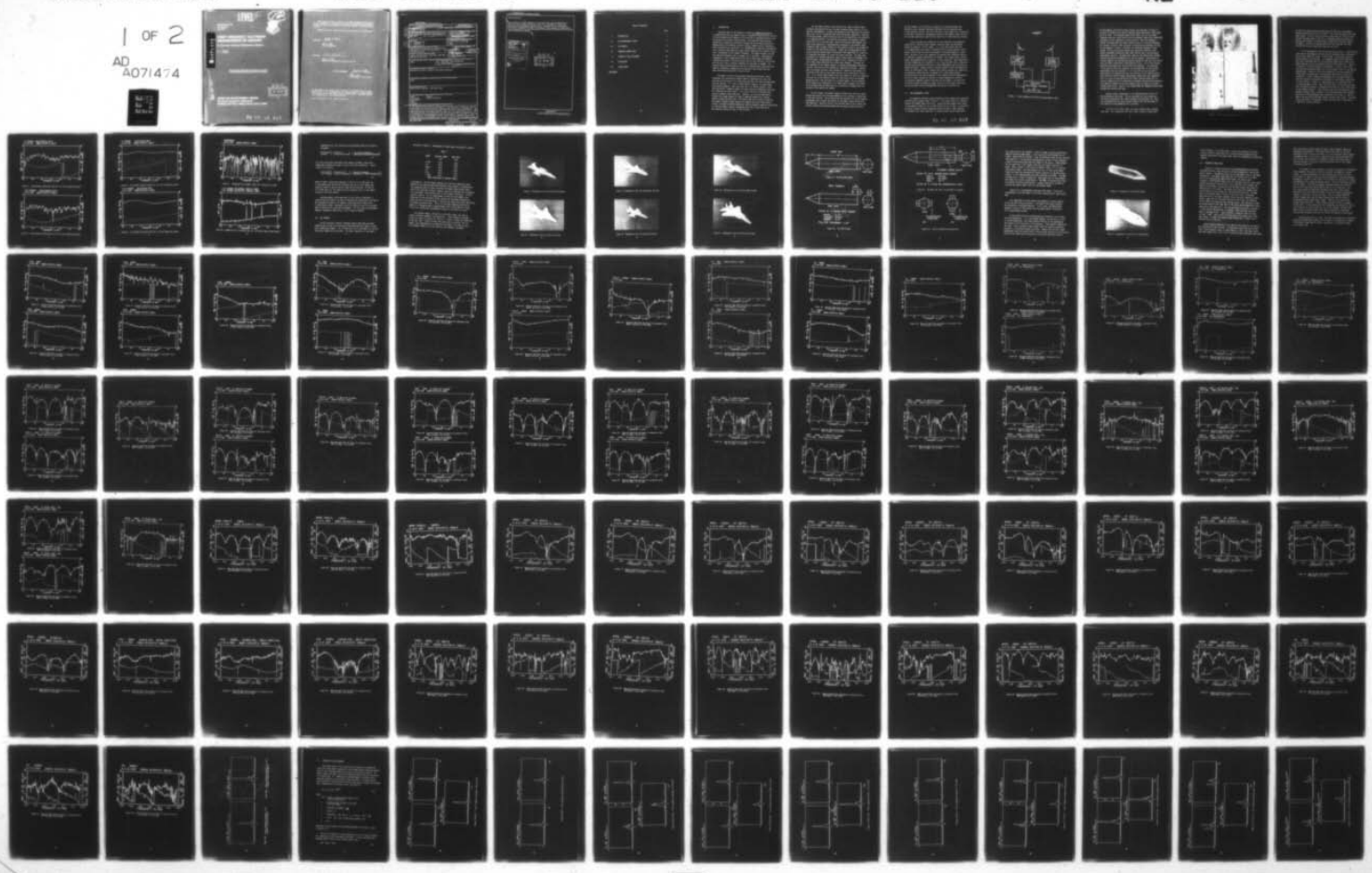

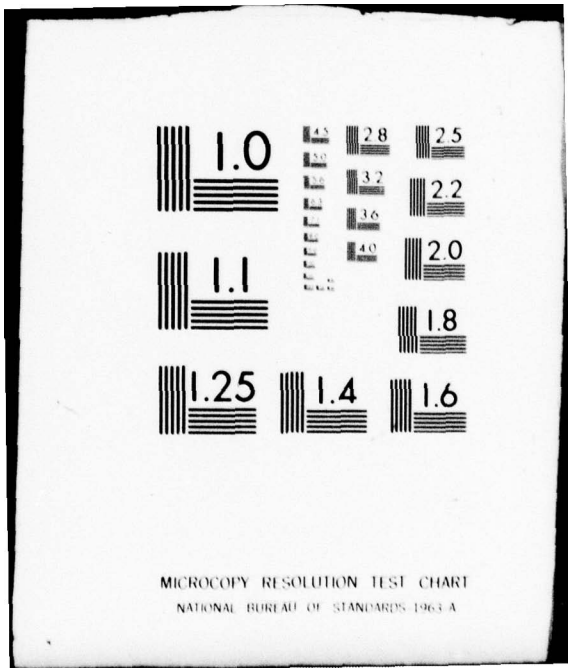
1.0
1.1
1.25
1.4
1.6
1.8
2.0
2.2
2.5
2.8
3.2
3.6
4.0
MICROCOPY RESOLUTION TEST CHART
NATIONAL BUREAU OF STANDARDS 1963-A

LEVEL II

12

RADC-TR-79-110
Interim Report
May 1979

AD A071474

# SWEPT FREQUENCY SCATTERING MEASUREMENTS OF AIRCRAFT

The Ohio State University of ElectroScience Laboratory

K. A. Shubert
D. L. Moffatt







ROME AIR DEVELOPMENT CENTER
Air Force Systems Command
Griffiss Air Force Base, New York 13441

This report has been reviewed by the RADC Information Office (OI) and is releasable to the National Technical Information Service (NTIS). At NTIS it will be releasable to the general public, including foreign nations.

RADC-TR-79-110 has been reviewed and is approved for publication.

APPROVED: Otto E. Kerr

OTTO E. KERR
Project Engineer

APPROVED: Allan C. Schell

ALLAN C. SCHELL
Chief, Electromagnetic Sciences Division

FOR THE COMMANDER: John P. Huss

JOHN P. HUSS
Acting Chief, Plans Office

If your address has changed or if you wish to be removed from the RADC mailing list, or if the addressee is no longer employed by your organization, please notify RADC (EEC), Hanscom AFB MA 01731. This will assist us in maintaining a current mailing list.

Do not return this copy. Retain or destroy.

UNCLASSIFIED

SECURITY CLASSIFICATION OF THIS PAGE (When Date Entered)

## REPORT DOCUMENTATION PAGE

READ INSTRUCTIONS BEFORE COMPLETING FORM

| | |
|---|---|
| 1. REPORT NUMBER: RADC-TR-79-110 | 2. GOVT ACCESSION NO. |
| 3. RECIPIENT'S CATALOG NUMBER | |
| 4. TITLE (and Subtitle): SWEPT FREQUENCY SCATTERING MEASUREMENTS OF AIRCRAFT. | 5. TYPE OF REPORT & PERIOD COVERED: Interim Report |
| 6. PERFORMING ORG. REPORT NUMBER: ESL-784677-1 | |
| 7. AUTHOR(s): K. A. Shubert, D. L. Moffatt | 8. CONTRACT OR GRANT NUMBER(s): F19628-77-C-0125 |
| 9. PERFORMING ORGANIZATION NAME AND ADDRESS: The Ohio State University of ElectroScience Department of Electrical Engineering Laboratory, Columbus OH 43212 | 10. PROGRAM ELEMENT, PROJECT, TASK AREA & WORK UNIT NUMBERS: 61102F, 23050425 |
| 11. CONTROLLING OFFICE NAME AND ADDRESS: Deputy for Electronic Technology (RADC/EEC), Hanscom AFB MA 01731 | 12. REPORT DATE: May 1979 |
| | 13. NUMBER OF PAGES: 127 |
| 14. MONITORING AGENCY NAME & ADDRESS(if different from Controlling Office): Same | 15. SECURITY CLASS. (of this report): UNCLASSIFIED |
| | 15a. DECLASSIFICATION/DOWNGRADING SCHEDULE: N/A |

16. DISTRIBUTION STATEMENT (of this Report)

Approved for public release; distribution unlimited.

17. DISTRIBUTION STATEMENT (of the abstract entered in Block 20, if different from Report)

Same

18. SUPPLEMENTARY NOTES

RADC Project Engineer: Otho Kerr (EEC)

19. KEY WORDS (Continue on reverse side if necessary and identify by block number)

Swept
Scattering
Measurements
Pulse
Response
Aircraft
Complex resonances

20. ABSTRACT (Continue on reverse side if necessary and identify by block number)

Measured swept frequency complex scattering data are presented for six 1/72 scale models of aircraft and one model of a typical pencil or aerospace vehicle-type target with various vertical stabilizer and simple cavity attachments. The measured data span the model frequency bands 2.2 to 4.0 GHz and/or 4.0 to 7.6 GHz. The measured data are predominantly for vertical polarization (perpendicular to a horizontal plane containing the wings and fuselage of the aircraft) at selected sparse aspects. The measurement system, which utilizes somewhat unique background subtraction techniques, has a bistatic angle of either 30 degrees (Cont'd)

→ next page

DD FORM 1 JAN 73 1473

UNCLASSIFIED

SECURITY CLASSIFICATION OF THIS PAGE (When Date Entered)

402 251

Item 20 (Cont'd)

(most targets) or eight degrees (a few pencil-type target orientations). Synthetic pulse response waveforms (only pulse envelopes are shown) are generated from the measured spectral data. Features of both the spectral and temporal responses are used to extrapolate the potential of substructure target features such as tail stabilizers and cavities in prediction-correlation type identification schemes.

TABLE OF CONTENTS

# I. INTRODUCTION

One major goal of the research on Contract F19628-77-C-0125 was to demonstrate that the complex natural resonances associated with certain so-called substructure features of an aircraft or aerospace vehicle could be exploited for target identification. The postulated exploitation method was a prediction-correlation process which has been successfully demonstrated using dominant (overall target) complex natural resonances. While the method was successful, its implementation required interrogation over a spectral span where the major target dimension was slightly larger than a wavelength at the highest frequency. For modern fighter aircraft the required frequency span is roughly 2.0 to 20.0 MHz. Interrogation frequencies in this range maximize the gross target physical property information content in the echo signal but are very difficult to utilize, particularly since a relative coherence of the echos is needed. The present study was motivated by a desire to significantly raise the interrogation frequencies needed while at the same time recognizing that some identification potential could be lost.

For modern aircraft and aerospace vehicles the two most likely candidates for substructure complex natural resonances are; one, the vertical and horizontal tail stabilizers and two, the cavities associated with jet engines. It is not a simple matter, however, to study these postulated phenomena. Note that what one is in effect saying is that over particular frequency ranges the return from the suggested structures will dominate the echo signal. It is very difficult to estimate the precise frequency spans required. Moreover, an existing experimental reflectivity range capable of rapidly sampling harmonically related complex scattering data over a 10:1 band could not be used to establish the proper frequency spans because the samples were too widely spaced. Finally, analytical methods employing reaction integral equation calculations to find the complex natural resonances could not be used because of the required electrical size of the aircraft.

For the above reasons a new reflectivity range to obtain swept frequency data basically over the model frequency span from 1.0 to 12.0 GHz was instrumented. To date, the system has only been used for measurements over 2.2 to 7.6 GHz but does have the broader capability. Features of the new system, some of which are felt to be innovative, are presented in a separate section. To establish the proper sub-frequency regions within the 1.0 to 12.0 GHz span, certain preliminary measurements were made using essentially a hand-operated prototype of the present swept frequency range (a major feature of the present system is the automation of much of the data taking process). These initial measurements were used to produce contour maps of scattered field amplitude as a function of frequency and aspect for three 1/72 scale aircraft. The maps were presented in a contract quarterly report letter dated 13 September 1977. From the maps, strong apparent evidence of tail resonances in the 2.2 to 4.0 GHz range covered by this report were deduced. The maps are not repeated in this report because a different measurement system was actually used and the error bounds are inherently different. Contour maps are perhaps the most useful method for reducing large amounts of scattered field data to two single pictures (for a particular viewing cut). It is also evident however that vast amounts of data are required, and that all of the contract funds and time could easily be consumed producing just a few "pictures" of a single target. For our purpose, which required an examination of at least several targets, the alternative of amplitude and phase data as a function of frequency but for selected fixed aspects was chosen.

In this report, the swept frequency reflectivity facility instrumented specifically for the requirements of this contract is described in the next section. The following section (Section III) gives figures, photographs and a verbal description of the model targets which have been measured. Sections IV and V are the main body of this report and present respectively measured amplitude and phase scattering curves

for the targets as a function of frequency for selected aspects and synthetic pulse response waveforms generated from the measured data in the previous section. The final sections of the report are a discussion of the major features of the measured spectral and temporal data (Section VI) and the conclusions (Section VII) which can be drawn from the results.

It has long been the contention of this laboratory that measured scattering or radiation data, however carefully taken and presented, cannot be viewed as a final answer. It is only when these data are in a format which can be easily integrated into a larger and more easily useful picture that the effort and expense of the measurements is justified. We have in fact also suggested the appropriate integrator-impulse or canonical response waveforms of an object. This report takes certain steps, the modulated pulse responses, in that direction. More importantly the data themselves are presented in such a way that the total scattering picture can be gradually obtained as other measurements and calculations become available. Modern reaction integral equation (RIE) and geometrical theory of diffraction (GTD) methods have greatly enhanced our capability of obtaining scattering data on geometrically complicated objects. With these tools the data presented in this report could be supplemented by RIE at lower frequencies and GTD at higher frequencies to obtain a relatively complete transfer function for the target. To those with this goal we would be happy to supply details of the targets which may not be available from the photographs and figures in Section III.

## II. THE MEASUREMENT SYSTEM

All measured scattering data obtained for this report were generated using the basic scheme shown in Figure 1. The signal source is a Hewlitt Packard (HP) 8690A Sweep Oscillator. Scattering measurements were taken in two spectral bands; 2.2 to 4.0 GHz and/or 4.0 to 7.6 GHz. In each band 201 evenly spaced discrete frequency points were used. When sweeping in frequency the signal generator is actually under closed loop control

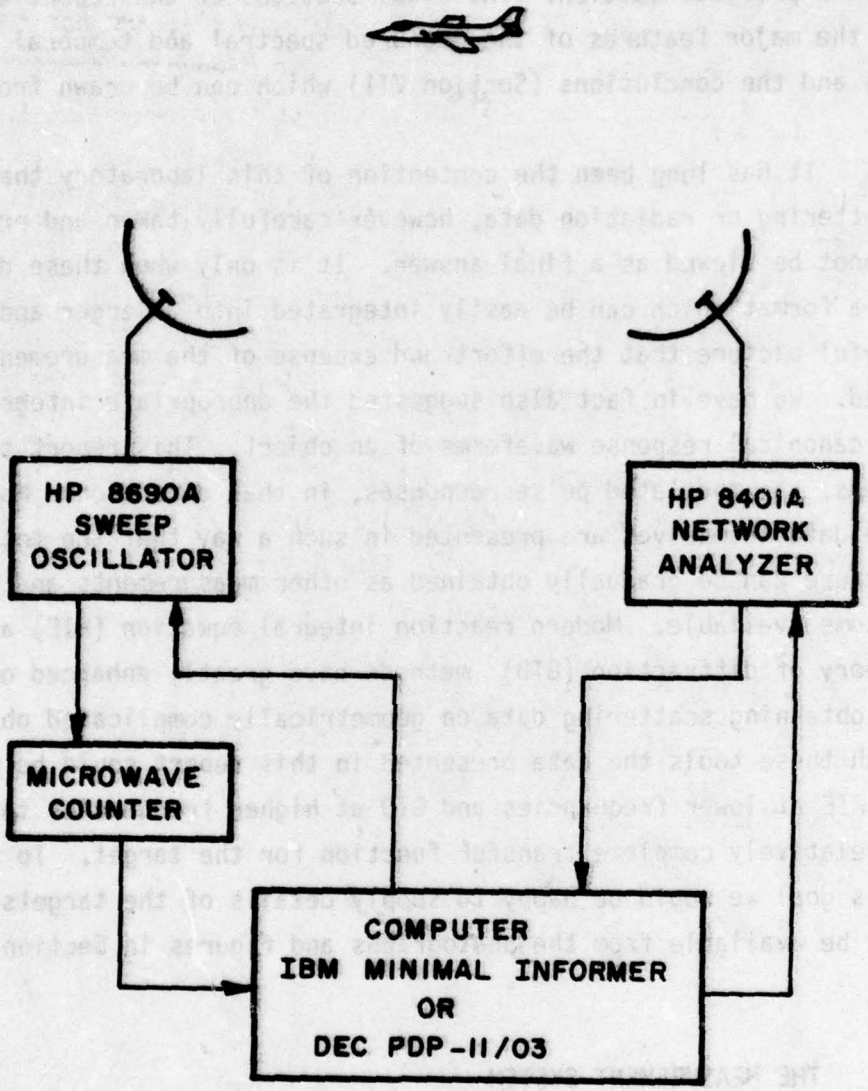


Figure 1. Block diagram of reflectivity measurement range.

of the computer with the microwave counter (as indicated in Figure 1) utilized to establish the actual frequency being generated at each given point in time. The frequency domain data, then, are not true swept frequency data but rather actual discrete frequency domain data (amplitude and phase) at 201 repeatable, distinct points. When the frequency counter indicated that the signal generator was at a desired frequency, the analog to digital (A/D) converter from the Network Analyzer is read by the computer. Figure 1 indicates two different computers in the system. During the contract period this laboratory received a new Digital Equipment Corporation (DEC) PDP11/03 for use in our microwave measurement facility. Extended down times for the IBM Minimal Informer required immediate implementation of the DEC system. Installation of the new computer was considered essential because of the very real threat that the older system would catastrophically fail. All of the original measured data planned for the contract were obtained. The time span of the contract was such, however, that any additions to the original measurements were not possible. It is also fair to say that had it been possible to complete the data runs earlier in the contract period, some additional spot frequency measurements might have been suggested. This in no way has detracted from the stated contract objectives in terms of demonstration of substructure resonance identification potential. The computer programs on the two computers were as identical as their systems would allow. There is no evidence that the computers being interchanged has affected the data.

Figure 2 shows a photograph of the system when the 4.0 to 7.6 GHz measurements were made. The two parabolas are fed by American Electronic Laboratories No. H1479 broadband horn antennas [1]. With this configuration the total bistatic angle is $20^{o}$ and the range to the bisector of the parabolas was 13.30 feet.

In the 2.2 to 4.0 GHz range, two lower frequency horn antennas were used. The transmitter horn had a total E-plane included angle

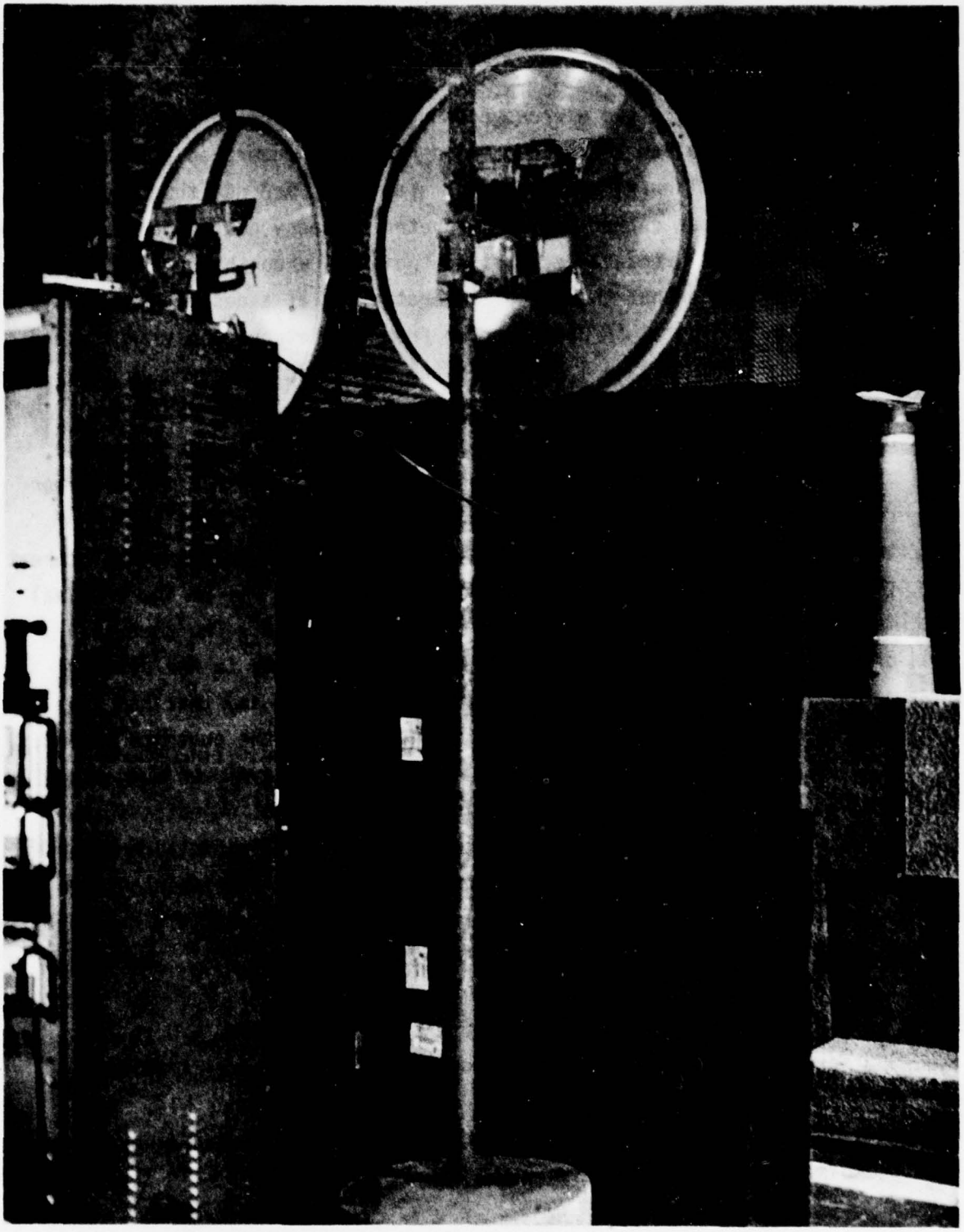

Figure 2. Photograph of reflectivity range.

of $20^{o}$ and a total H-plane included angle of $28^{o}$ with a rectangular aperture measuring 14.5 by 10.5 inches. The receiving antenna was somewhat larger. It had a total E-plane included angle of $14^{o}$ and a total H-plane included angle of $18^{o}$ with a rectangular aperture measuring 46.0 by 34.0 inches. This measurement system had a bistatic angle of 8 degrees. For the $8^{o}$ bistatic angle data the range was 19.5 feet. For the $30^{o}$ bistatic angle the range was 18.0 feet.

In all measurements vertical polarization was used. A few horizontal polarization measurements were obtained by changing target orientation. The bistatic angle was always in the H-plane. Calibration used conducting spheres as references. The computer program which generated the exact calculated data for the conducting sphere was written on another contract [2,3] using equations given by Harrington [4]. Figures 3 through 8 illustrate a typical calibration. Figures 3 and 4 show the uncalibrated measured data on 5 inch (diameter) and 3.5 inch spheres respectively. Figures 5 and 6 show respective calculated scattering values where the magnitude in dB represents dB above (or below) one centimeter. Figure 7 shows the background (or no target) condition. Figure 8 compares the measured, calibrated 3.5 inch sphere return with its exact values. Figure 8 is representative of the possible errors in the measurement system. Note that the spikes in the phase occurred when the measured target or background data were near the $\pm$ $180^{o}$ points on the network analyzer. These "branch cuts" were considered to give minimal problems since, in general, very few data points were affected. The errors in the magnitudes were considered to be within $\pm$ 1 dB for 90% of the data with occasional spikes causing larger errors. The phase errors are within $\pm$ 10 degrees, except at points near $\pm$ $180^{o}$ where a $\pm$ $20^{o}$ error is more realistic.

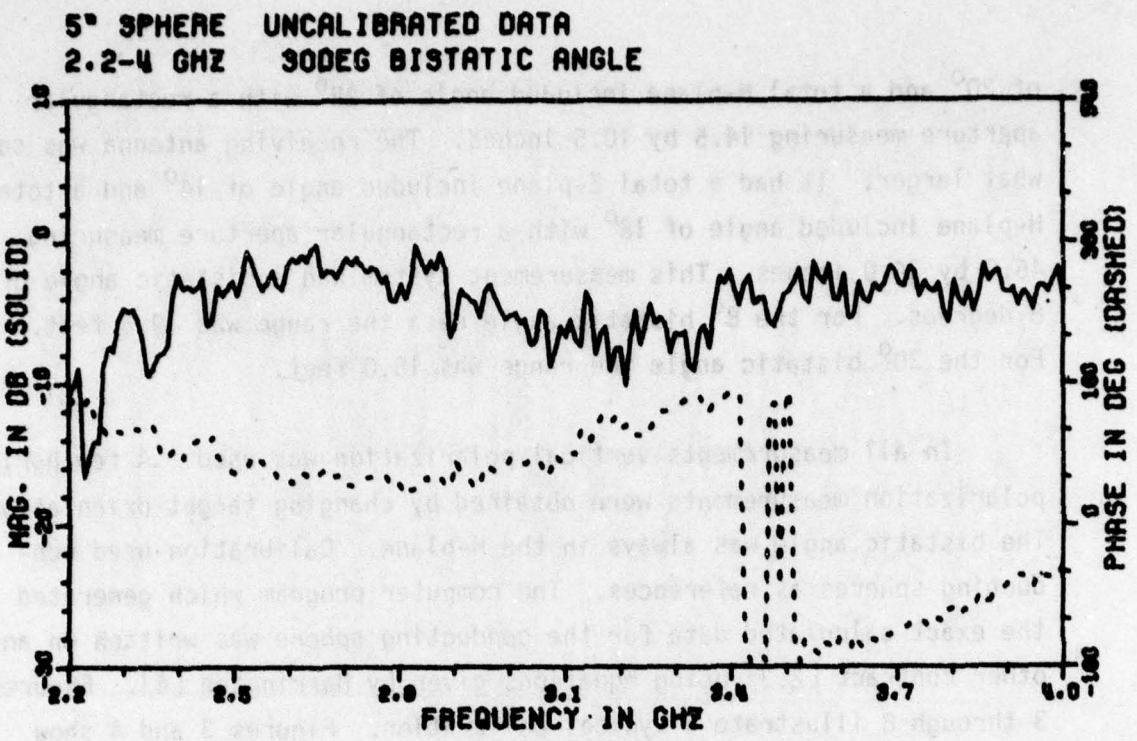


Figure 3. Uncalibrated scattering data for 5.0 inch conducting sphere.

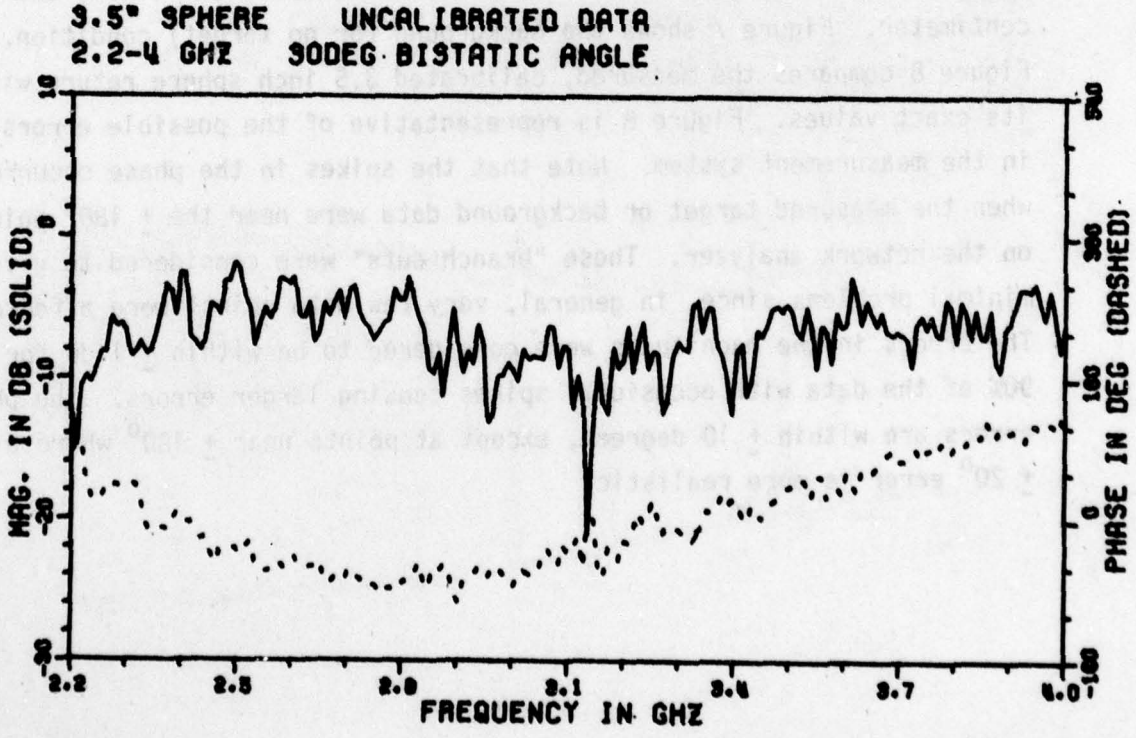


Figure 4. Uncalibrated scattering data for 5.0 inch conducting sphere.

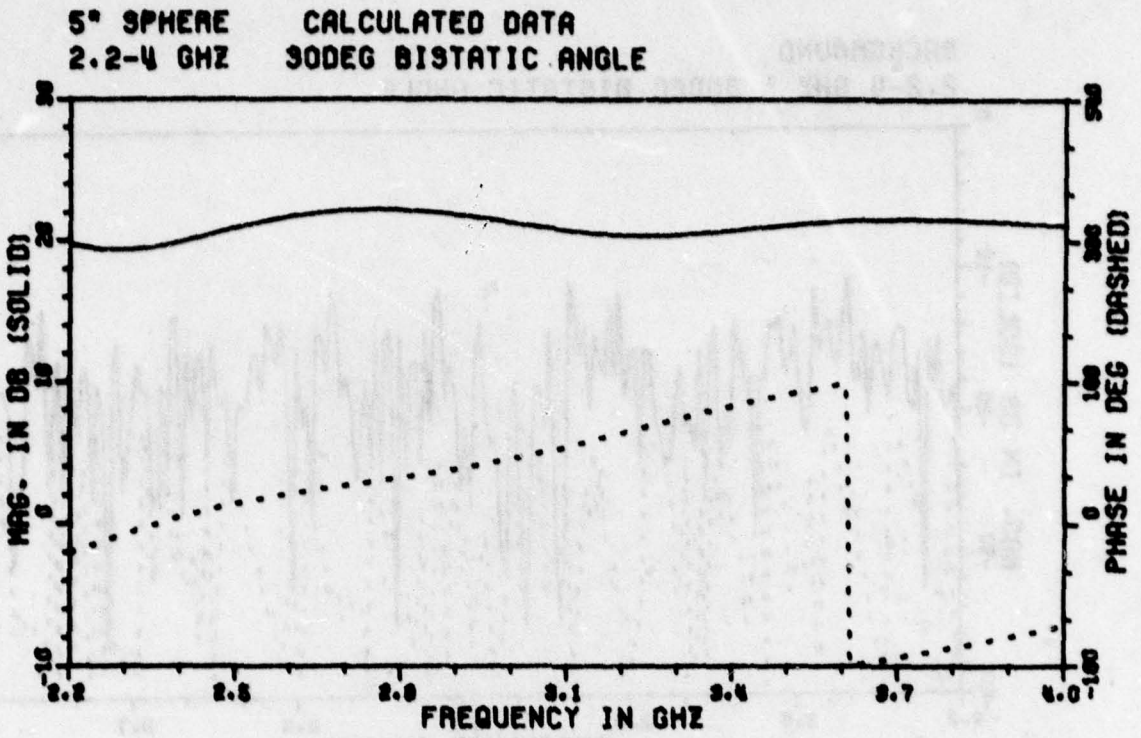


Figure 5. Calculated scattering data for 5.0 inch conducting sphere.

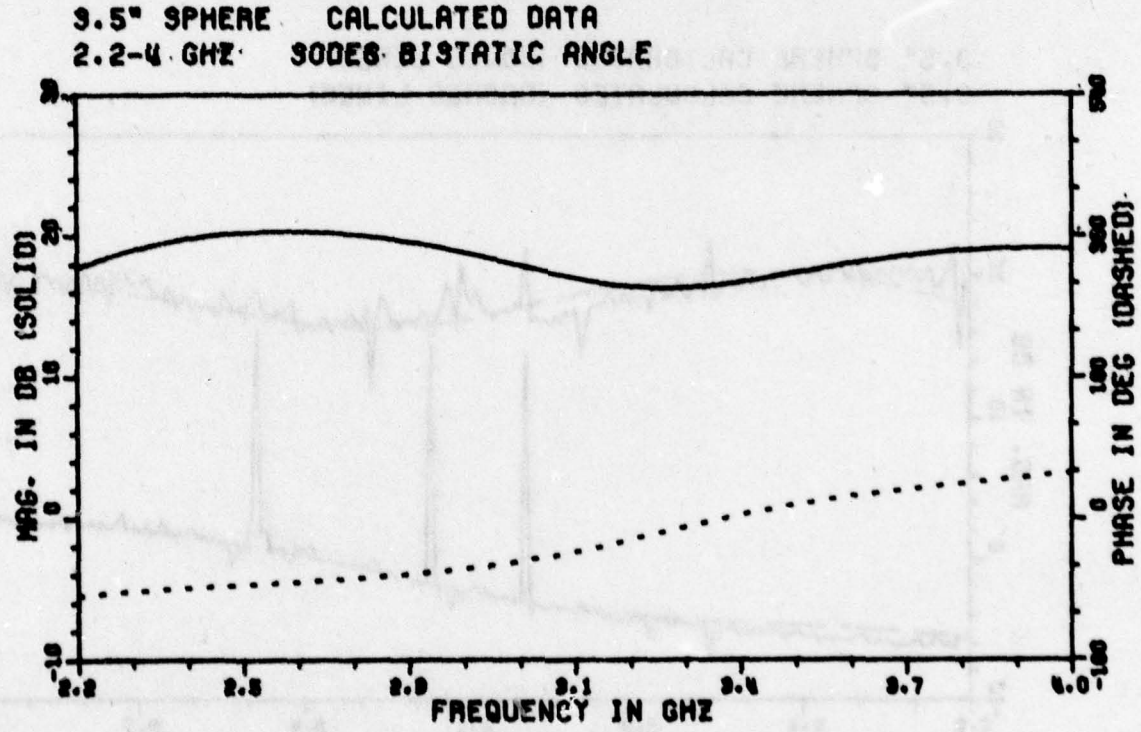


Figure 6. Calculated scattering data for 3.5 inch conducting sphere.

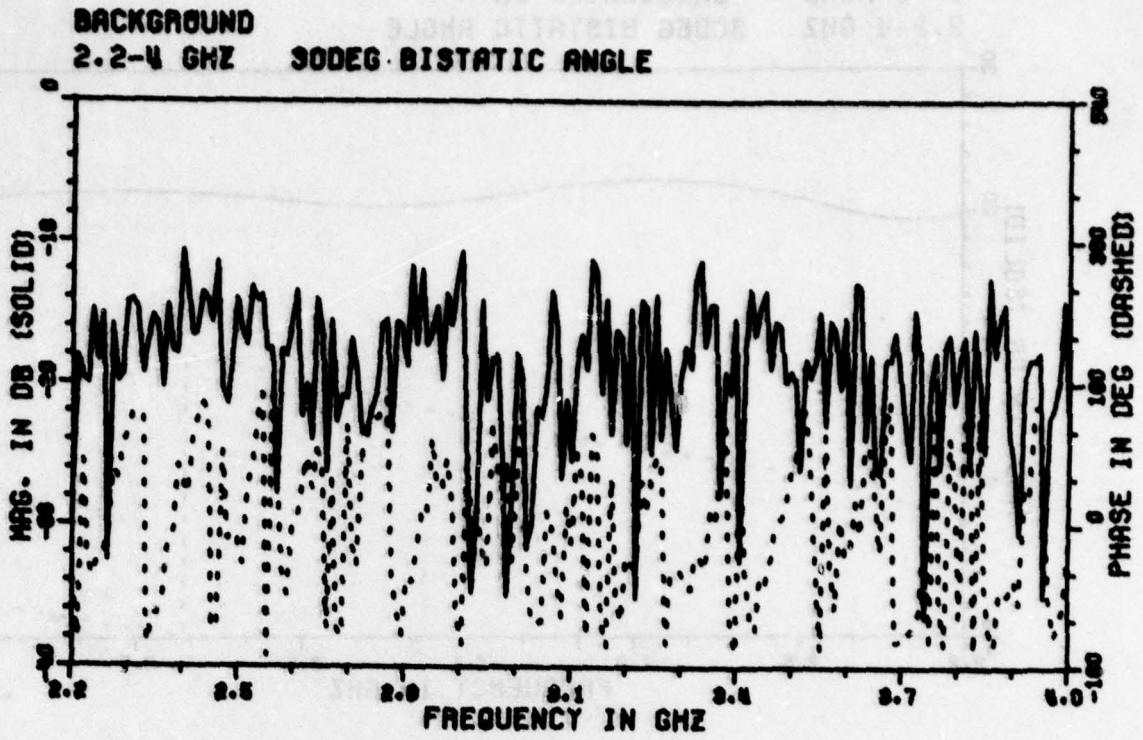


Figure 7. Background (no target) signal for reflectivity range.

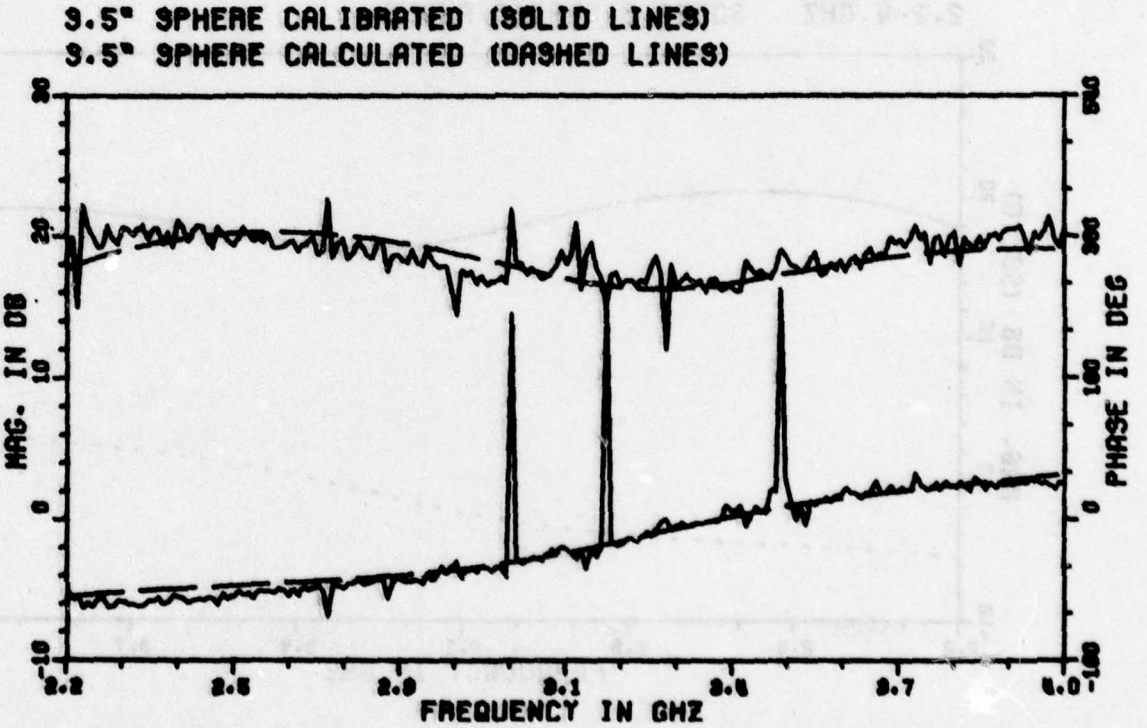


Figure 8. Comparison of calculated data vs. calibrated sphere measurements.

Mathematically, the calibration was performed using the following procedure:

$$\begin{pmatrix}\text{calibrated}\\ \text{target}\end{pmatrix} = \begin{pmatrix}\text{measured}\\ \text{target-background}\end{pmatrix} \times \left( \frac{\text{calculated reference}}{\text{measured reference-background}} \right) \tag{1}$$

All calculations were performed using complex arithmetic operations (magnitude and phase included) at each of the 201 frequencies. Specifically, for Figure 8,

$$\begin{pmatrix}\text{calibrated}\\ \text{3.5" sphere}\end{pmatrix} = \begin{pmatrix}\text{measured 3.5"}\\ \text{sphere-background}\end{pmatrix} \times \left( \frac{\text{(exact 5" sphere)}}{\text{(measured 5" sphere-background)}} \right) \tag{2}$$

When the other targets were measured in the 2.2 to 4.0 GHz span the 5 inch sphere was used as the calibrator and the 3.5 inch sphere was used as a check to verify that no large errors occurred. In the 4.0 to 7.6 GHz band a 6 inch sphere was the reference with a 5 inch sphere serving as the check sphere.

The measurement system described in this section represents a state-of-the-art advance in terms of reflectivity ranges which can rapidly and reproducibly measure the complex scattering from an object over a wide spectral band. Admittedly the error bounds are not all one might hope to achieve with continued development. For this type of measurement, however, background subtraction is not a normal procedure.

## III. THE TARGETS

On this contract, bistatic frequency domain amplitude and phase (square root of radar cross section) scattering data were taken on seven basic conducting targets. Six of these were 1/72 scale models of aircraft which were commercially available. The major dimensions of the models

are given in Table I. Photographs of these models are given in Figures

TABLE I

| TARGET | FUSELAGE LENGTH (cm) | WING SPAN (cm) |
|---|---|---|
| F-104 | 23.5 | 10.8 |
| F-4 | 23.0 | 15.8 |
| MIG-21 | 18.5 | 10.5 |
| F-5 | 18.8 | 10.8 |
| F-15 | 27.0 | 17.6 |
| F-104N | 23.8 | 10.8 |

GROSS DIMENSIONS OF AIRCRAFT MODELS

9 through 14. The two targets denoted as F-104 and F-104N were scale models of the same aircraft which differed only slightly in construction. The conducting paint on their surfaces (all models were plastic which were silver-painted) differed, however, and this difference was considered to be the major contributing factor in the dramatic differences in their spectral returns. For all measurements of the aircraft models, the wings were in the horizontal plane, except for the target denoted F4V which was the F4 with the wings in the vertical plane (the plane containing the electric polarization). The 2.2 to 4.0 GHz frequency band corresponds to a frequency span of approximately 30.0 to 56.0 MHz full scale. The 4.0 to 7.6 GHz band corresponds to 60.0 to 112.0 MHz full scale.

The seventh target, referred to as the PEN target, was used in several different geometric configurations. Three classes of the PEN target are shown in Figures 15, 16 and 17. Figure 15 shows the dimensions of the bare PEN. Figure 16 shows the target with a vertical rear fin added. This configuration is referred to as PENT3. (3.0 inch vertical tail height), PENT2.5 (2.5 inch vertical tail height), and PENT2.

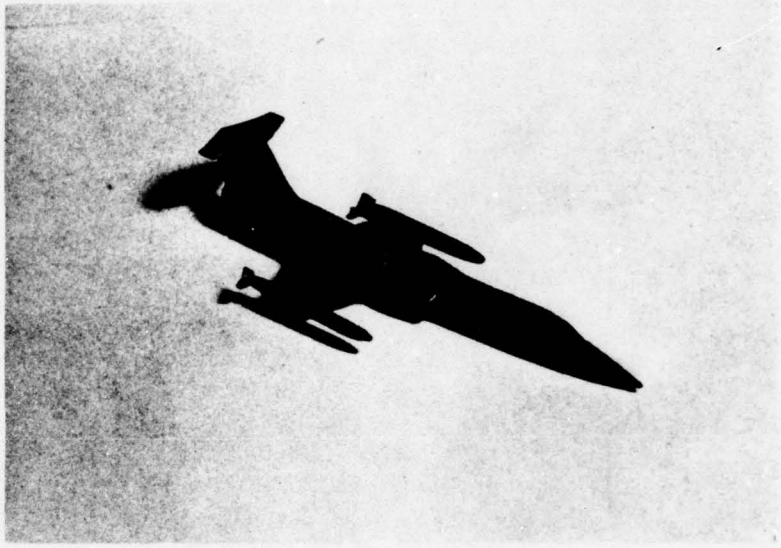

Figure 9. Photograph of the 1/72 scale F104 aircraft.

Figure 10. Photograph of the 1/72 scale F4 aircraft.

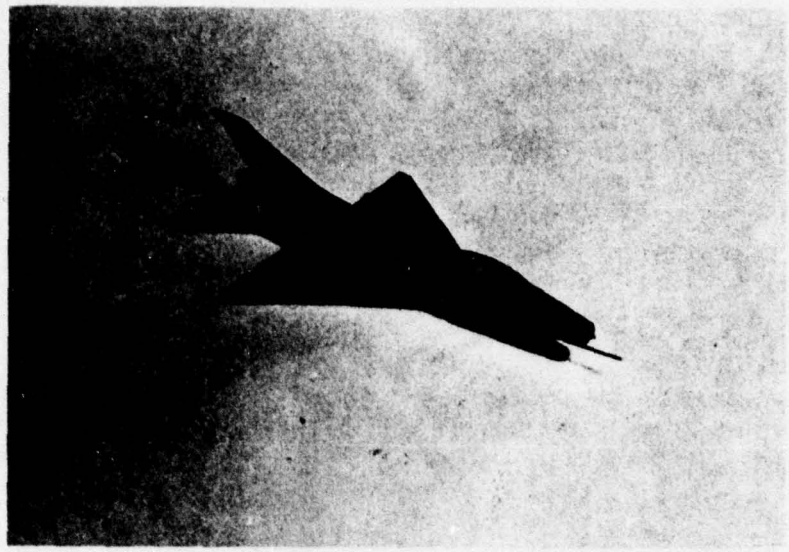

Figure 11. Photograph of the 1/72 scale MIG-21 aircraft.

Figure 12. Photograph of the 1/72 scale F5 aircraft.

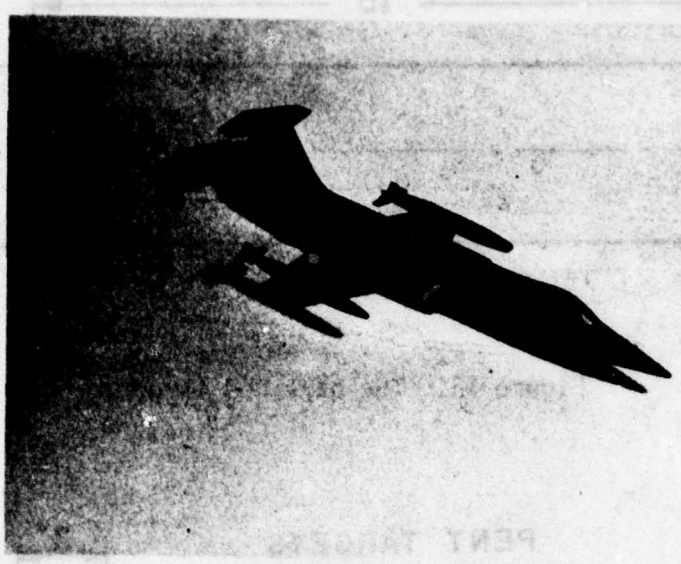

Figure 13. Photograph of the 1/72 scale F104N aircraft.

Figure 14. Photograph of the 1/72 scale F15 aircraft.

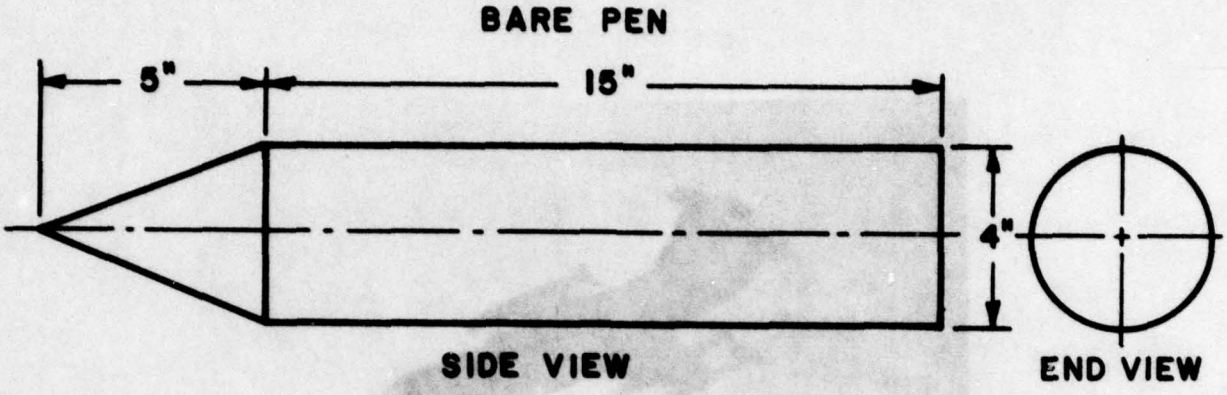


Figure 15. The bare PEN target.

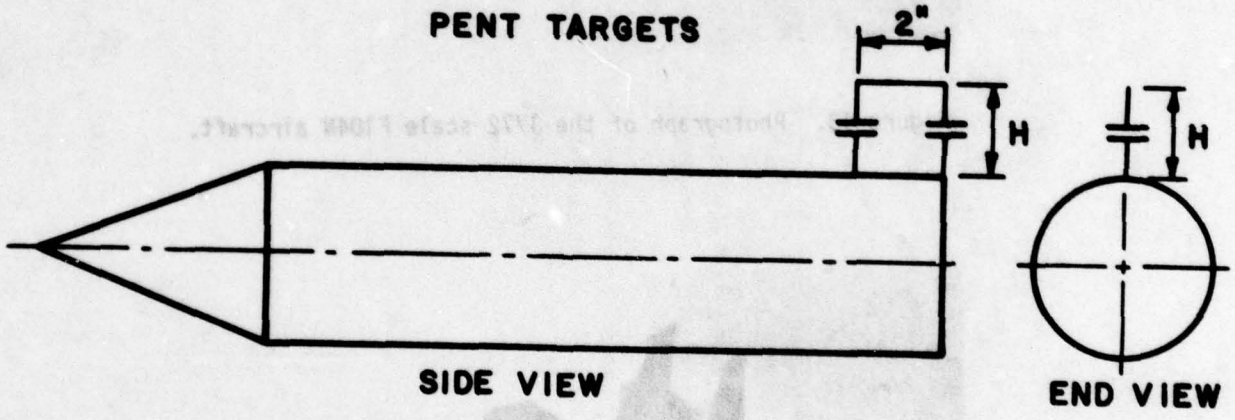


VALUE OF H VARIES WITH TARGET

| | |
|---|---|
| PENT2. | H = 2" |
| PENT2.5 | H = 2.5" |
| PENT3. | H = 3" |

TAIL FIN THICKNESS = 1/16"

Figure 16. The PENT target.

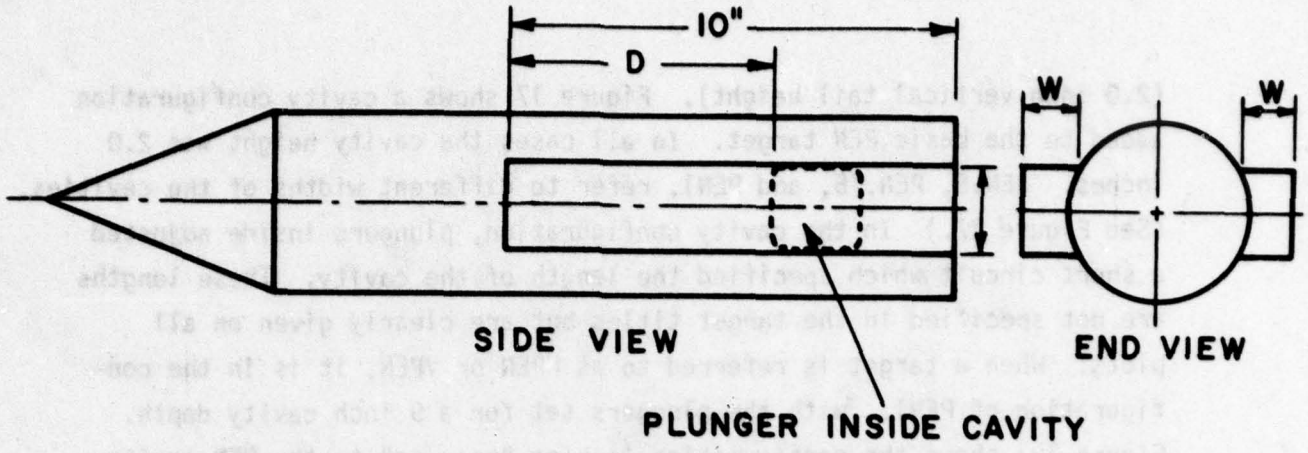


VALUE OF W,D VARIES WITH TARGET

| | |
|---|---|
| PEN.5 | W = 0.5" |
| PEN.75 | W = 0.75" |
| PENI. | W = 1" |

VALUE OF D GIVEN ON APPROPRIATE PLOT

Figure 17. The PEN 1.50, PEN 1.75 and PEN 2.0 targets.

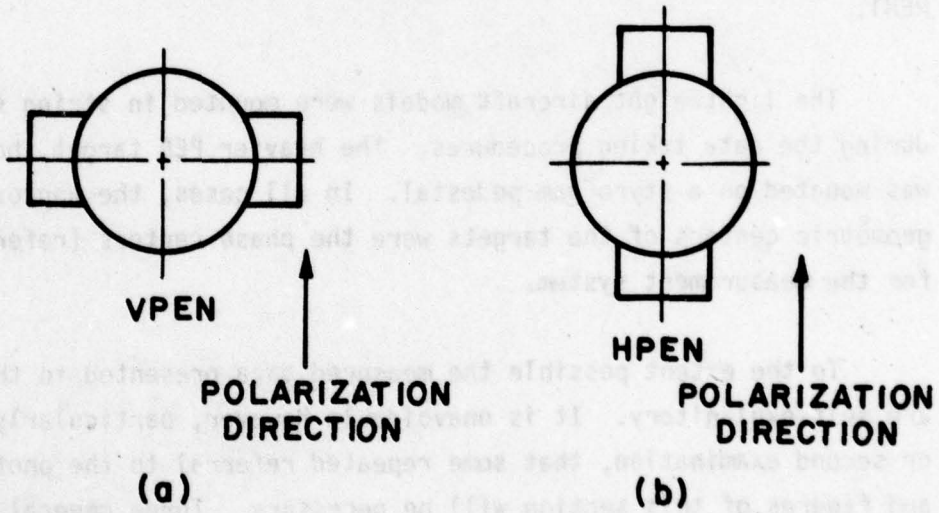


Figure 18. Cavity orientation designations.

(2.0 inch vertical tail height). Figure 17 shows a cavity configuration added to the basic PEN target. In all cases the cavity height was 2.0 inches. PEN.5, PEN.75, and PEN1. refer to different widths of the cavities. (See Figure 17.) In the cavity configuration, plungers inside adjusted a short circuit which specified the length of the cavity. These lengths are not specified in the target titles but are clearly given on all plots. When a target is referred to as HPEN or VPEN, it is in the configuration of PEN1. with the plungers set for a 9 inch cavity depth. Figure 18a shows the configuration looking "nose-on" to the PEN cavity targets, in all configurations but those referred to as HPEN. The HPEN configuration is shown in Figure 18b. Note again that all measurements were taken with vertical polarization. The HPEN configuration was used to simulate horizontal polarization. Targets referred to as VPEN are actually the same as PEN1. with a 9 inch plunger depth.

Figure 19 is a photograph of the bare PEN target. Figure 20 is a photograph of the PEN target in the cavity configuration, specifically PEN1.

The lightweight aircraft models were mounted in string supports during the data taking procedures. The heavier PEN target, however, was mounted on a styrofoam pedestal. In all cases, the approximate geometric centers of the targets were the phase centers (reference) for the measurement system.

To the extent possible the measured data presented in this report are self-explanitory. It is unavoidable however, particularly on first or second examination, that some repeated referral to the photographs and figures of this section will be necessary. Three general suggestions are made: First, the pencil-type target should be examined separately because of its different nature and scale. Second, the aircraft target photographs should be studied with a view to those portions of the structure which can be significantly excited by a vertically polarized electric

Figure 19. Photograph of the bare PEN target.

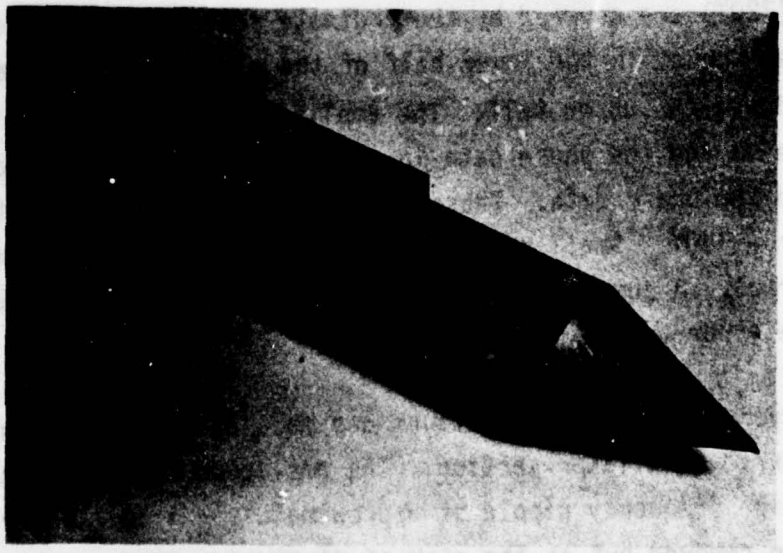

Figure 20. Photograph of the PEN cavity configuration.

field incident in the flight plane. Third, the scattered field data are for a bistatic angle which for relatively gross purposes can be ignored (backscatter) but places some limits on refinements of scattering centers.

## IV. FREQUENCY DOMAIN DATA

Figures 21 through 94 present the calibrated measured amplitude and phase bistatic radar data on six aircraft targets plus the various pencil targets. The data as given, are for the model sizes at the model frequencies. The labels above each plot are interpreted as follows: the first line gives the name of the target; the aspect angle (bisector of the bistatic angle thus, $0^{o}$ represents nose-on, other aspect angles are measured from nose-on), and on the PEN cavity targets, the depth of the plunger is given next (on the PENT targets the height of the vertical fin is given). The second line gives the frequency band and the actual bistatic angle for that particular data set. On some plots, the bistatic angle is given on the first line. Calibrated amplitude (solid) and phase (dashed) curves are given together on each figure. Note that for the phase portions of the plots, two complete cycles ($720^{o}$) are covered by the ordinate scale. This was done to keep the phase curves in the lower half of the plots and the magnitude curves generally in the upper half. The amplitude data are given in dB above 1 square cm and the phase data in degrees. Note also the occasional jumps in the phase data. These occurred, in general, when the phase was near $\pm$ $180^{o}$. Small errors at these points then appear much larger than normal. A jump of $2\pi$ degrees means nothing but it looks like a possible error on the plot.

Several general observations are made at this point but the details are deferred to a later section. The amplitude curves for the aircraft show a high frequency ripple of approximately $\pm$ 1 dB. The ripple could have been removed but at the risk of distorting other meaningful excursions.

The F-104 target at $90^{o}$ (Figure 23) shows a much stronger ripple, but was generally repeatable. We do not believe the ripple is real but, admittedly weakly, can only attribute it to an unfortunate string support arrangement which is not really supported by the associated phase data. The aircraft data show much less dramatic changes than do the pencil data but one must include the relative electrical size of the targets in drawing conclusions.

It is helpful in many instances to examine the spectral and synthetic pulse responses (discussed in the next section) in tandem for a given target. A second examination of the calibrated sphere data in Figure 8 is helpful in deducing the anticipated bandwidth of suspected resonance phenomena. We seek, in most cases, to illustrate for the aircraft targets the dominance of a single scattering center - the tail stabilizer sections of the targets. The interval between frequency samples is 9.0 MHz for the 2.2 to 4.0 GHz data and 18 MHz for the 4.0 to 7.6 GHz data. One will note on both the amplitude and phase plots that certain abrupt departures from the relatively smooth curves occur where corresponding changes in the other curve do not occur. That is, abrupt amplitude (phase) changes occur but the same frequency span does not reveal a corresponding phase (amplitude) change. There are also such abrupt changes where both occur. These changes represent at most two sample points and it is not believed that the scattering can change that rapidly with frequency for this electrical size of the targets. At most such points occur for perhaps 10% of the data and should be disregarded. The accuracy estimates given earlier reflect the neglect of such points.

The amplitude scale is in dB. This type of presentation conveniently confines the amplitude changes but the reader is cautioned that a gentle 5 dB change in amplitude is really a substantial (1.8 factor) change on a linear scale.

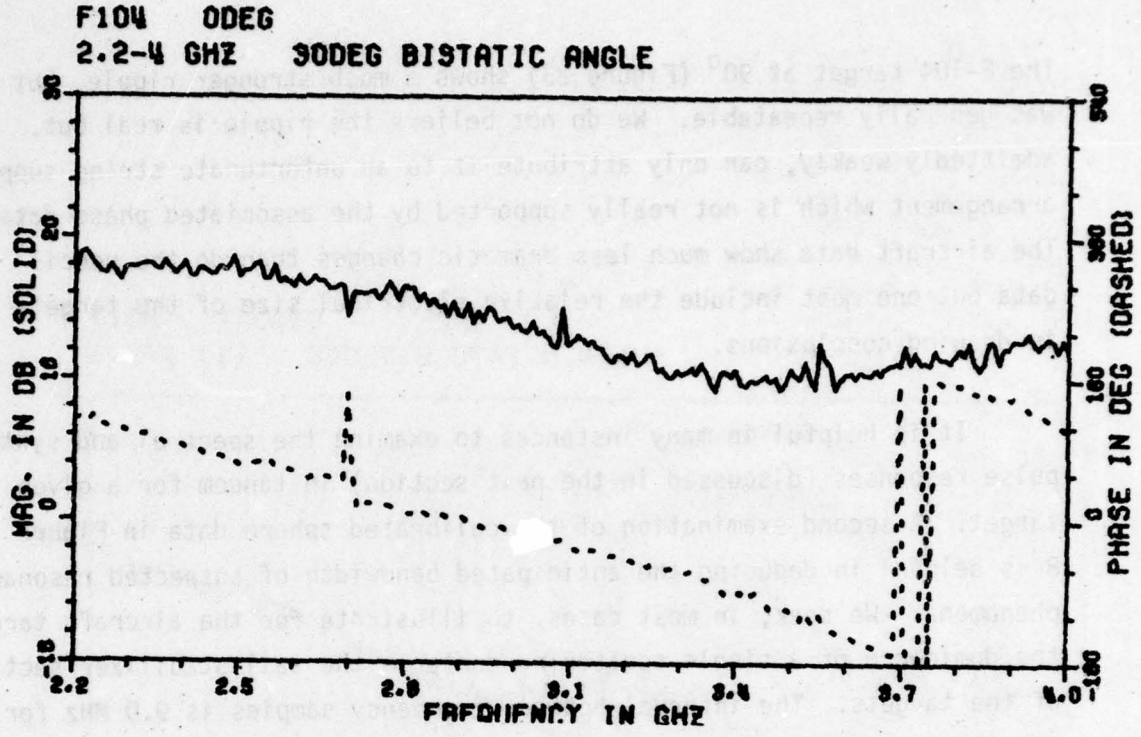


Figure 21. Measured amplitude and phase of scattered field, F-104 aircraft, 2.2-4.0 GHz.

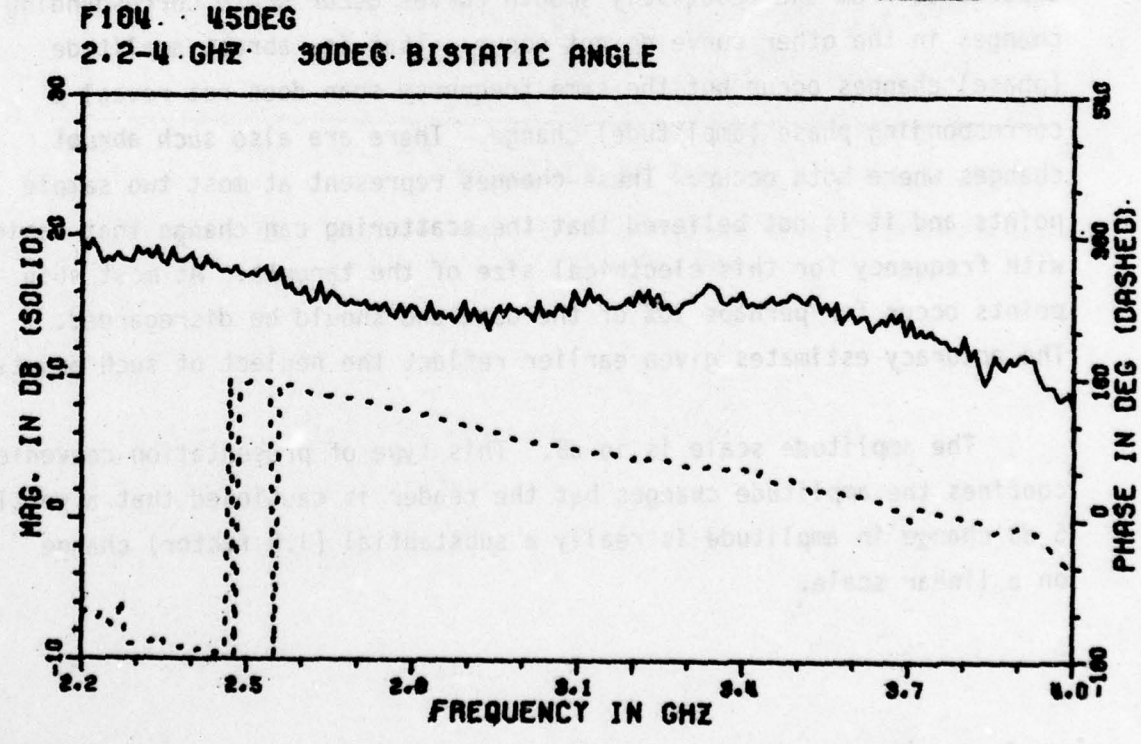


Figure 22. Measured amplitude and phase of scattered field, F-104 aircraft, 2.2-4.0 GHz.

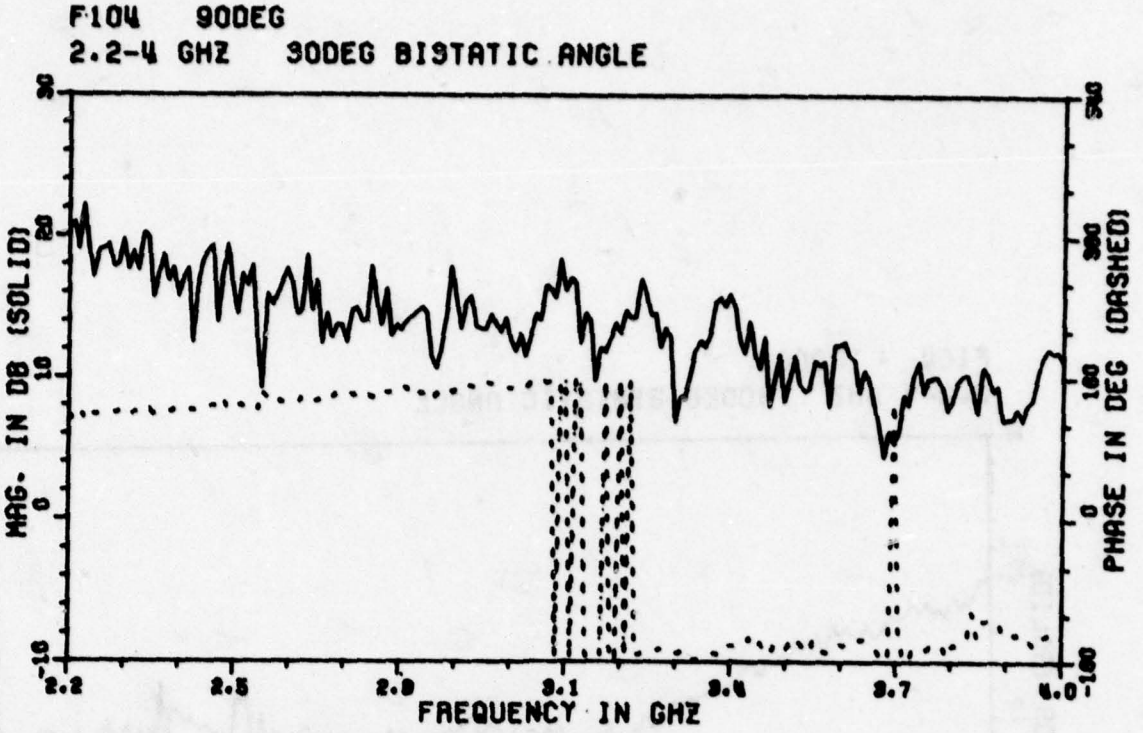


Figure 23. Measured amplitude and phase of scattered field, F-104 aircraft, 2.2-4.0 GHz.

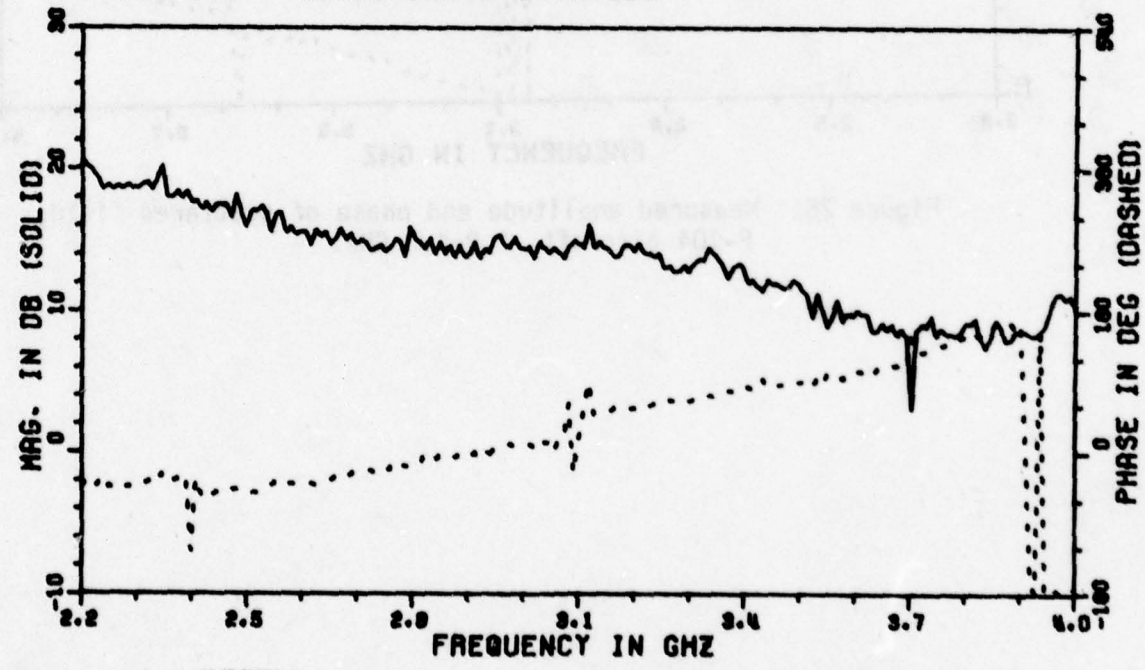


Figure 24. Measured amplitude and phase of scattered field, F-104 aircraft, 2.2-4.0 GHz.

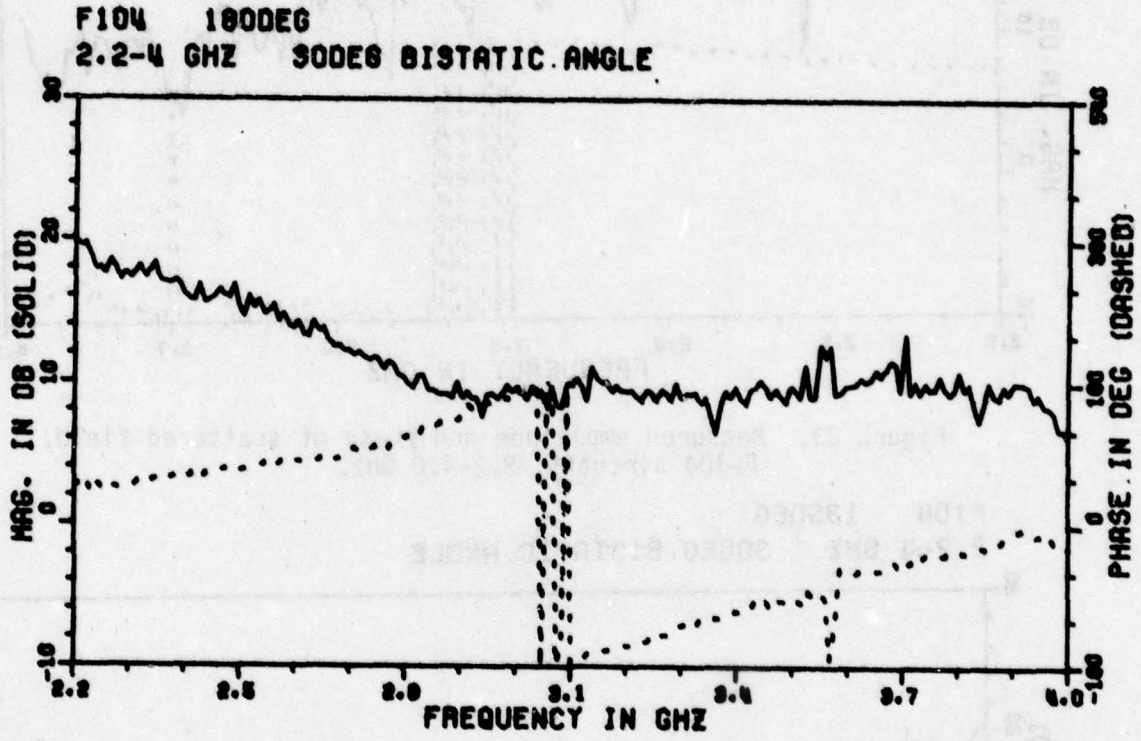


Figure 25. Measured amplitude and phase of scattered field, F-104 aircraft, 2.2-4.0 GHz.

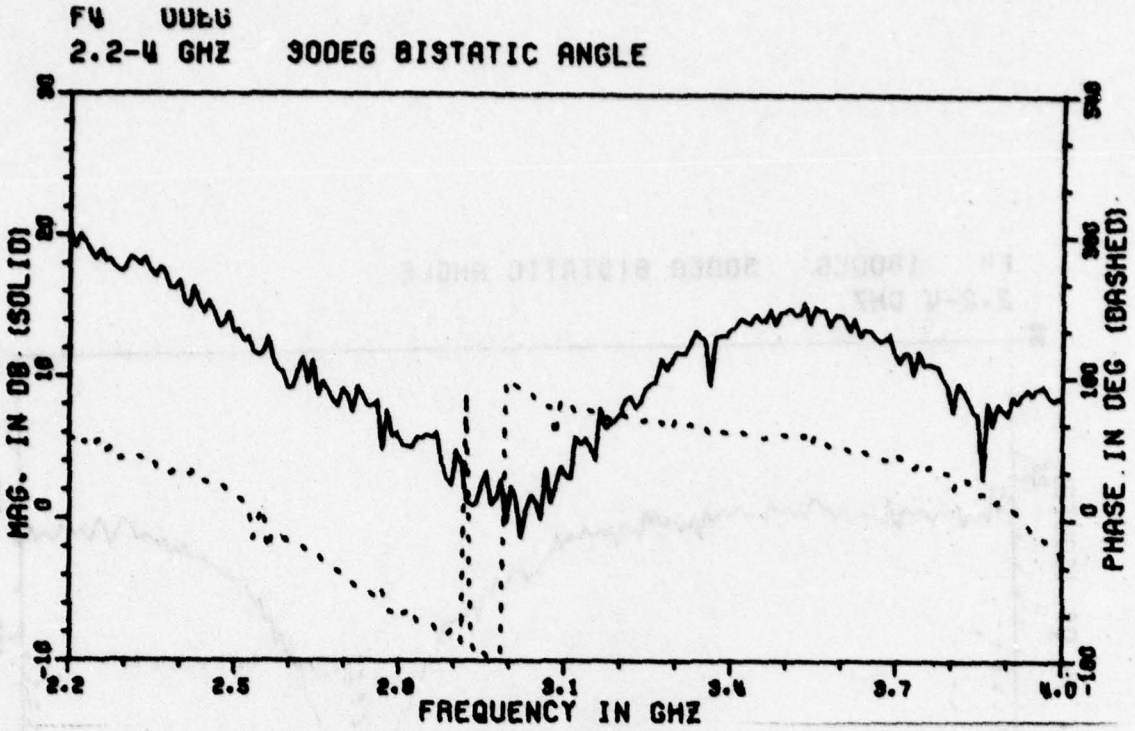


Figure 26. Measured amplitude and phase of scattered field, F-4 aircraft, 2.2-4.0 GHz.

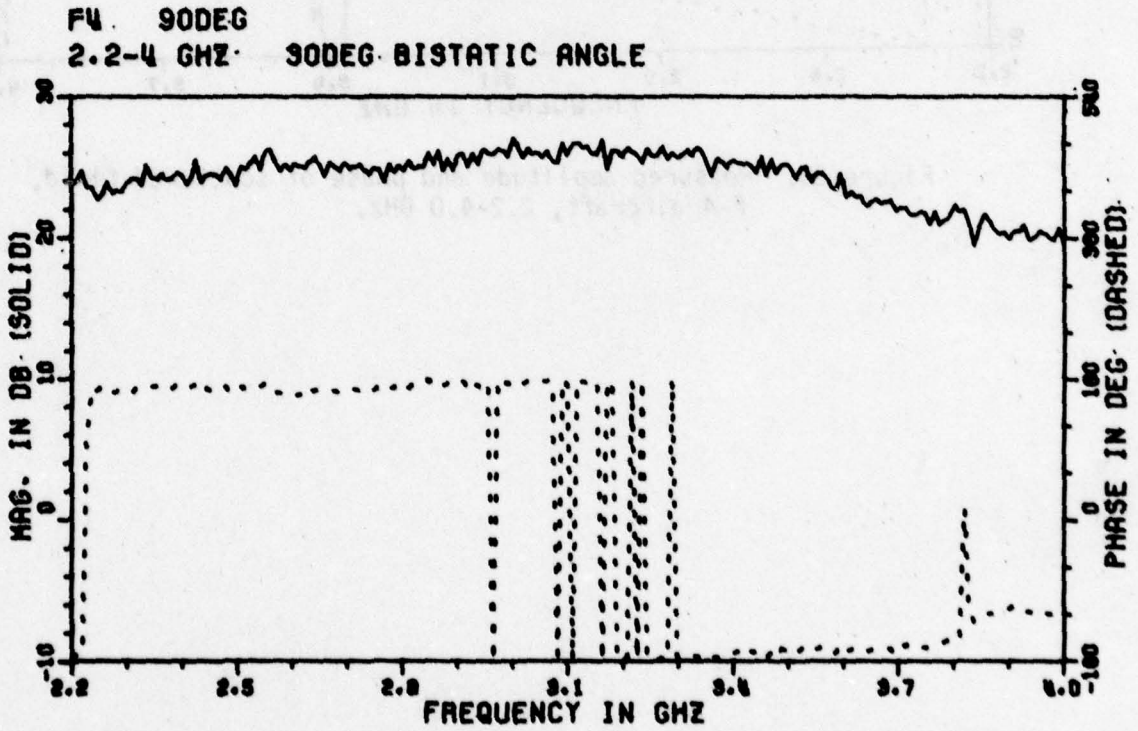


Figure 27. Measured amplitude and phase of scattered field, F-4 aircraft, 2.2-4.0 GHz.

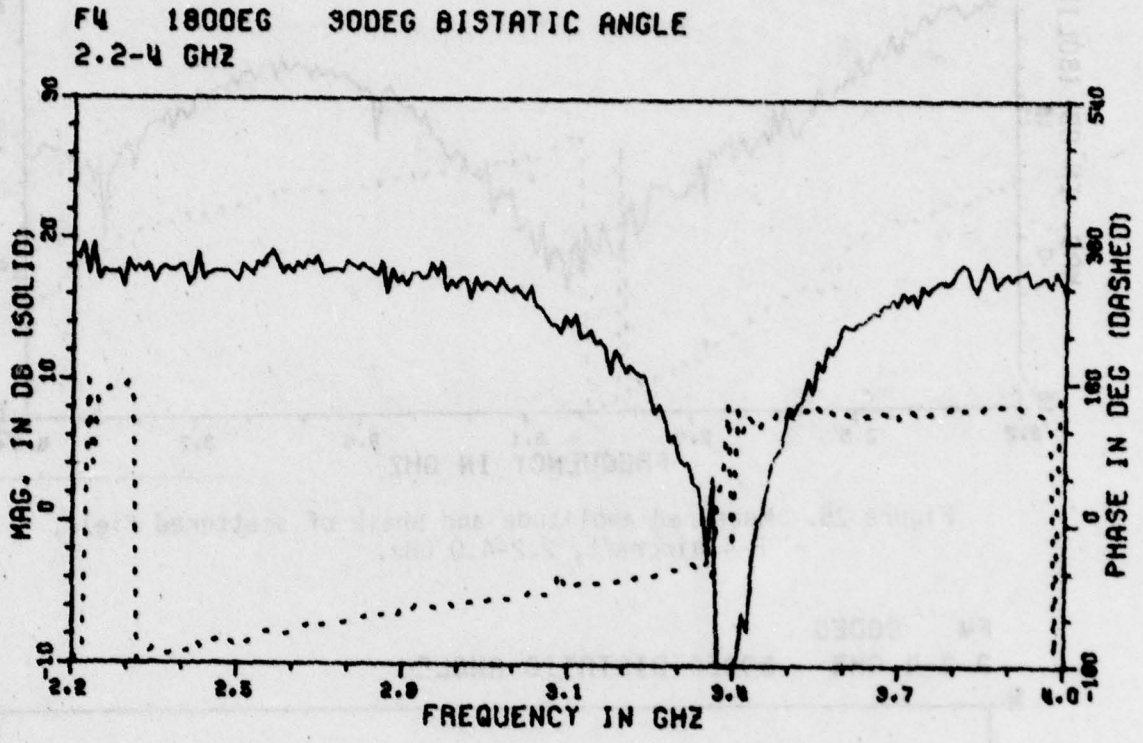


Figure 28. Measured amplitude and phase of scattered field, F-4 aircraft, 2.2-4.0 GHz.

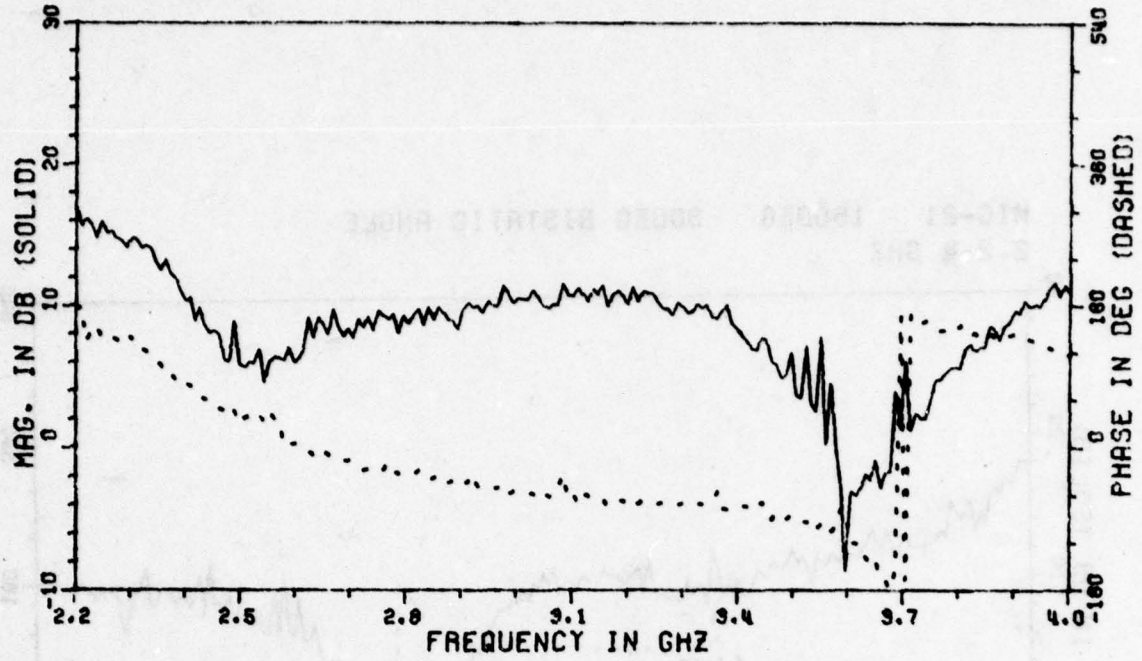


Figure 29. Measured amplitude and phase of scattered field, MIG-21 aircraft, 2.2-4.0 GHz.

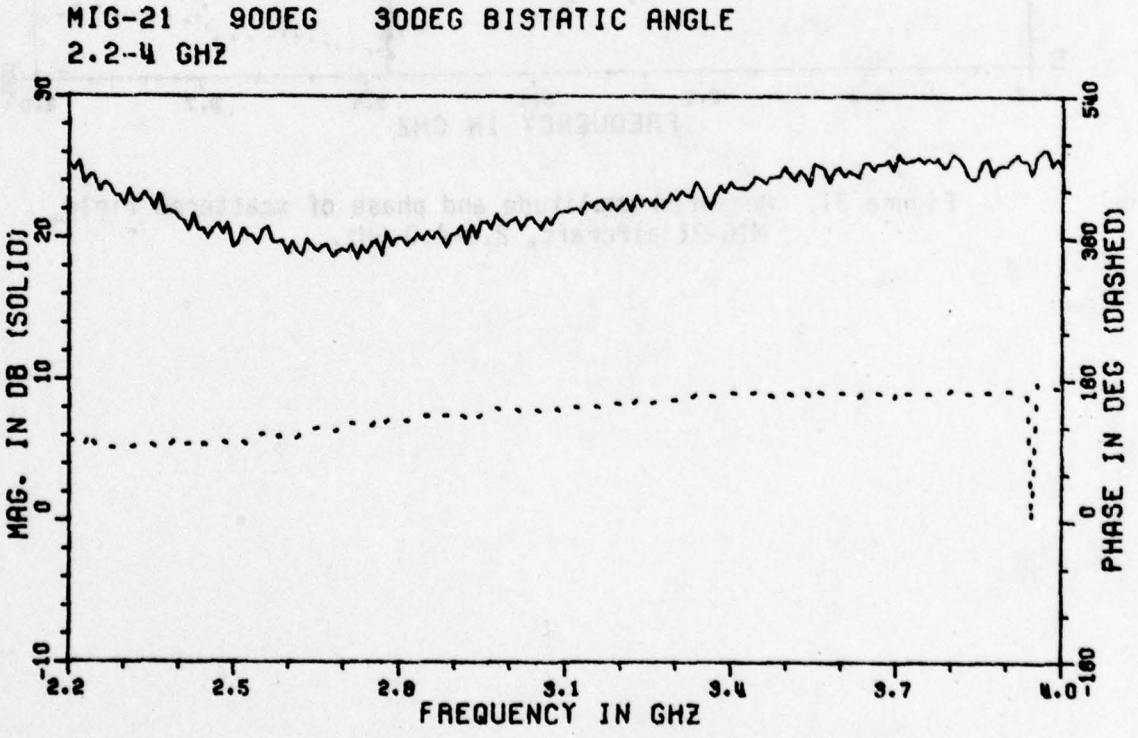


Figure 30. Measured amplitude and phase of scattered field, MIG-21 aircraft, 2.2-4.0 GHz.

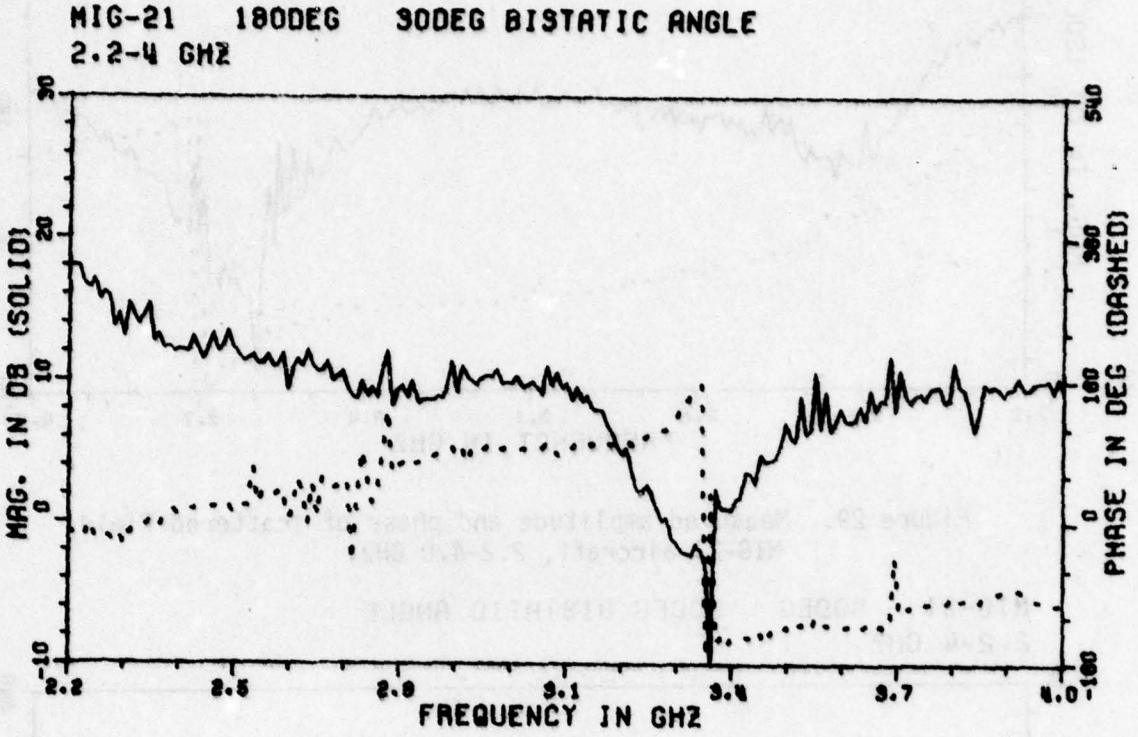


Figure 31. Measured amplitude and phase of scattered field, MIG-21 aircraft, 2.2-4.0 GHz.

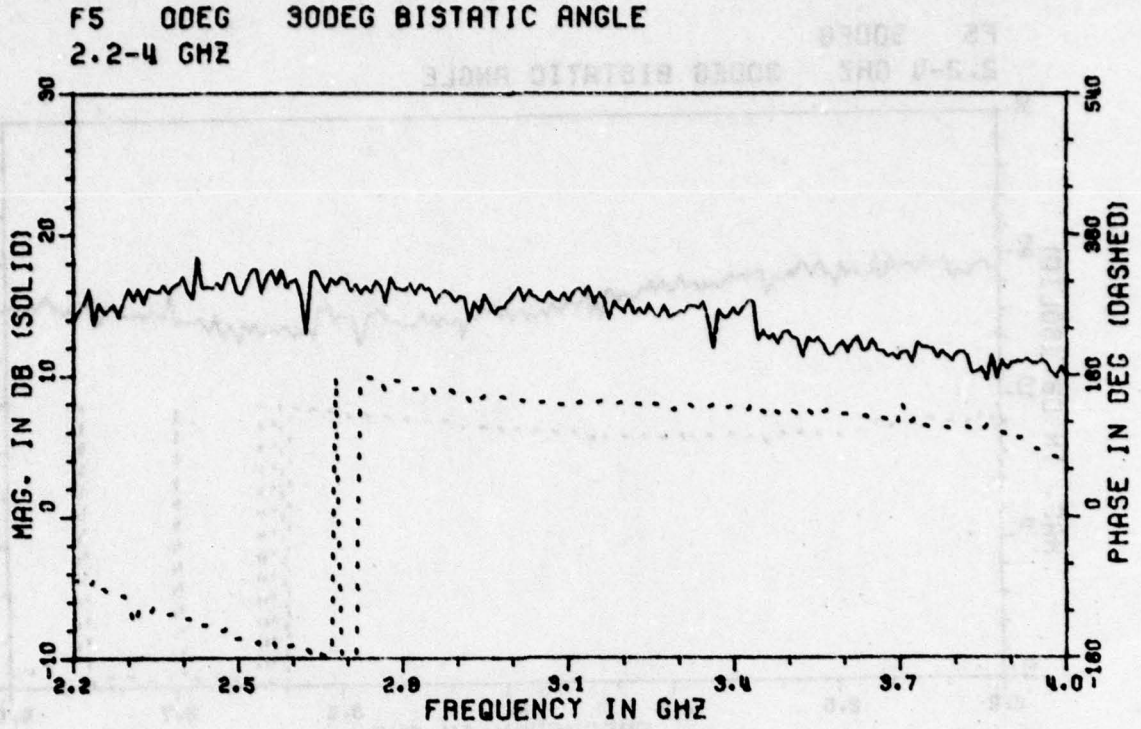


Figure 32. Measured amplitude and phase of scattered field, F5 aircraft, 2.2-4.0 GHz.

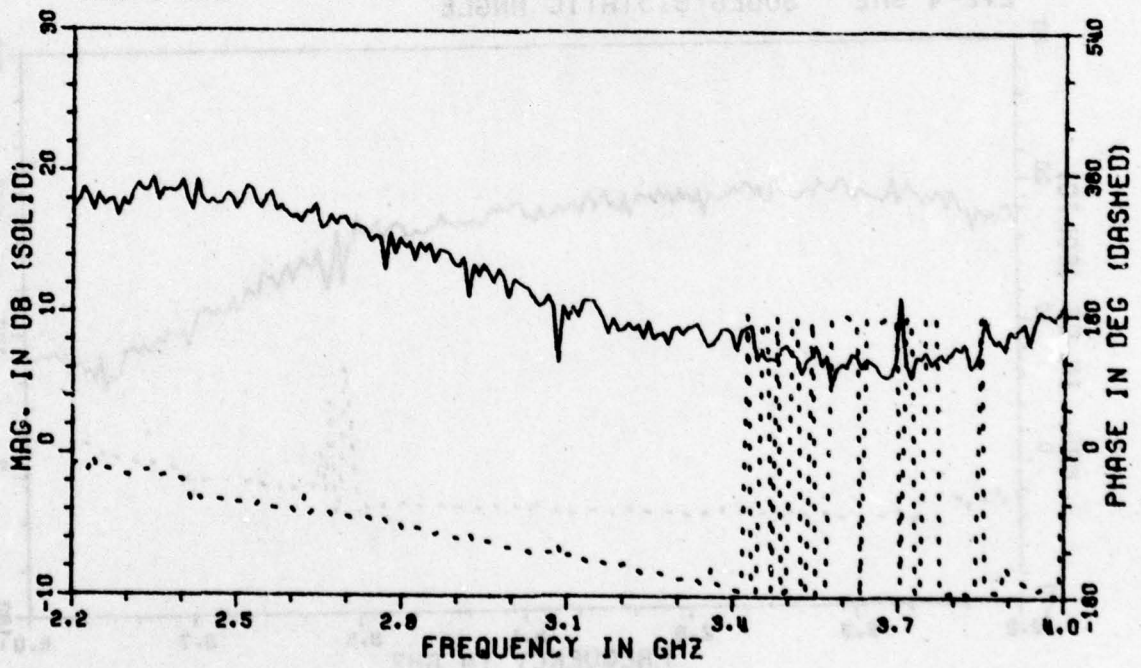


Figure 33. Measured amplitude and phase of scattered field, F5 aircraft, 2.2-4.0 GHz.

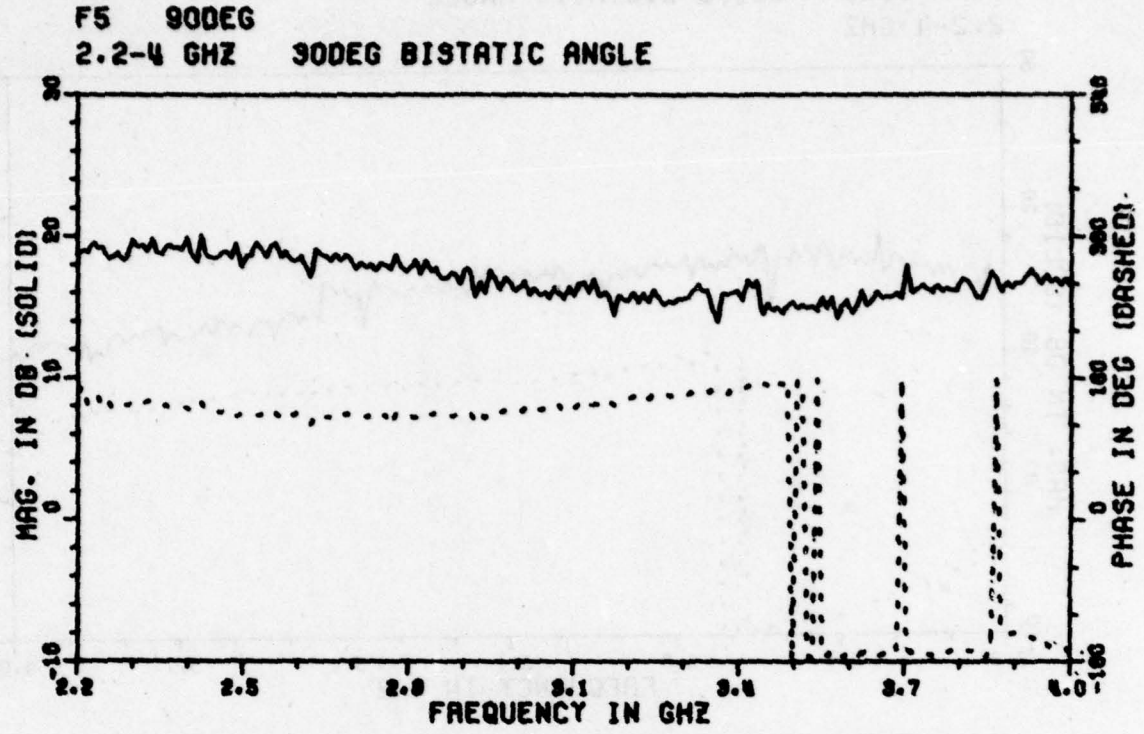


Figure 34. Measured amplitude and phase of scattered field, F5 aircraft, 2.2-4.0 GHz.

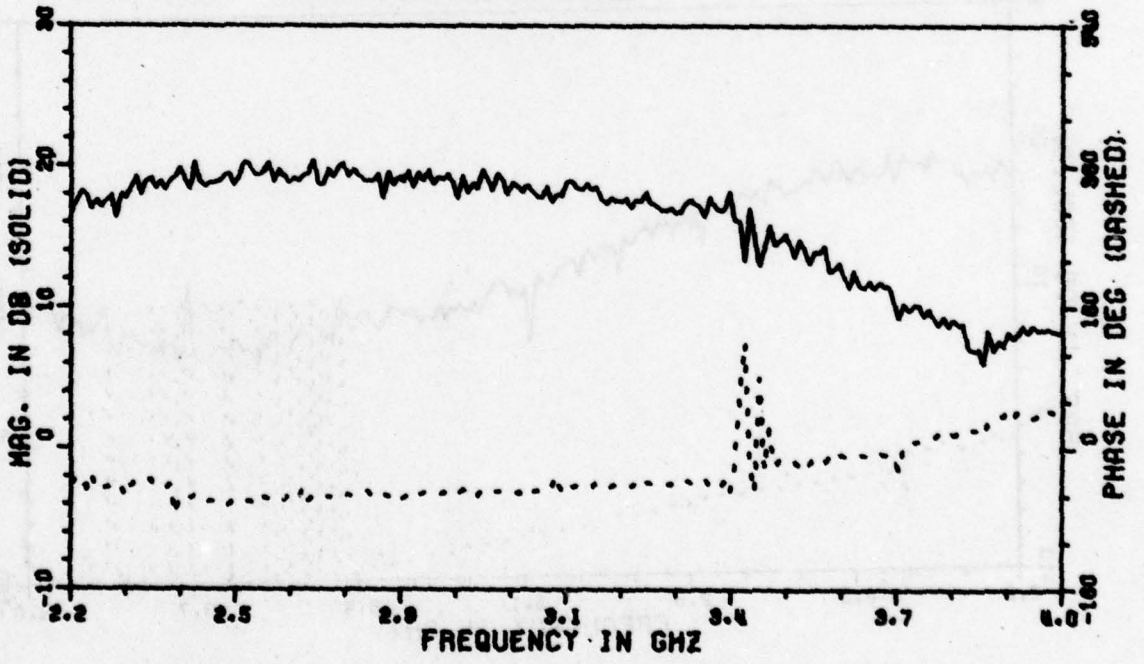


Figure 35. Measured amplitude and phase of scattered field, F5 aircraft, 2.2-4.0 GHz.

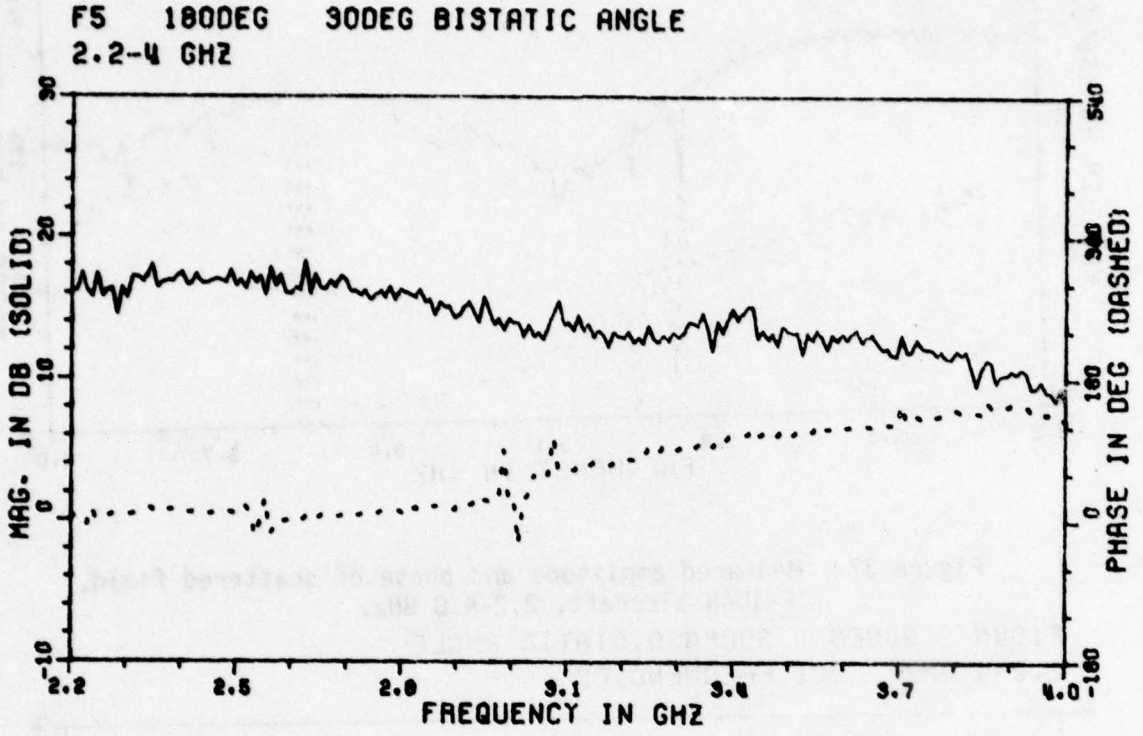


Figure 36. Measured amplitude and phase of scattered field, F5 aircraft, 2.2-4.0 GHz.

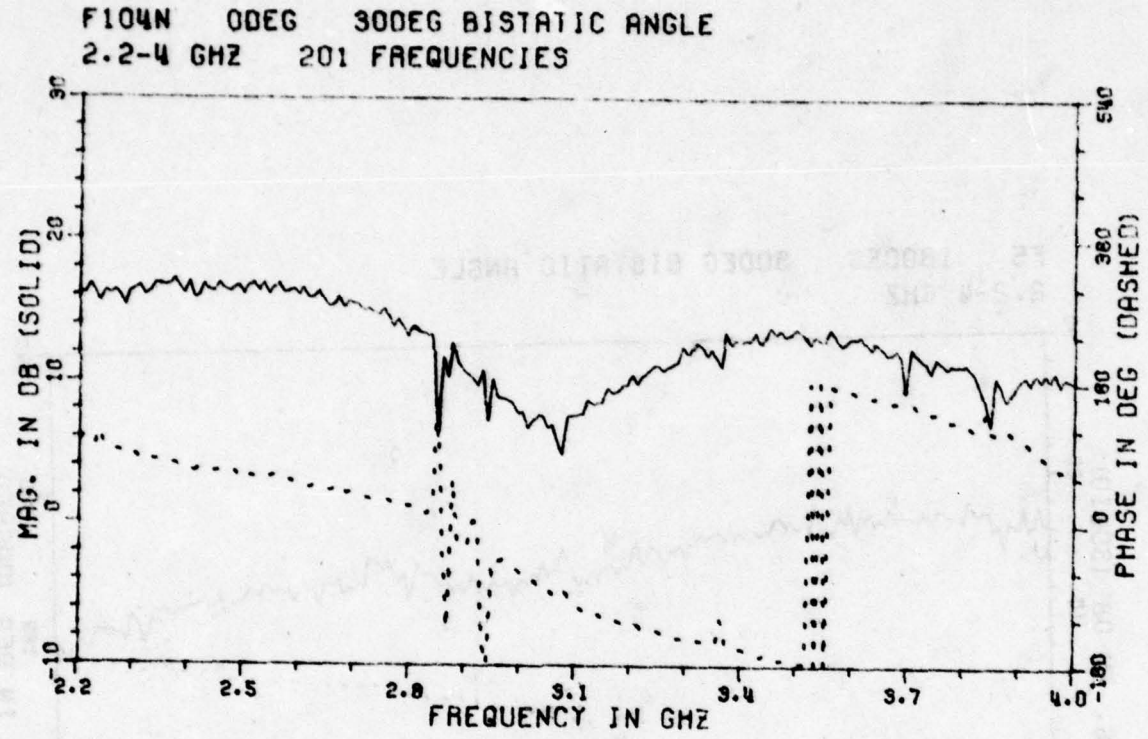


Figure 37. Measured amplitude and phase of scattered field, F-104N aircraft, 2.2-4.0 GHz.

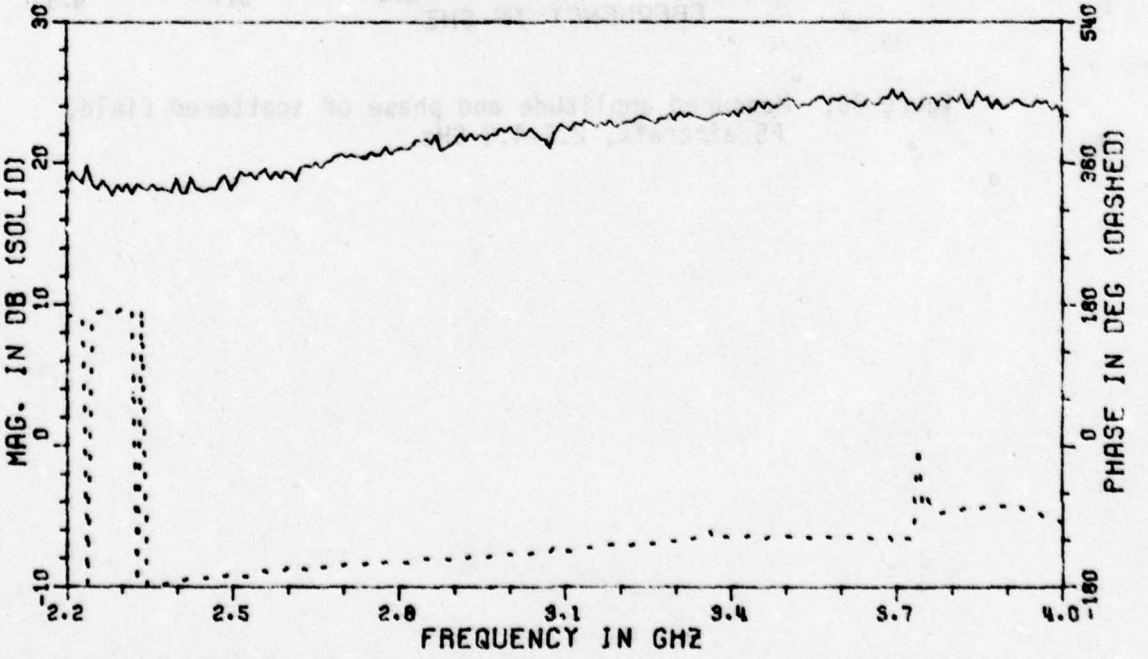


Figure 38. Measured amplitude and phase of scattered field, F-104N aircraft, 2.2-4.0 GHz.

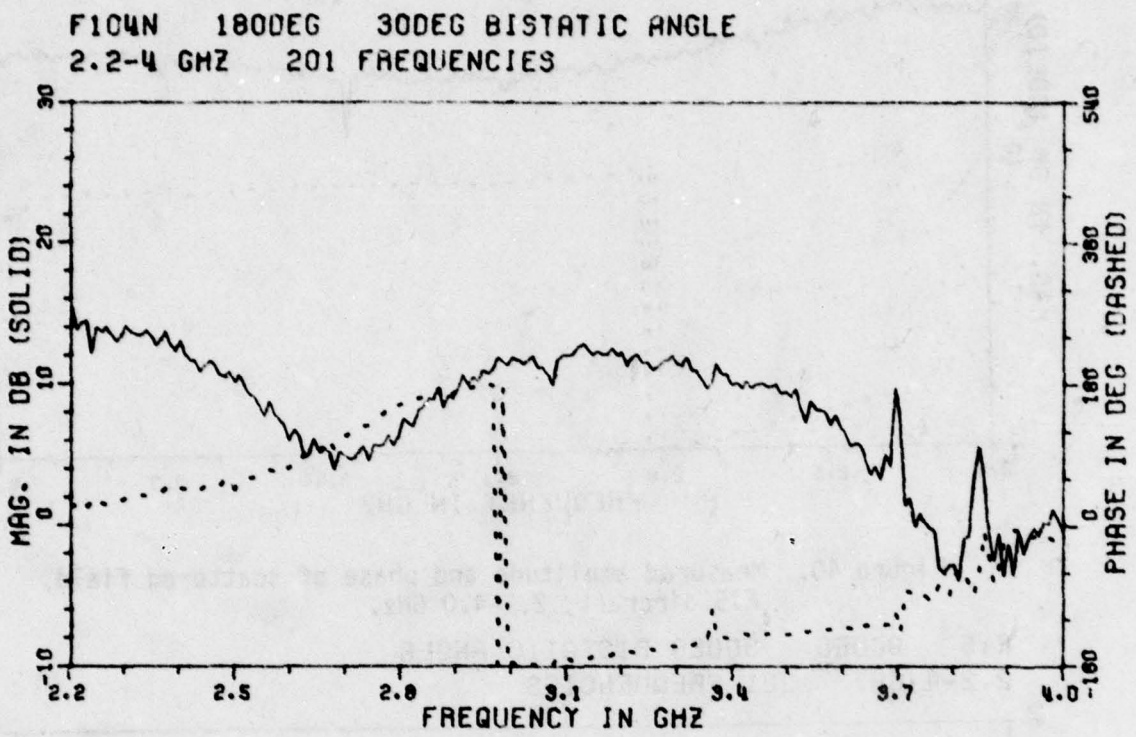


Figure 39. Measured amplitude and phase of scattered field, F-104N aircraft, 2.2-4.0 GHz.

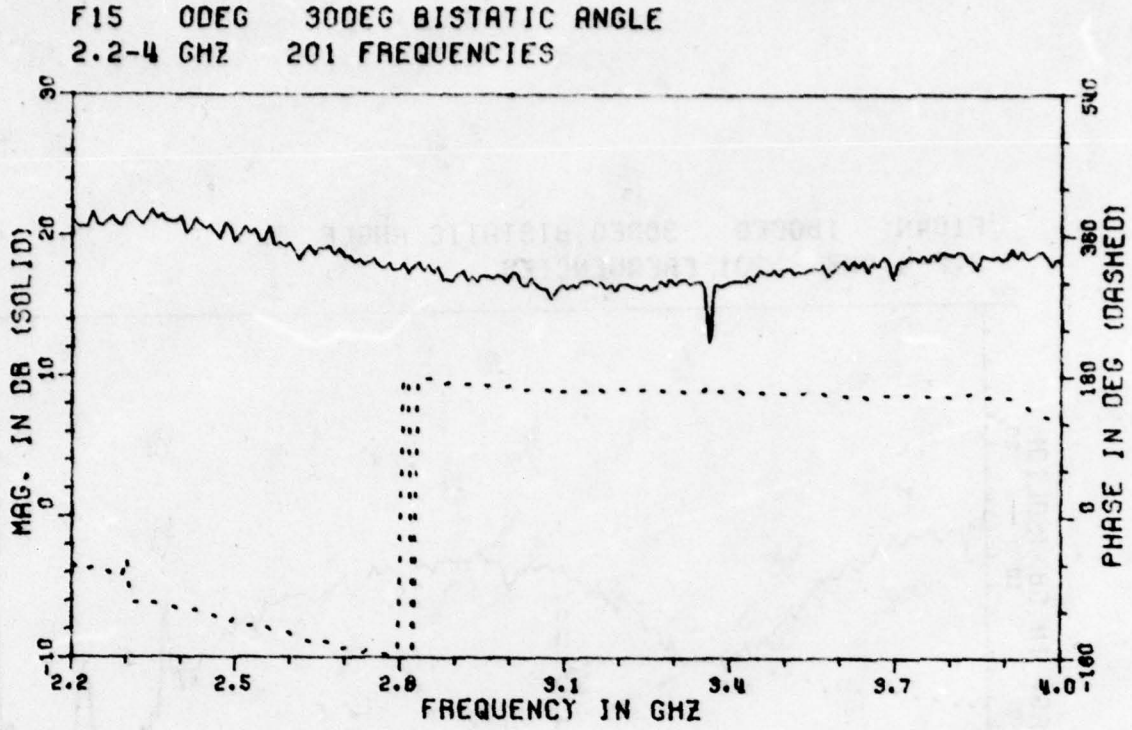


Figure 40. Measured amplitude and phase of scattered field, F15 aircraft, 2.2-4.0 GHz.

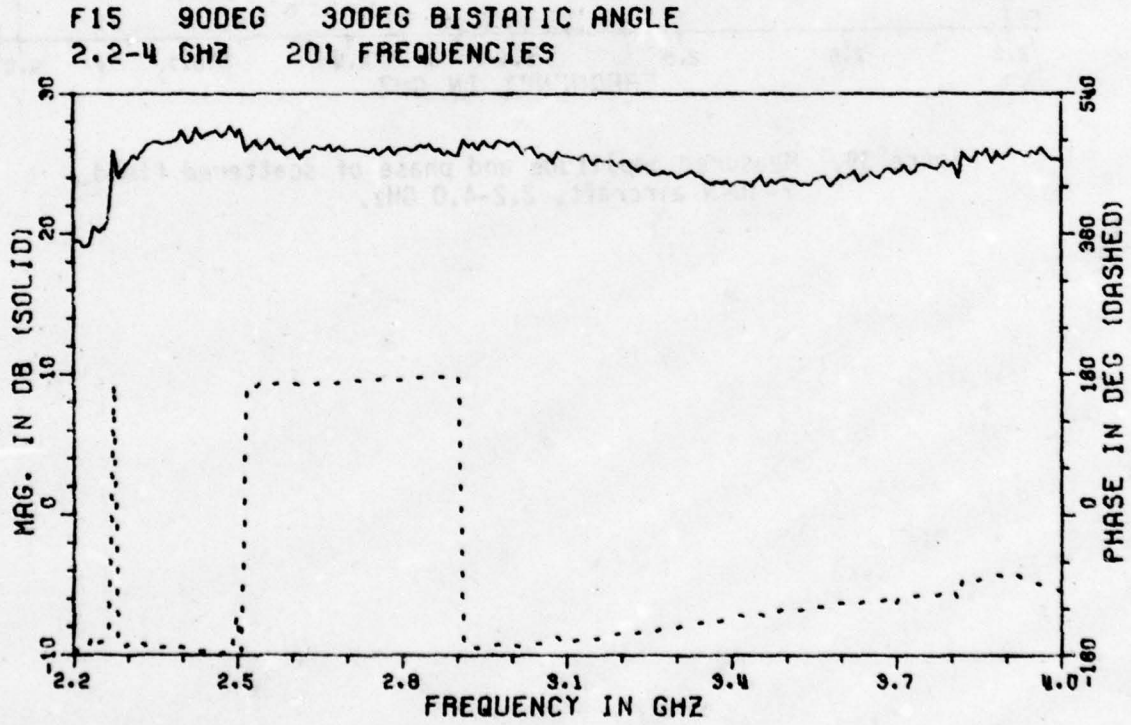


Figure 41. Measured amplitude and phase of scattered field, F15 aircraft, 2.2-4.0 GHz.

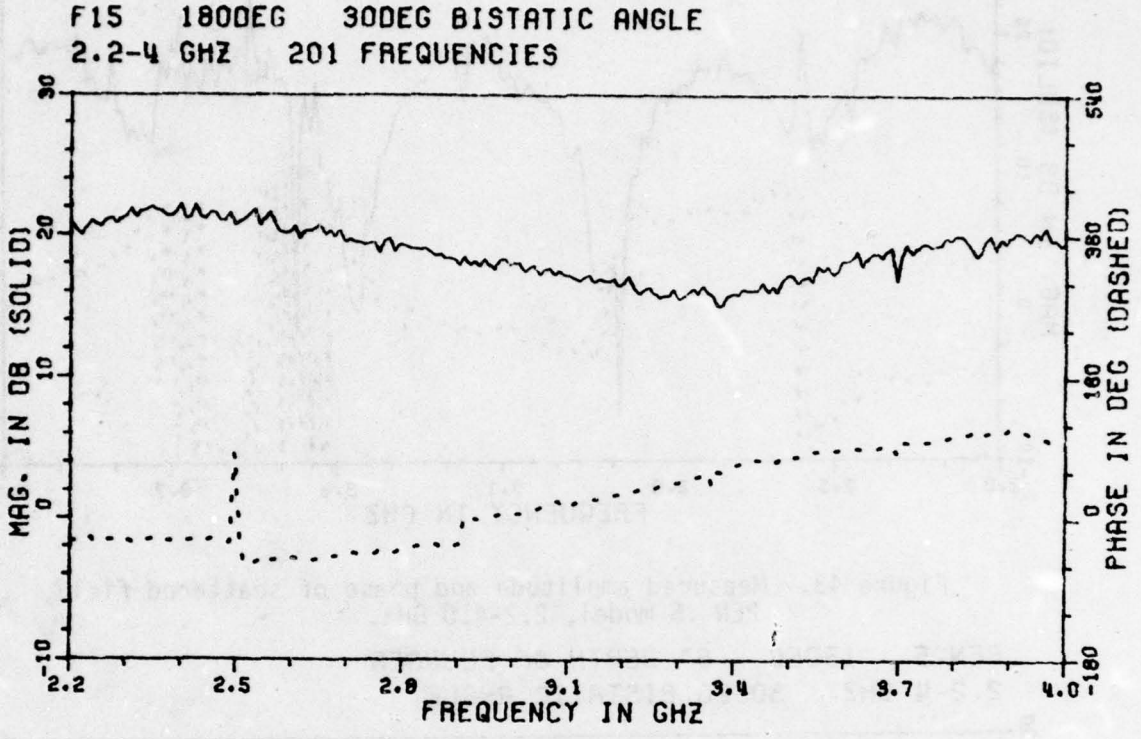


Figure 42. Measured amplitude and phase of scattered field, F15 aircraft, 2.2-4.0 GHz.

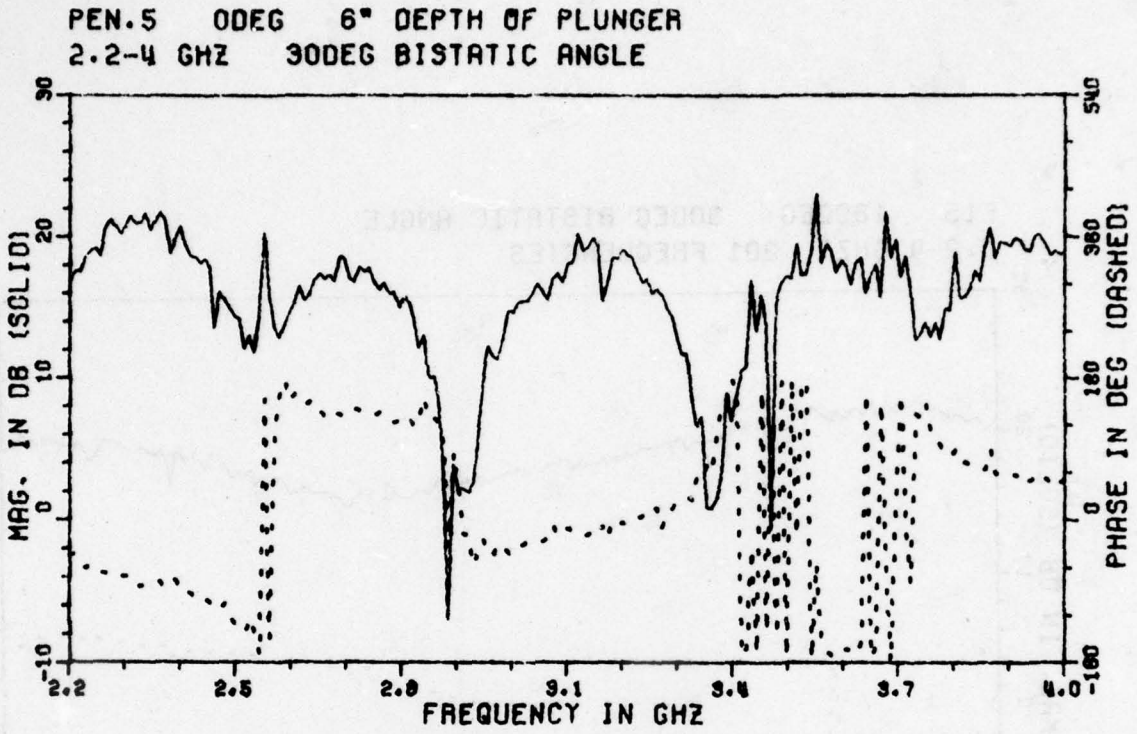


Figure 43. Measured amplitude and phase of scattered field, PEN .5 model, 2.2-4.0 GHz.

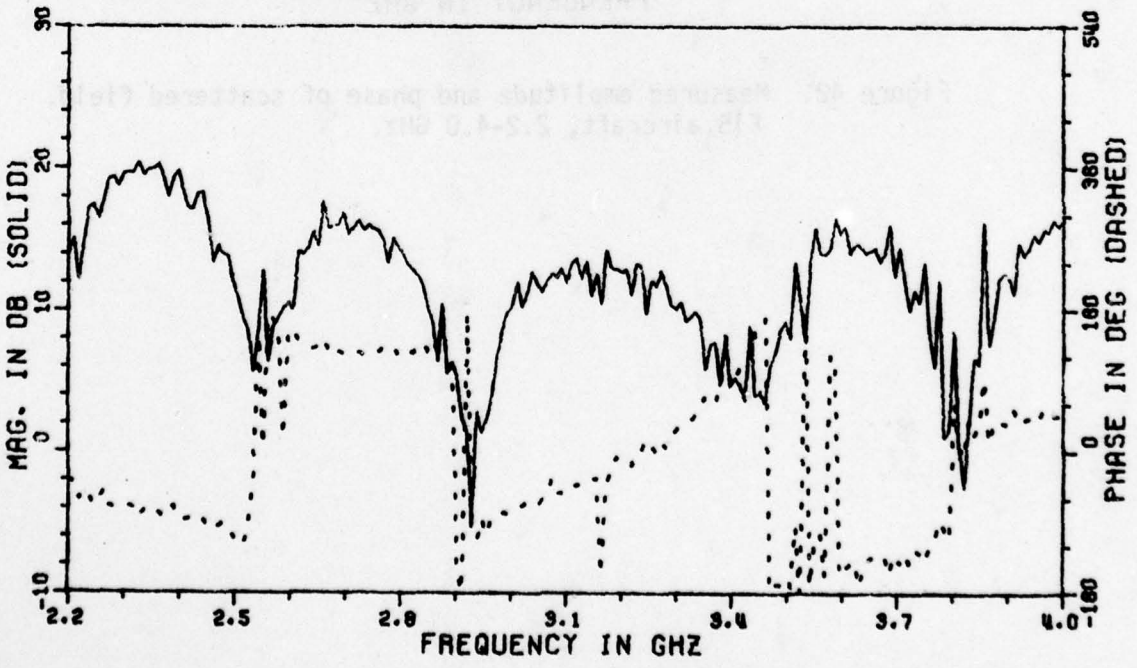


Figure 44. Measured amplitude and phase of scattered field, PEN .5 model, 2.2-4.0 GHz.

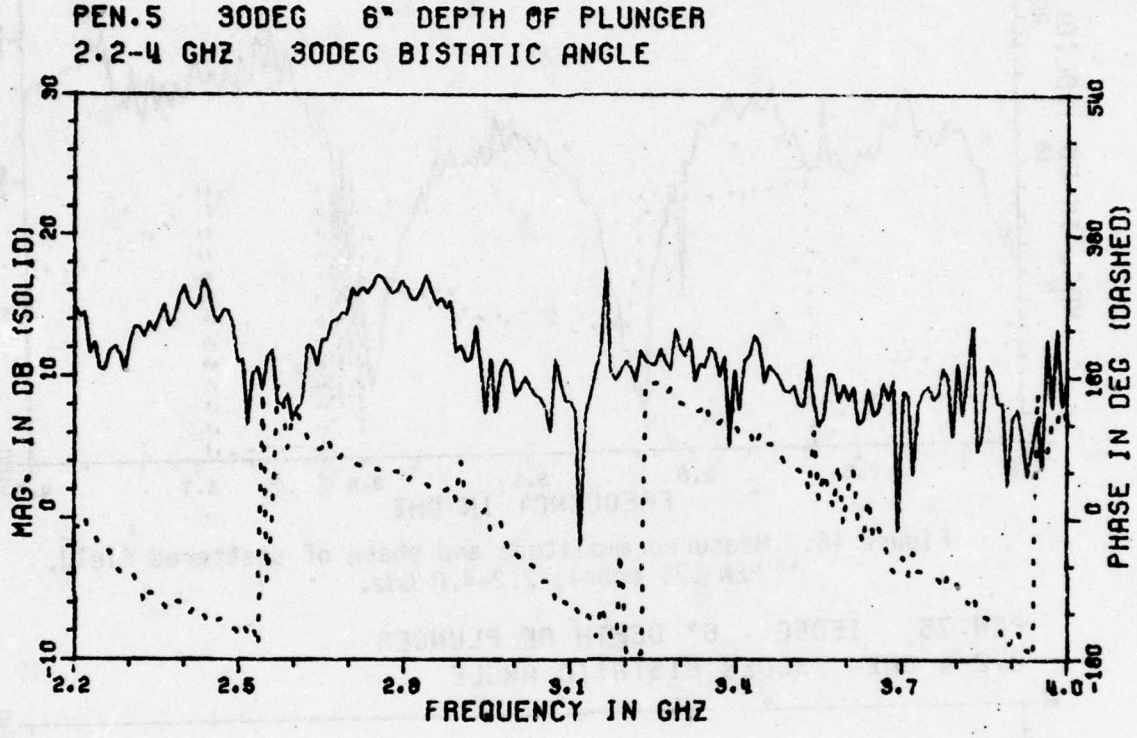


Figure 45. Measured amplitude and phase of scattered field, PEN .5 model, 2.2-4.0 GHz.

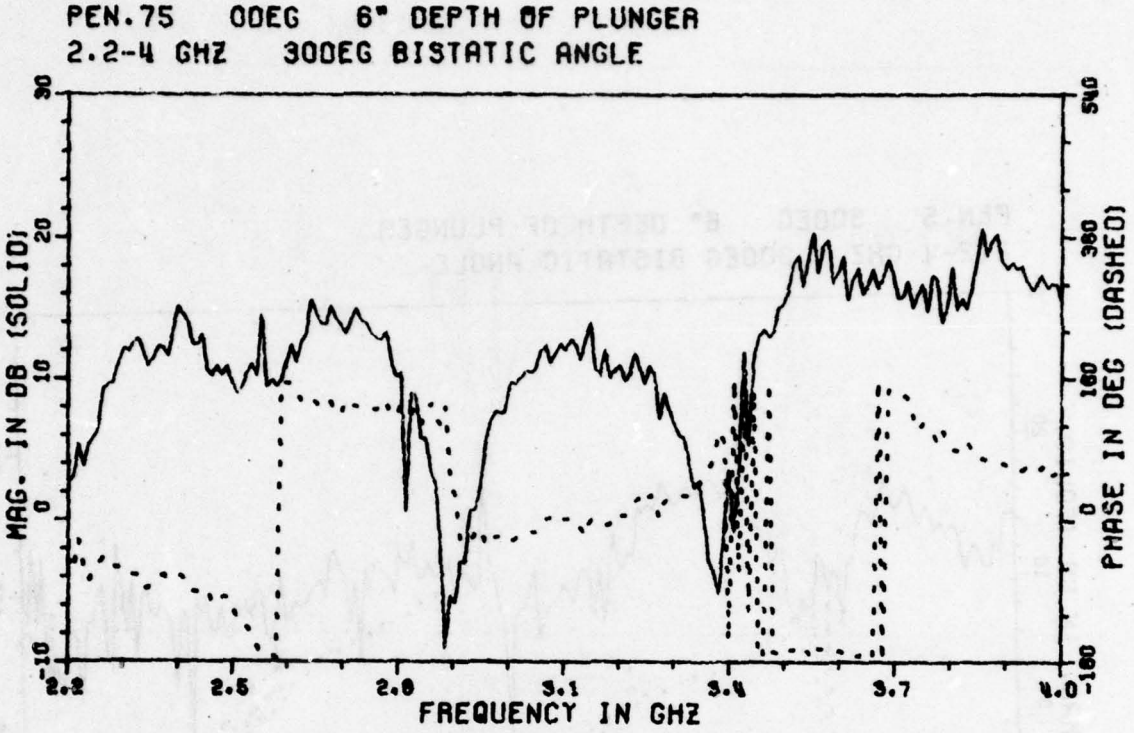


Figure 46. Measured amplitude and phase of scattered field, PEN .75 model, 2.2-4.0 GHz.

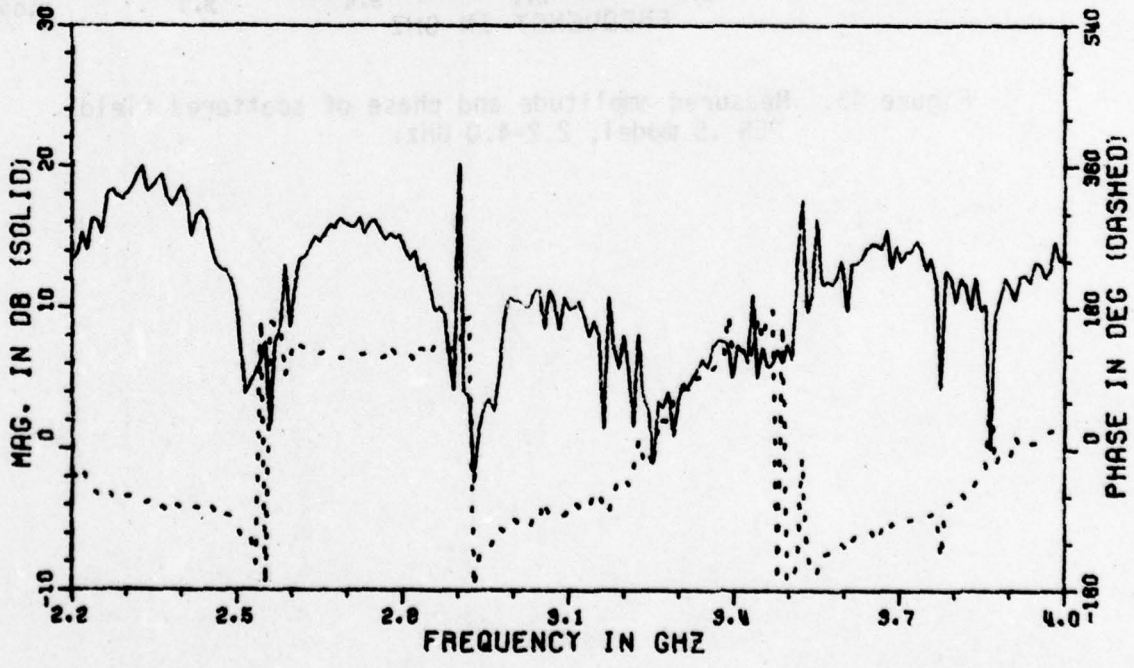


Figure 47. Measured amplitude and phase of scattered field, PEN .75 model, 2.2-4.0 GHz.

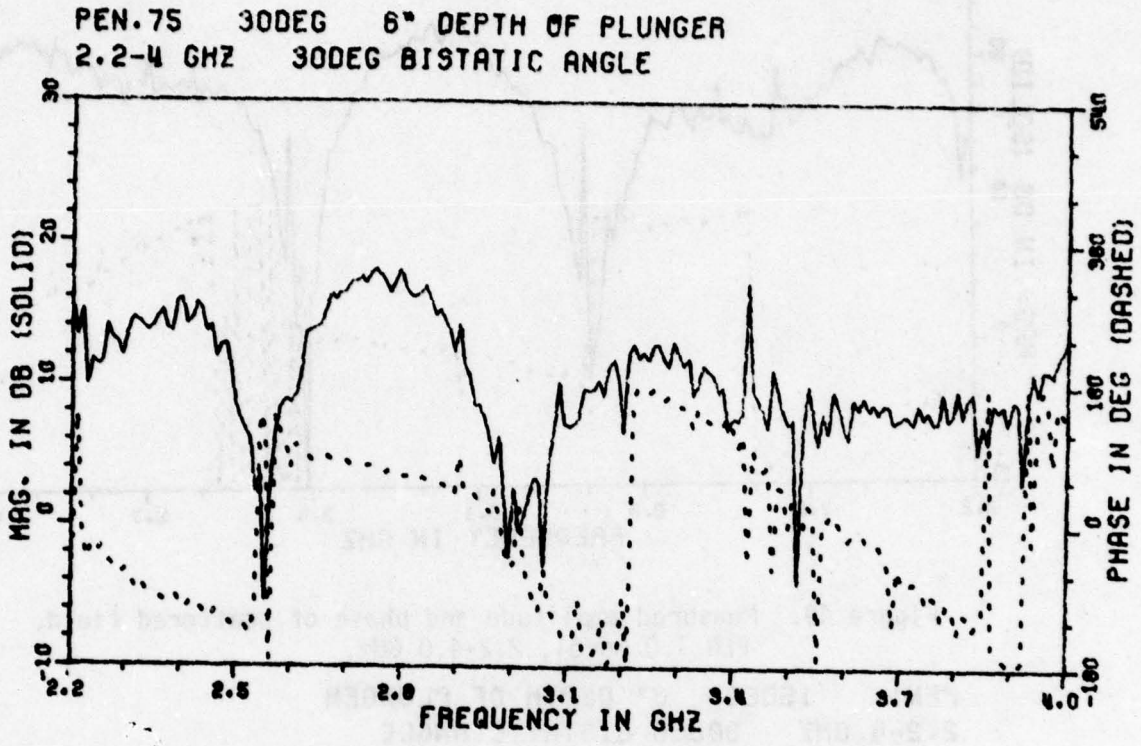


Figure 48. Measured amplitude and phase of scattered field, PEN .75 model, 2.2-4.0 GHz.

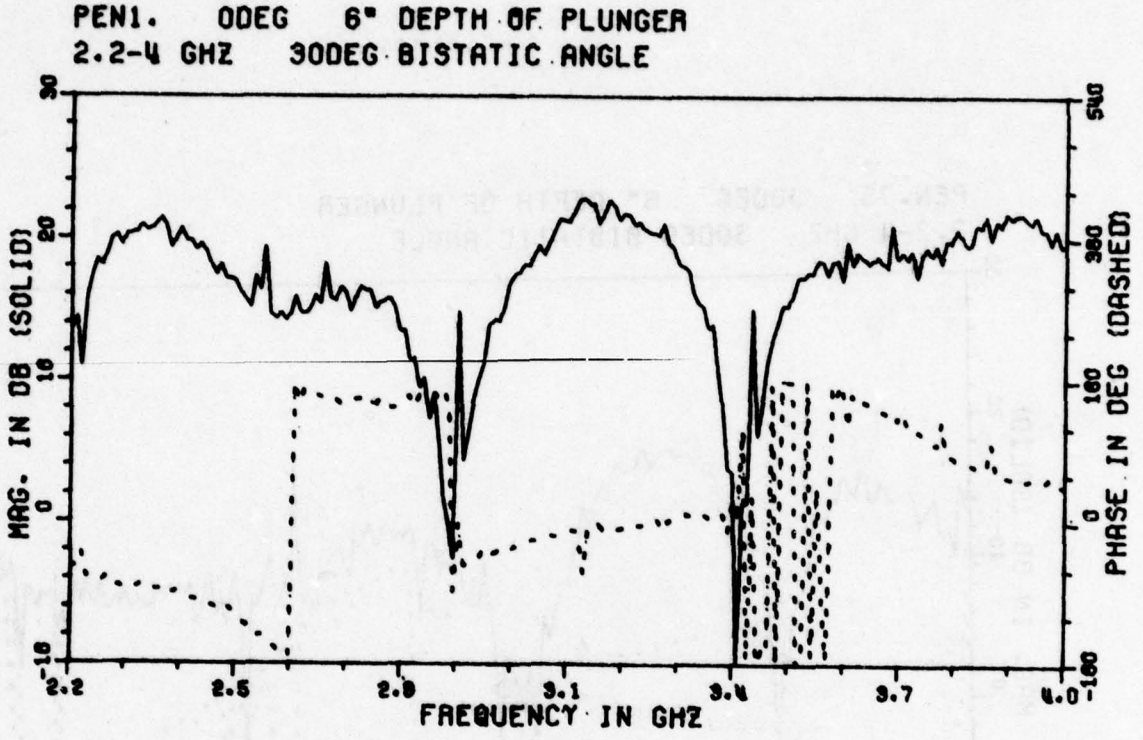


Figure 49. Measured amplitude and phase of scattered field, PEN 1.0 model, 2.2-4.0 GHz.

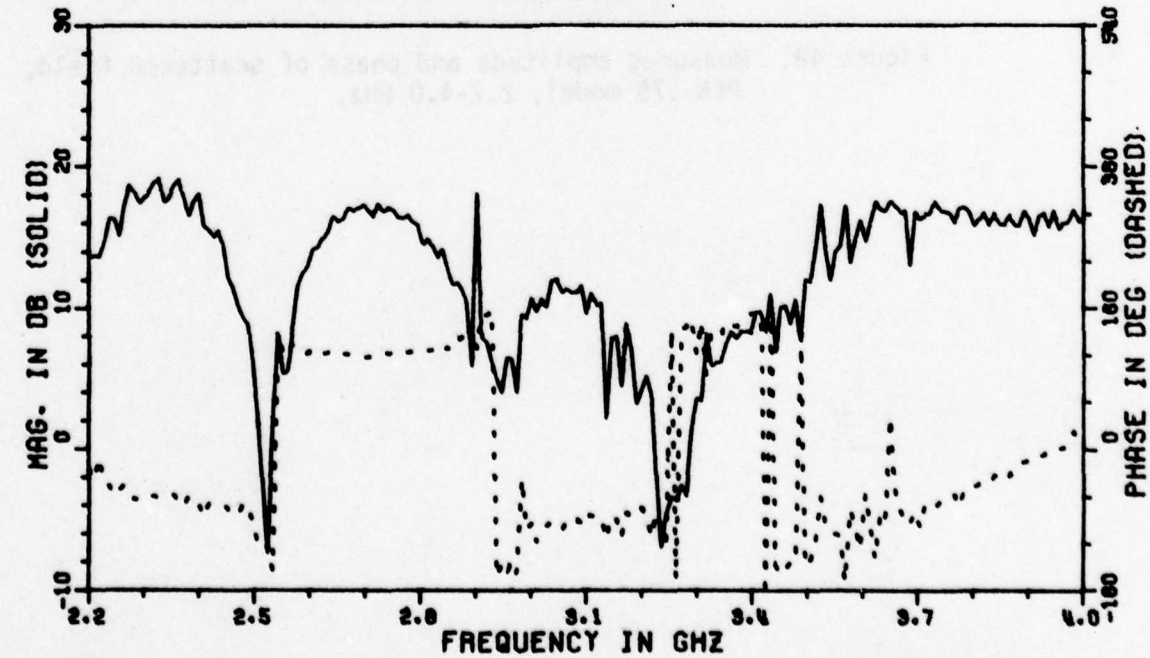


Figure 50. Measured amplitude and phase of scattered field, PEN 1.0 model, 2.2-4.0 GHz.

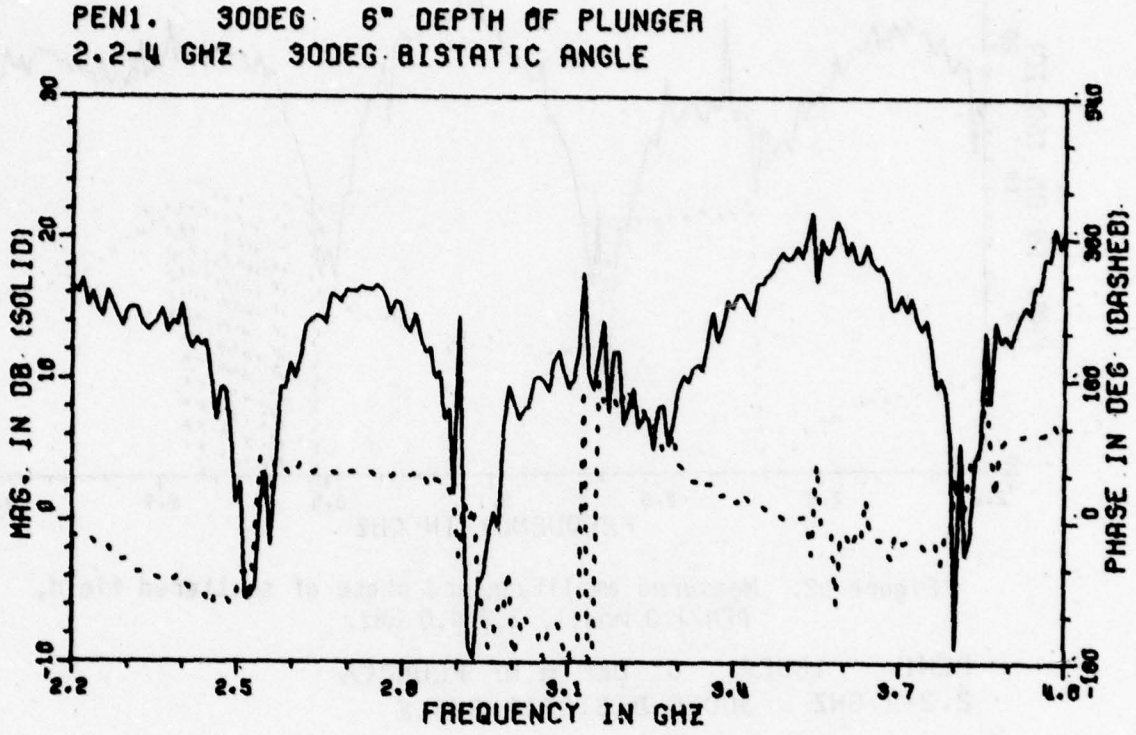


Figure 51. Measured amplitude and phase of scattered field, PEN 1.0 model, 2.2-4.0 GHz.

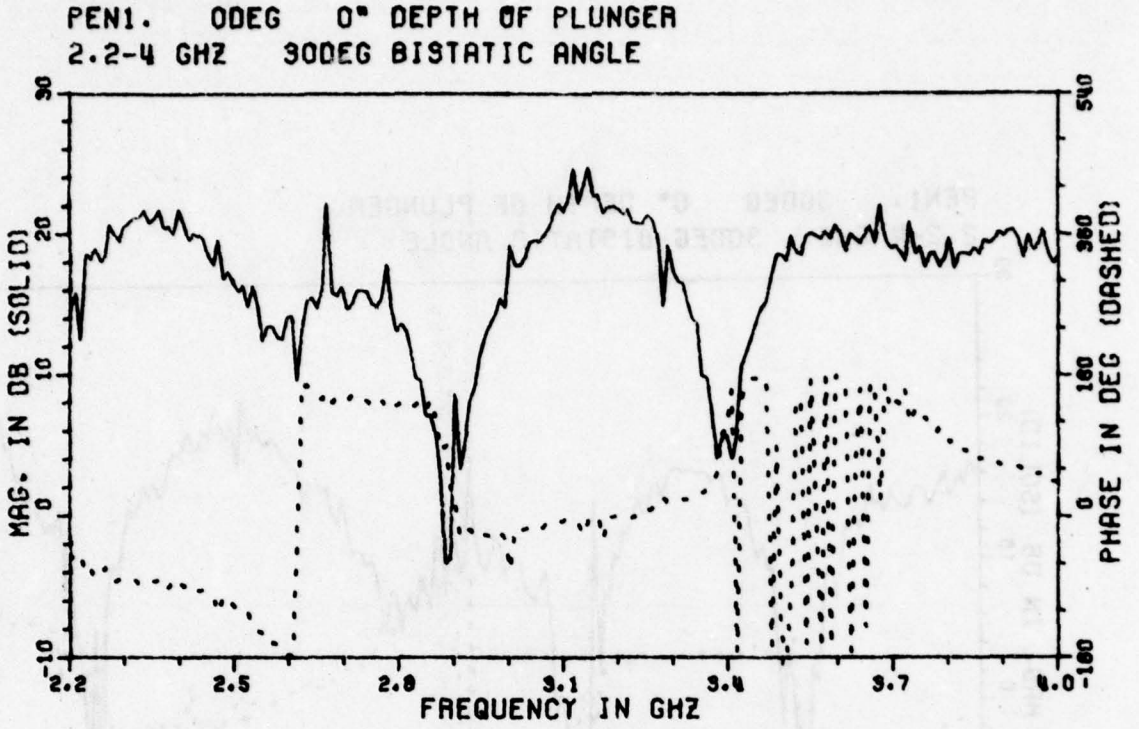


Figure 52. Measured amplitude and phase of scattered field, PEN 1.0 model, 2.2-4.0 GHz.

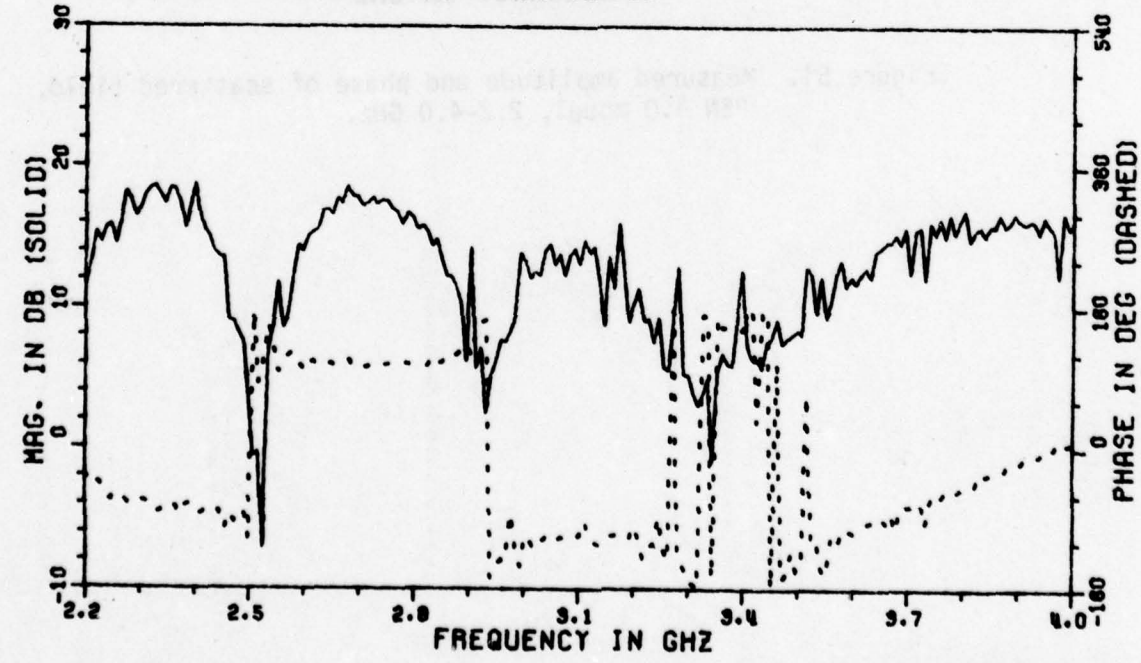


Figure 53. Measured amplitude and phase of scattered field, PEN 1.0 model, 2.2-4.0 GHz.

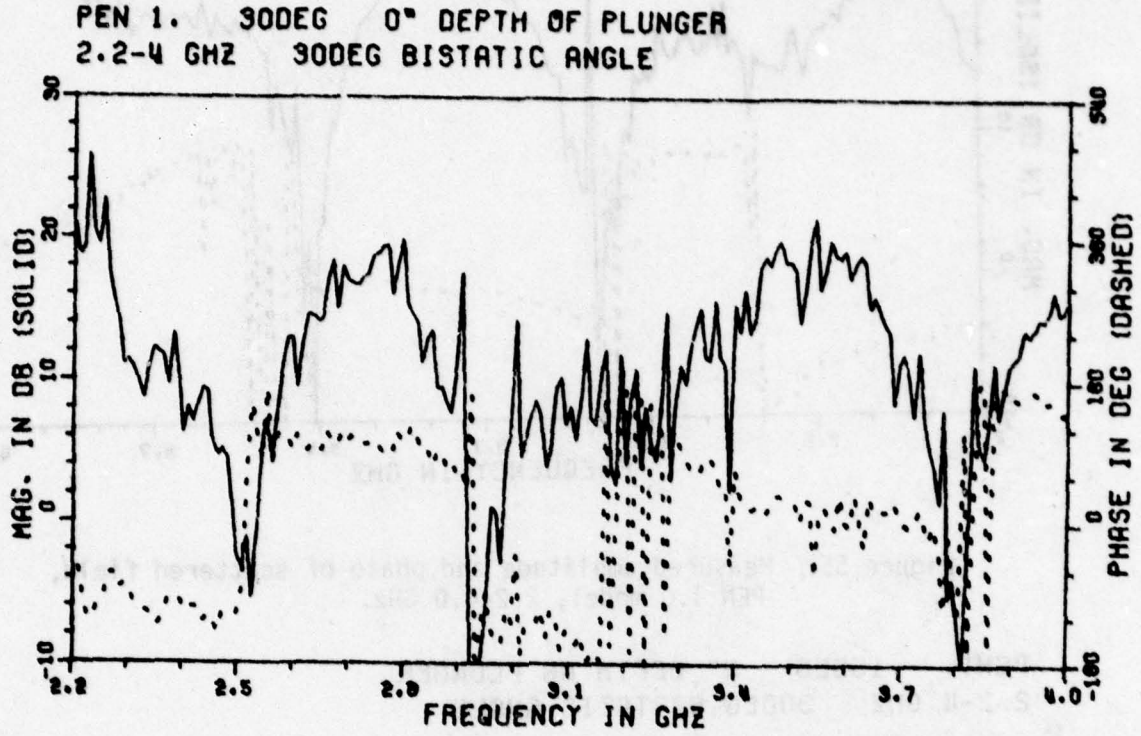


Figure 54. Measured amplitude and phase of scattered field, PEN 1.0 model, 2.2-4.0 GHz.

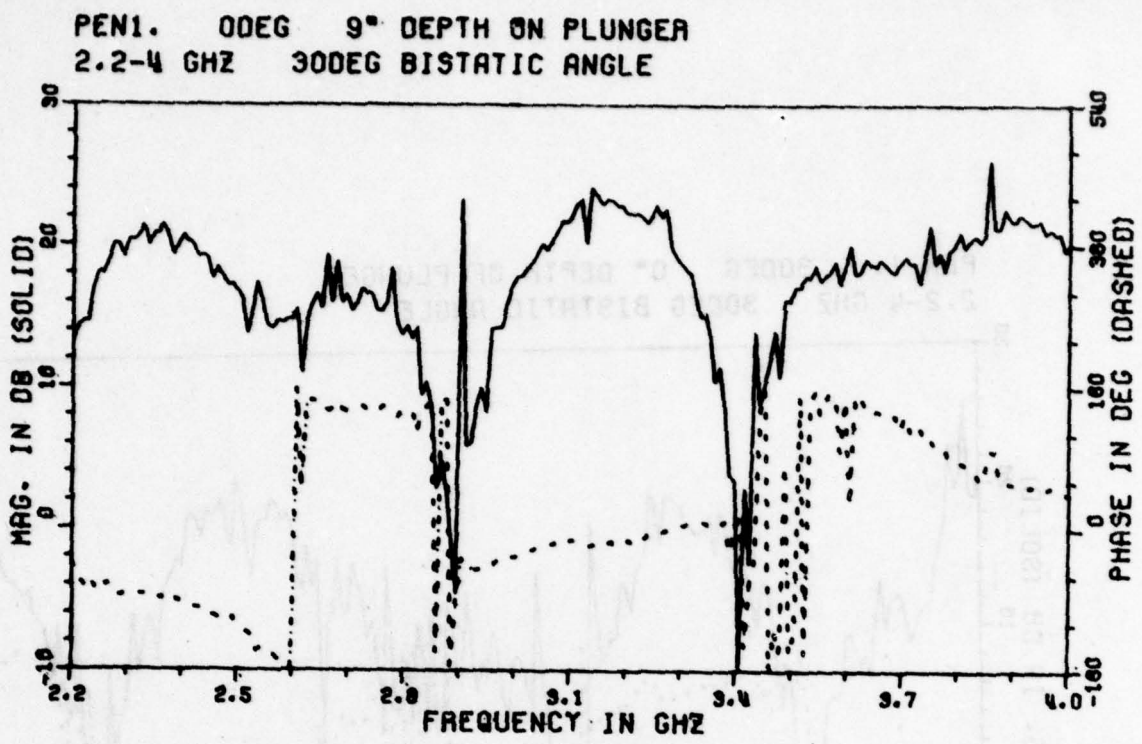


Figure 55. Measured amplitude and phase of scattered field, PEN 1.0 model, 2.2-4.0 GHz.

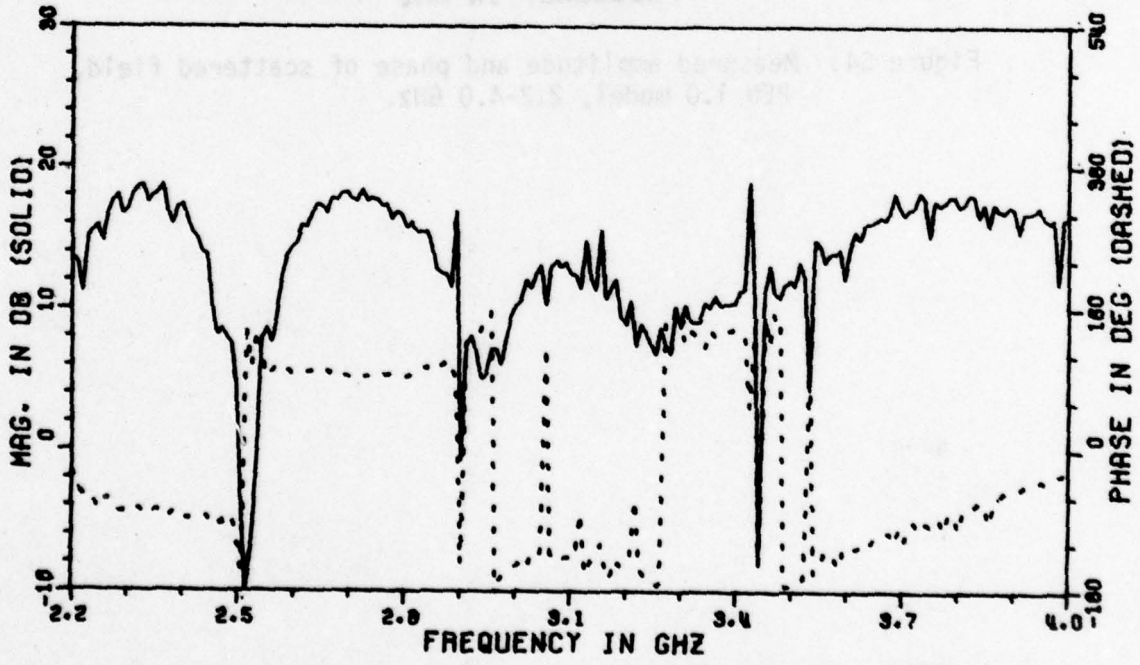


Figure 56. Measured amplitude and phase of scattered field, PEN 1.0 model, 2.2-4.0 GHz.

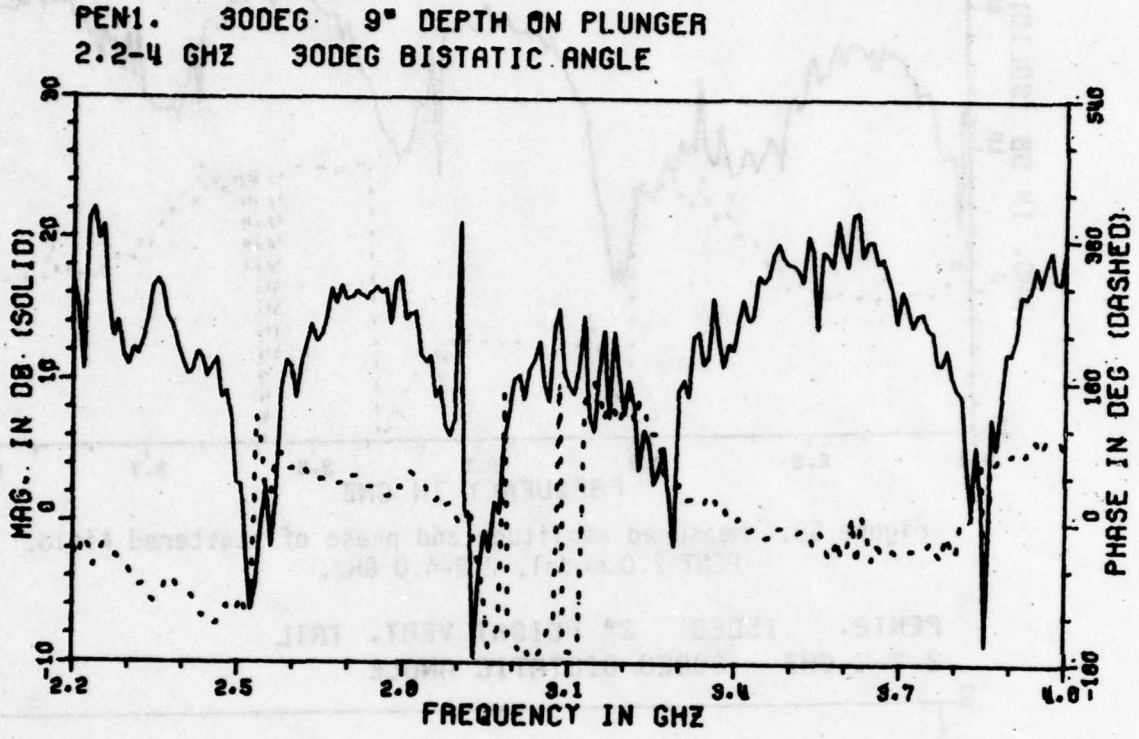


Figure 57. Measured amplitude and phase of scattered field, PEN 1.0 model, 2.2-4.0 GHz.

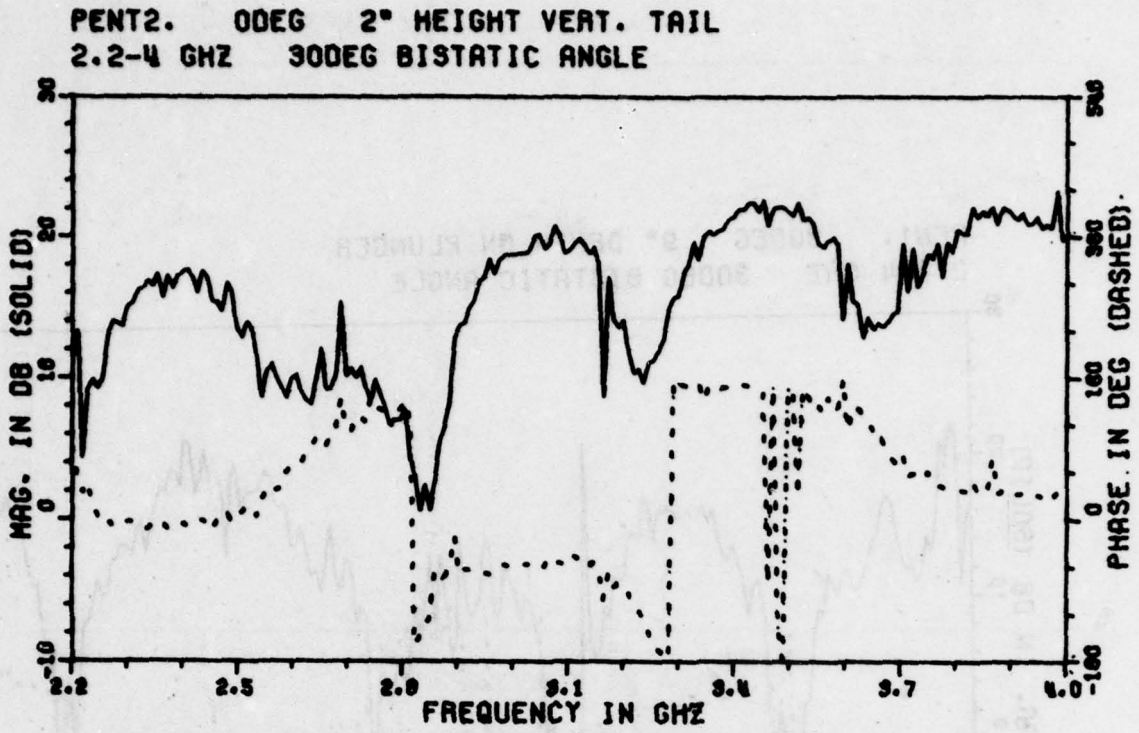


Figure 58. Measured amplitude and phase of scattered field, PENT 2.0 model, 2.2-4.0 GHz.

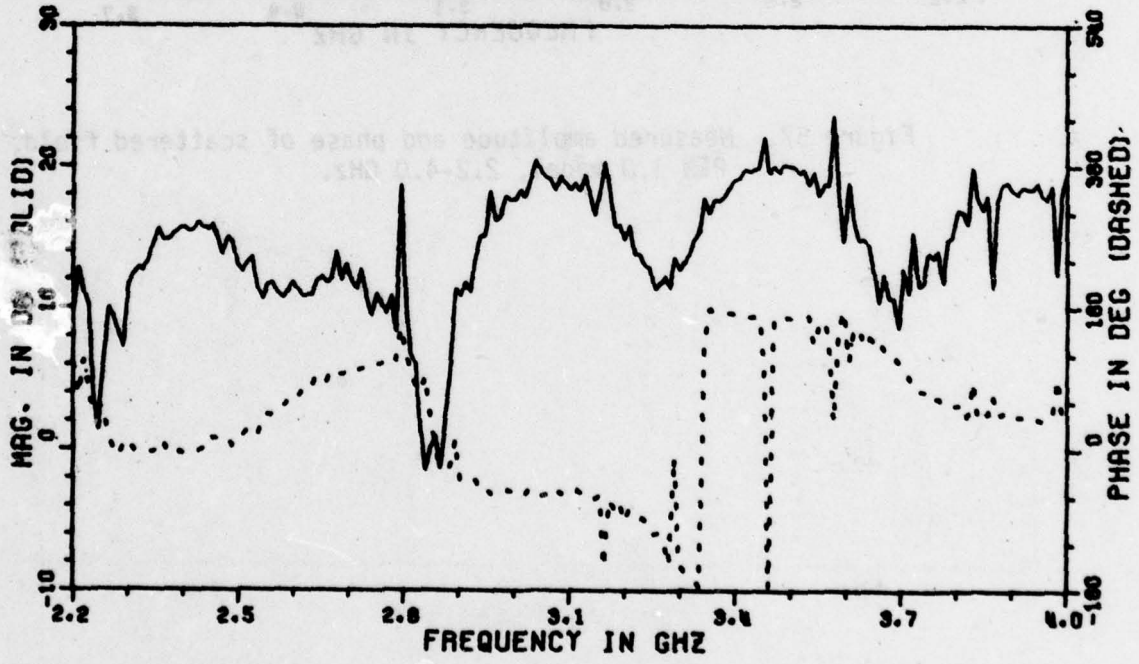


Figure 59. Measured amplitude and phase of scattered field, PENT 2.0 model, 2.2-4.0 GHz.

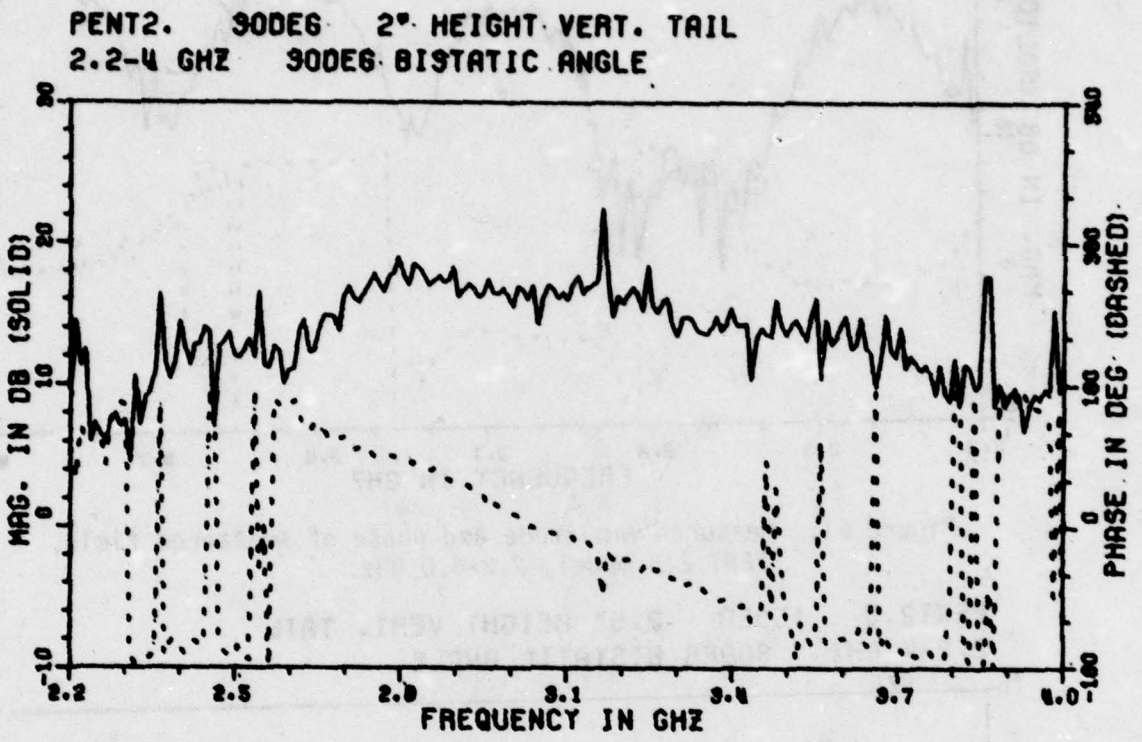


Figure 60. Measured amplitude and phase of scattered field, PENT 2.0 model, 2.2-4.0 GHz.

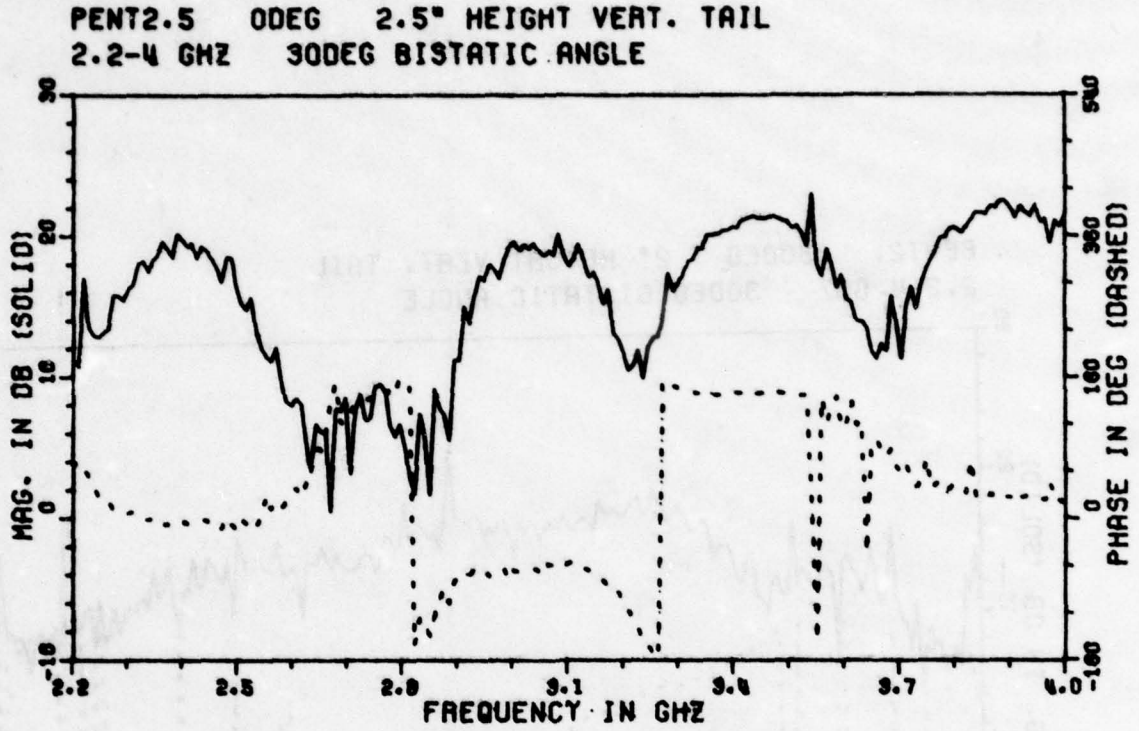


Figure 61. Measured amplitude and phase of scattered field, PENT 2.5 model, 2.2-4.0 GHz.

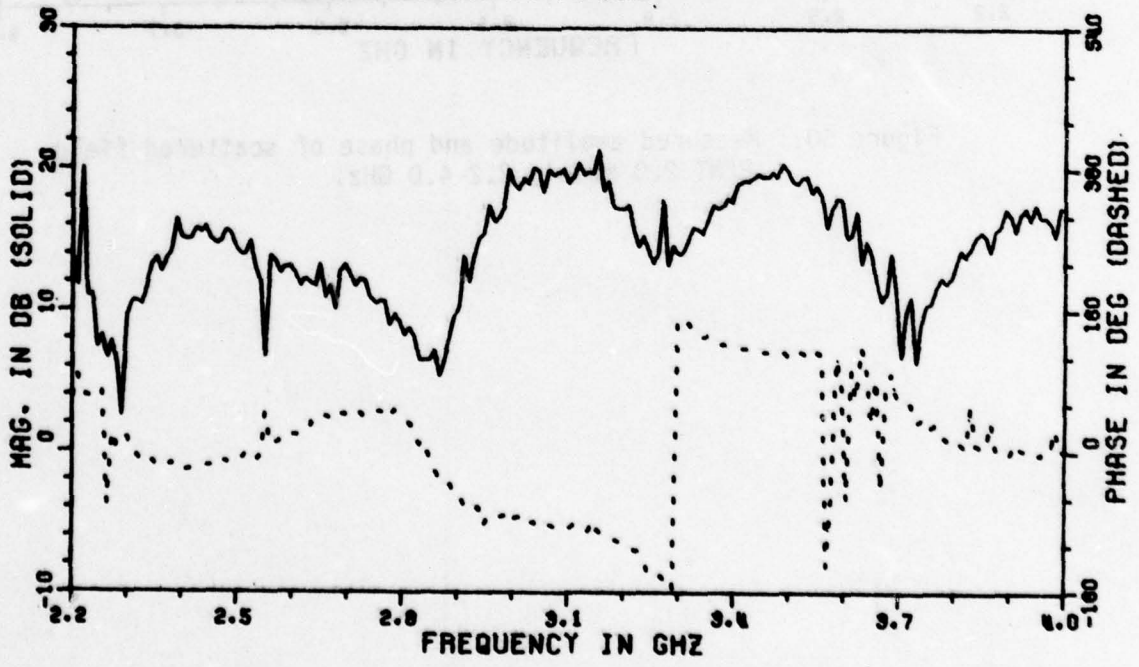


Figure 62. Measured amplitude and phase of scattered field, PENT 2.5 model, 2.2-4.0 GHz.

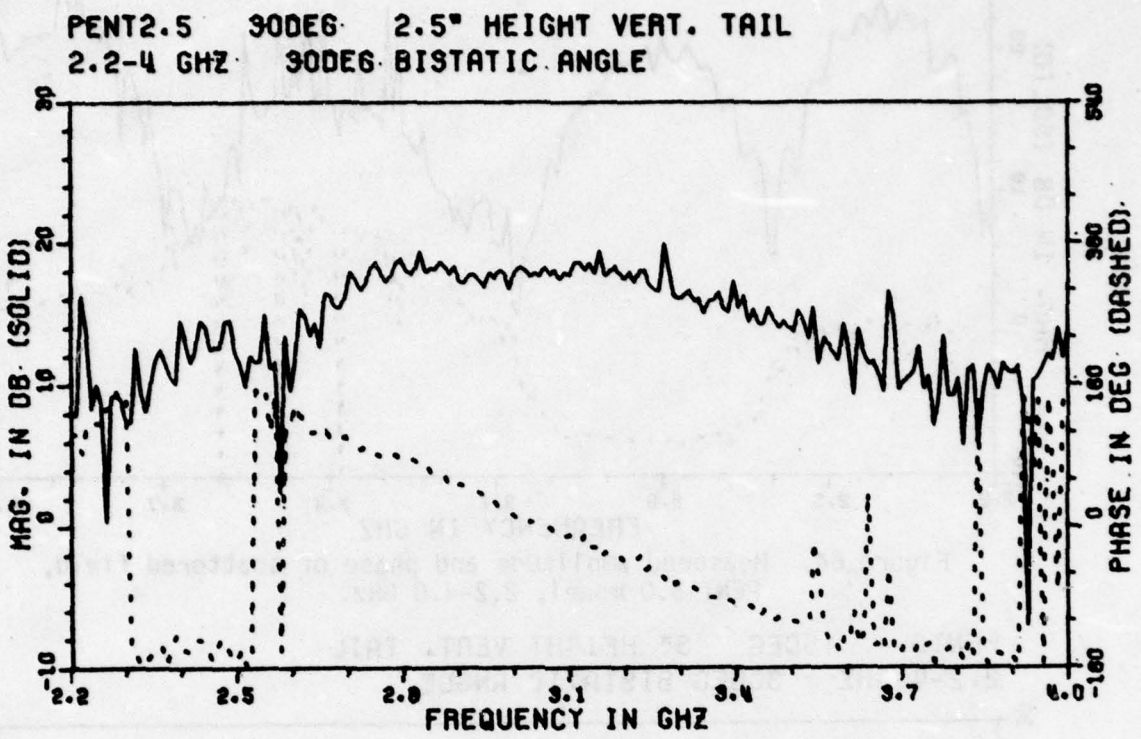


Figure 63. Measured amplitude and phase of scattered field, PENT 2.5 model, 2.2-4.0 GHz.

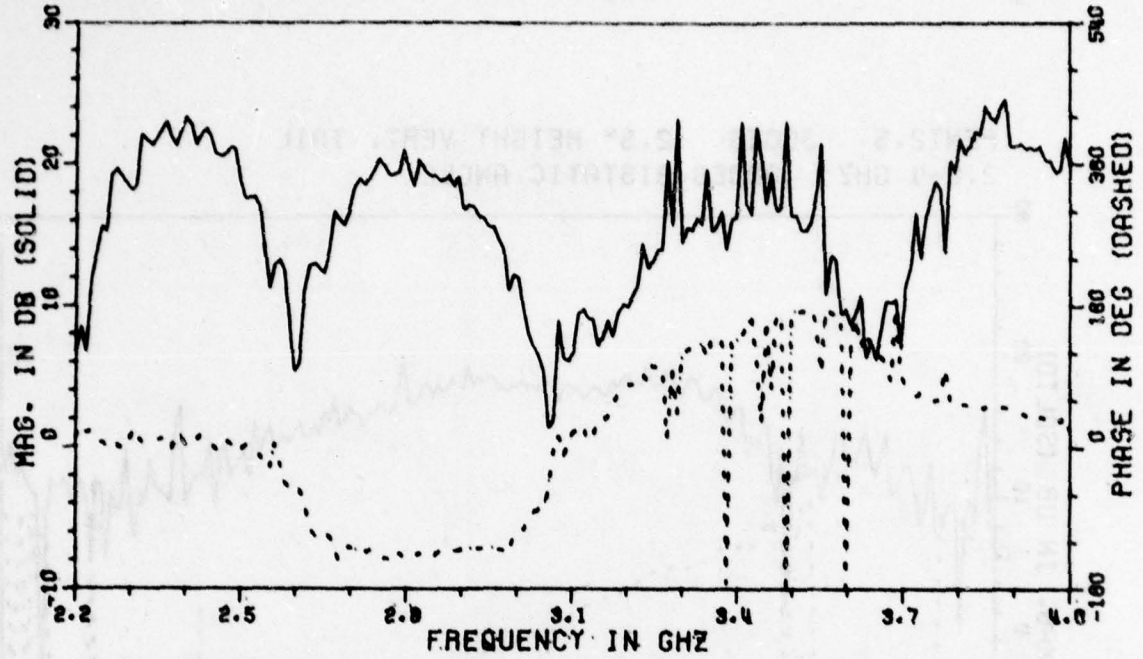


Figure 64. Measured amplitude and phase of scattered field, PENT 3.0 model, 2.2-4.0 GHz.

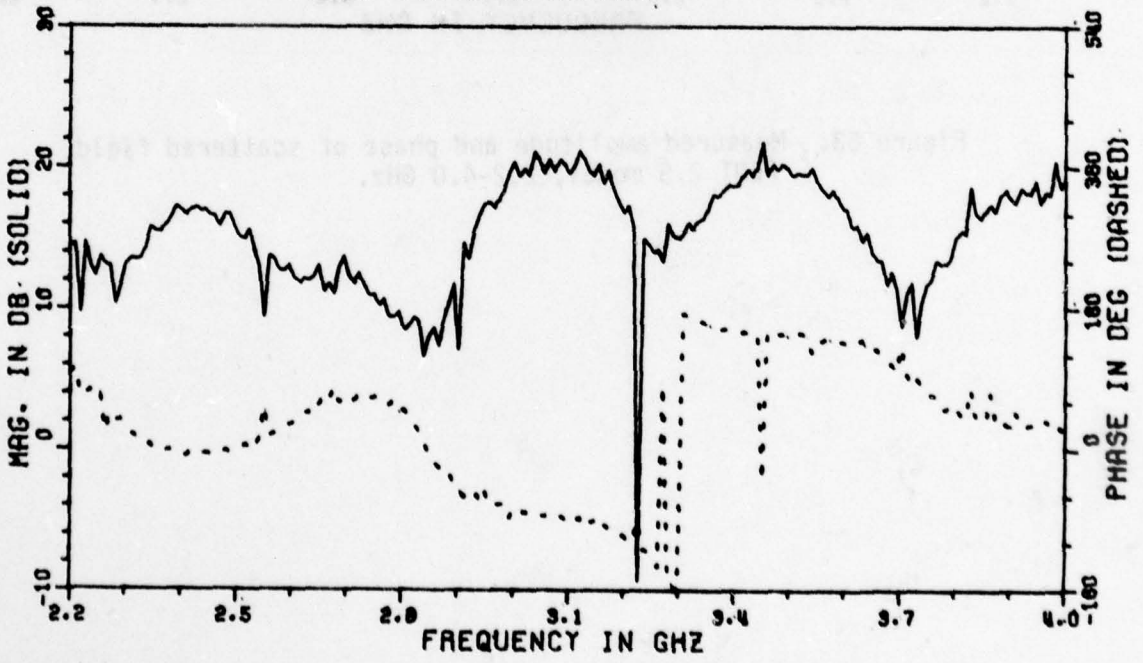


Figure 65. Measured amplitude and phase of scattered field, PENT 3.0 model, 2.2-4.0 GHz.

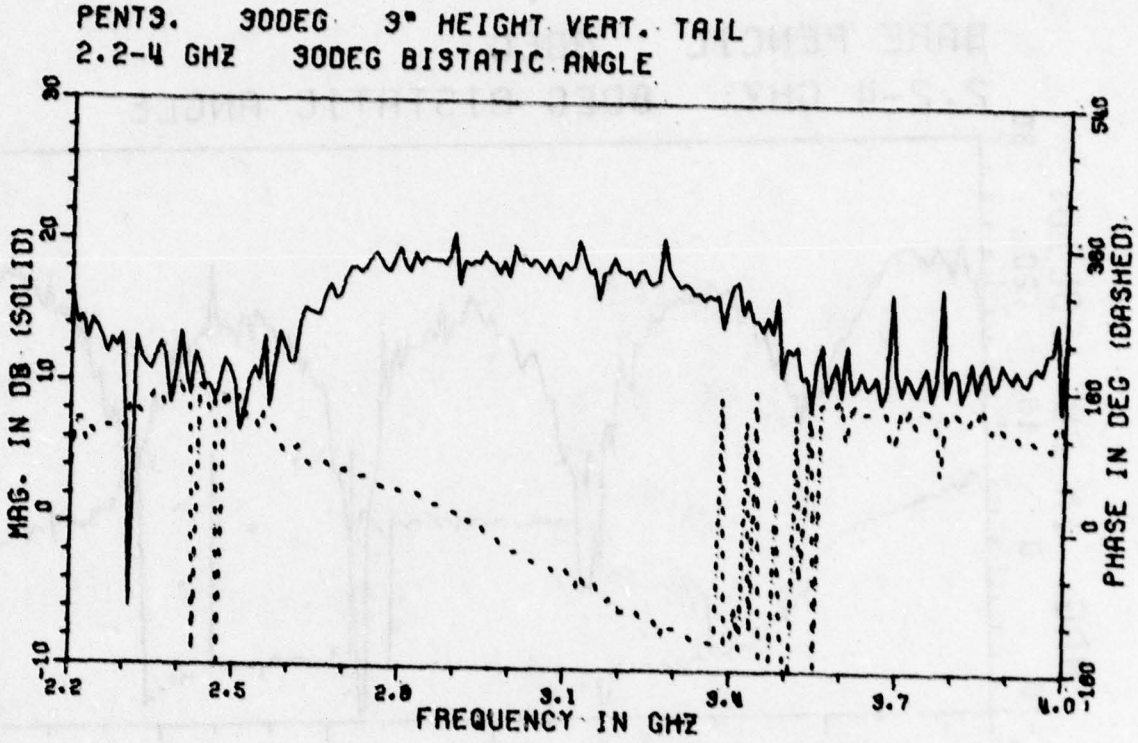


Figure 66. Measured amplitude and phase of scattered field, PENT 3.0 model, 2.2-4.0 GHz.

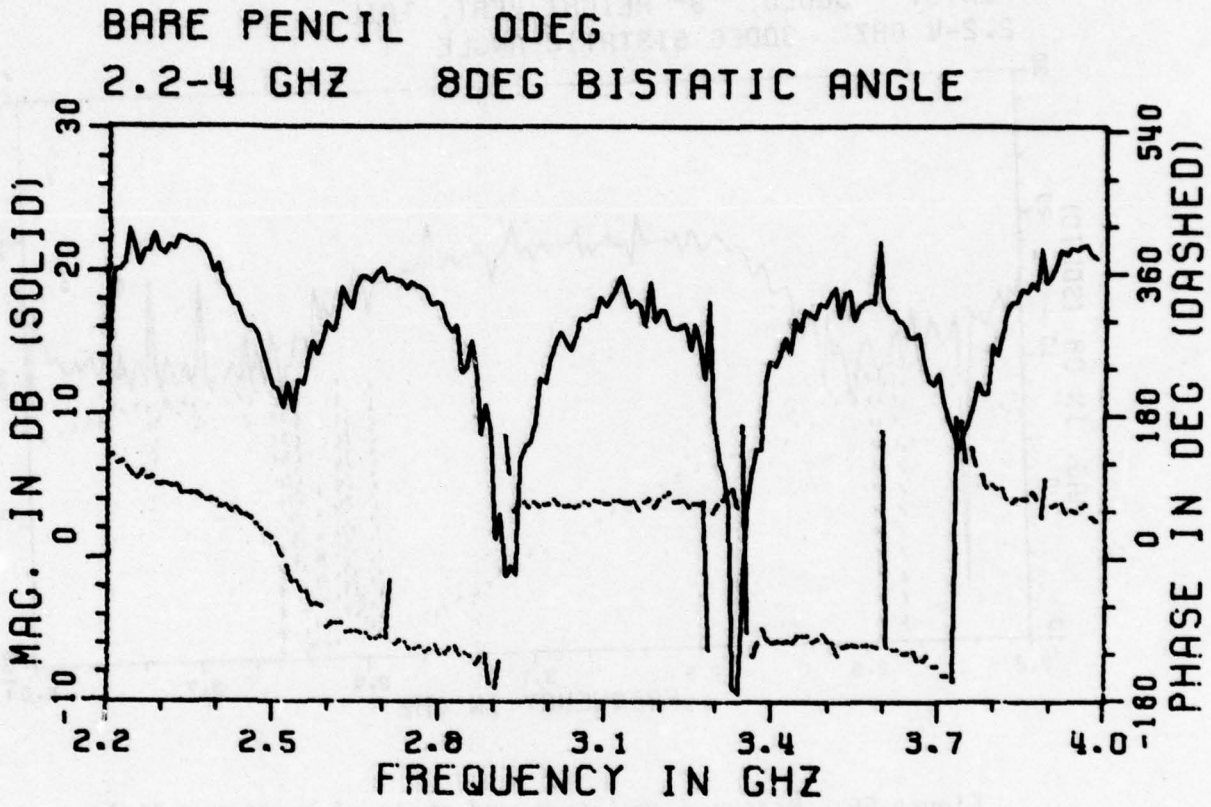


Figure 67. Measured amplitude and phase of scattered field, Bare PEN model, 2.2-4.0 GHz.

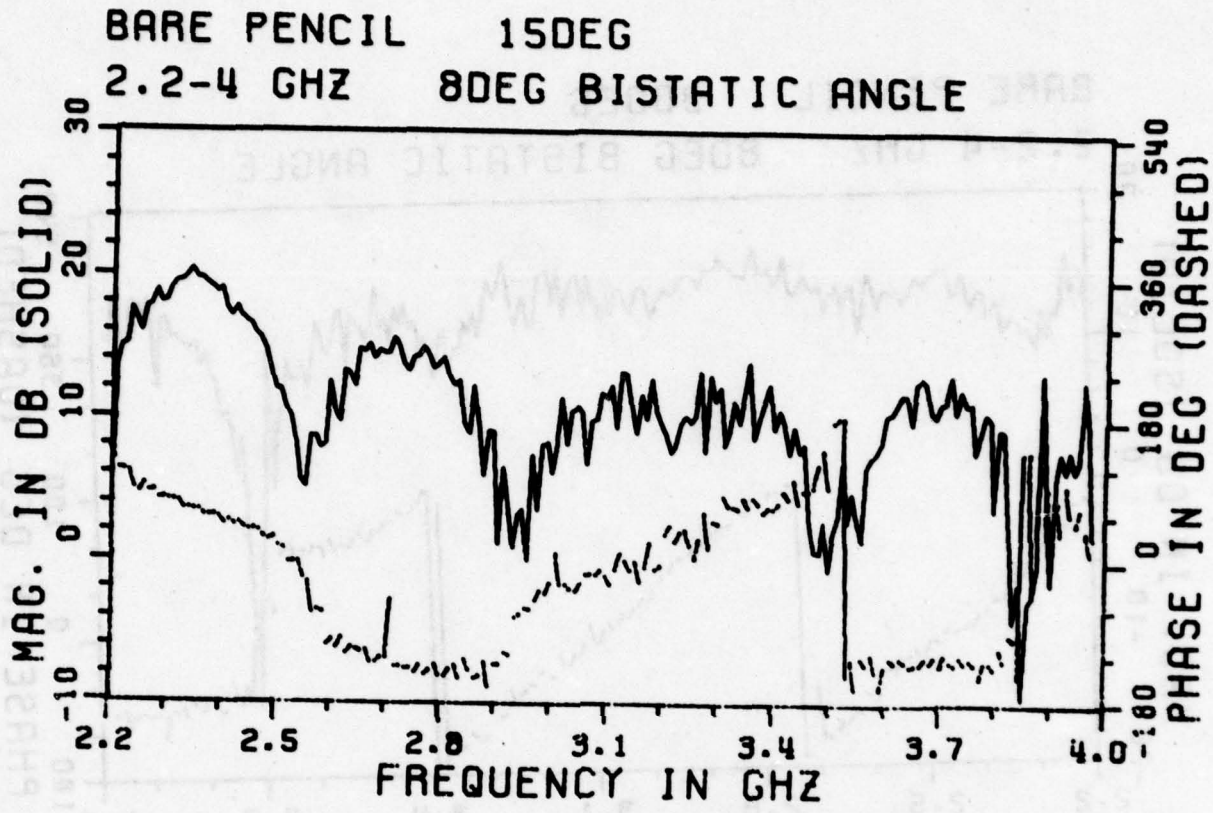


Figure 68. Measured amplitude and phase of scattered field, Bare PEN model, 2.2-4.0 GHz.

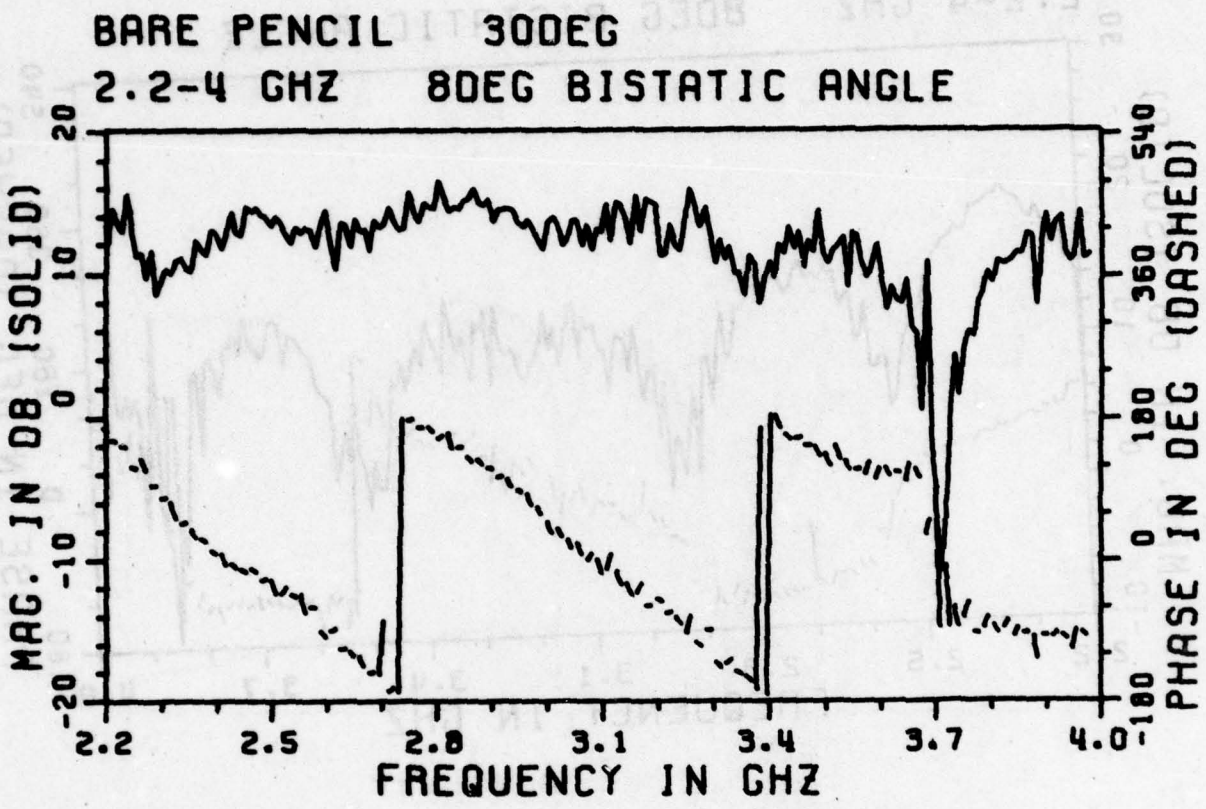


Figure 69. Measured amplitude and phase of scattered field, Bare PEN model, 2.2-4.0 GHz.

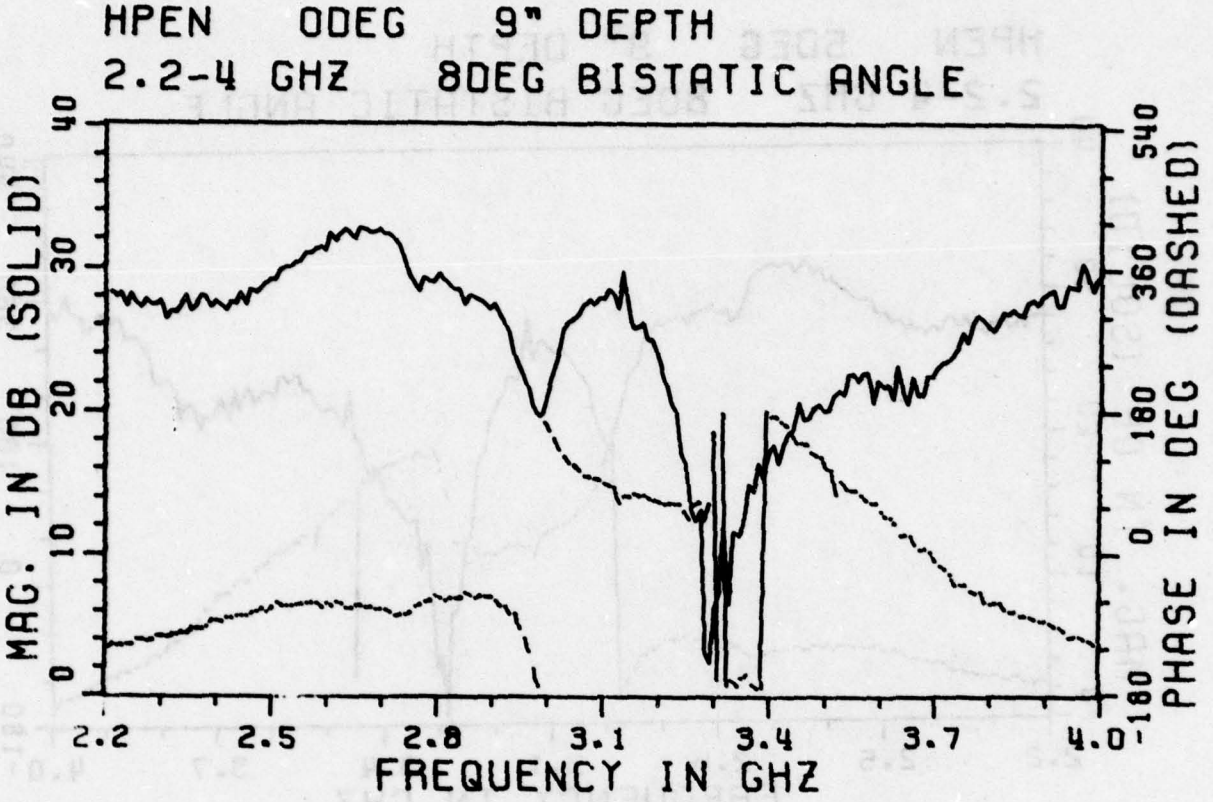


Figure 70. Measured amplitude and phase of scattered field, HPEN model, 2.2-4.0 GHz.

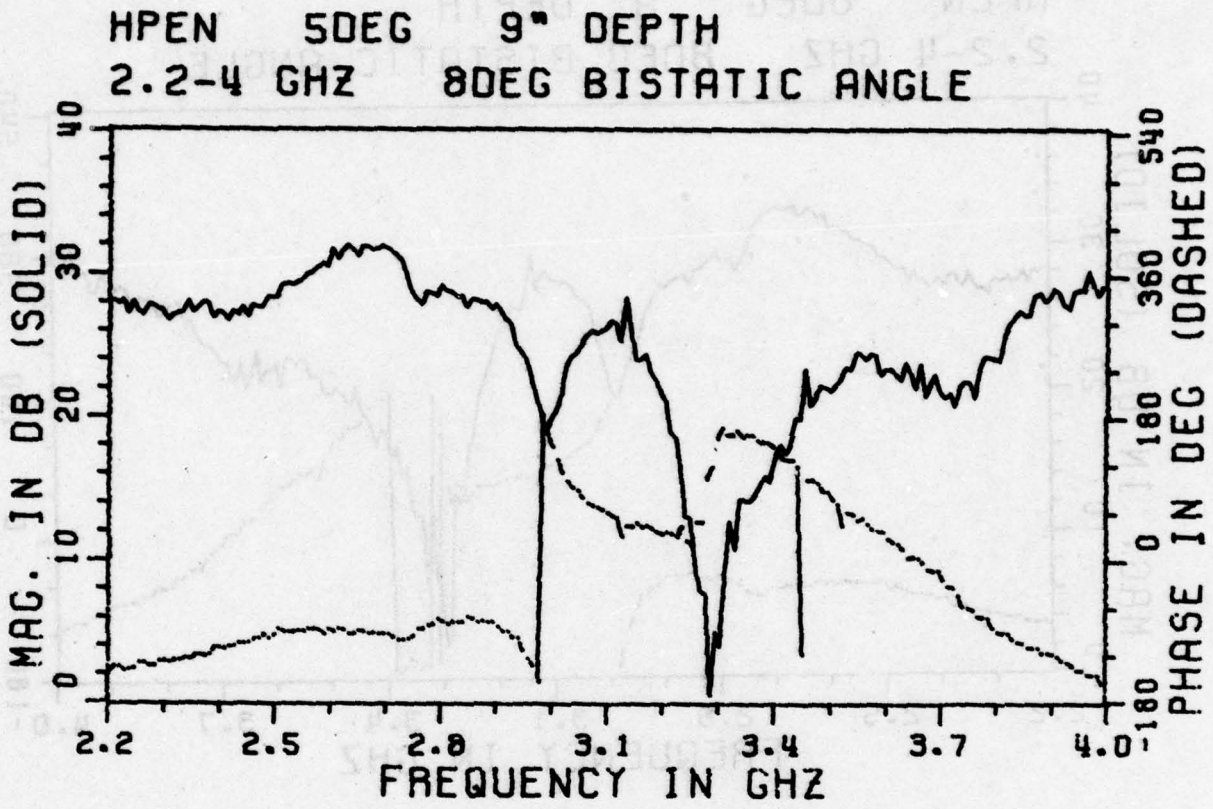


Figure 71. Measured amplitude and phase of scattered field, HPEN model, 2.2-4.0 GHz.

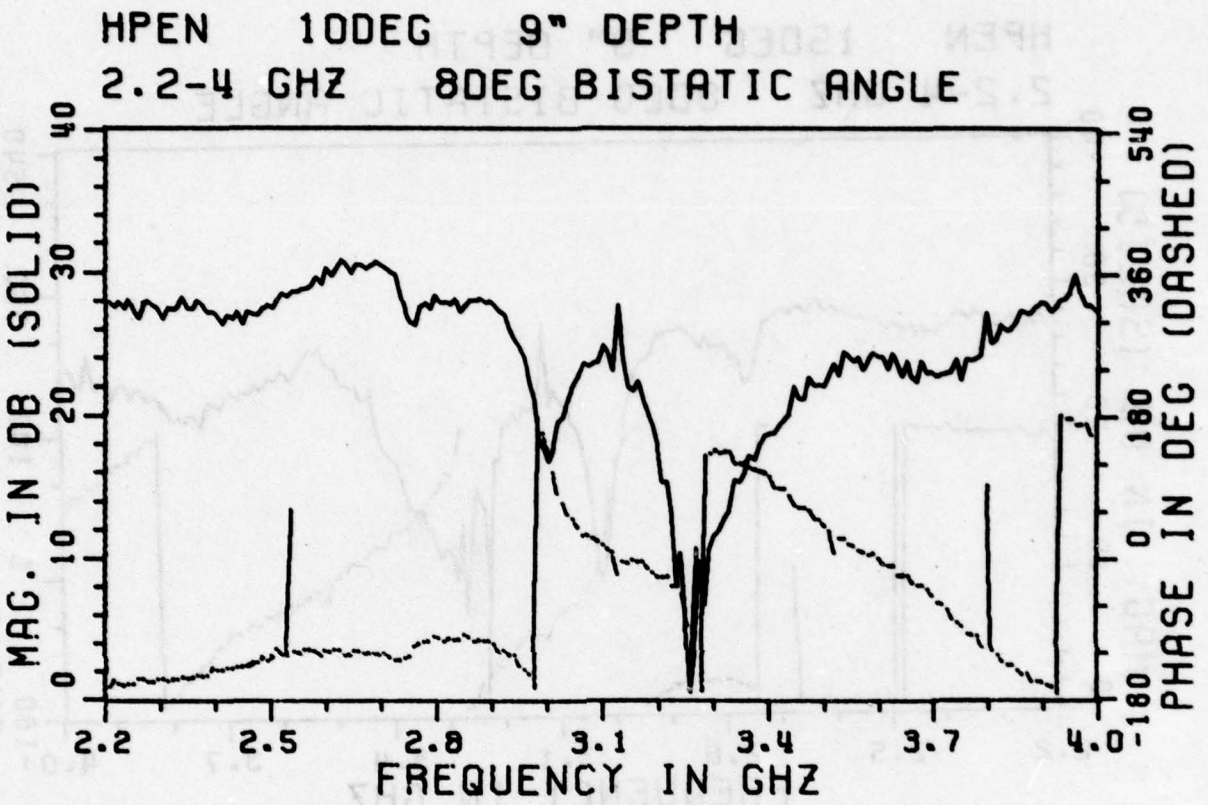


Figure 72. Measured amplitude and phase of scattered field, HPEN model, 2.2-4.0 GHz.

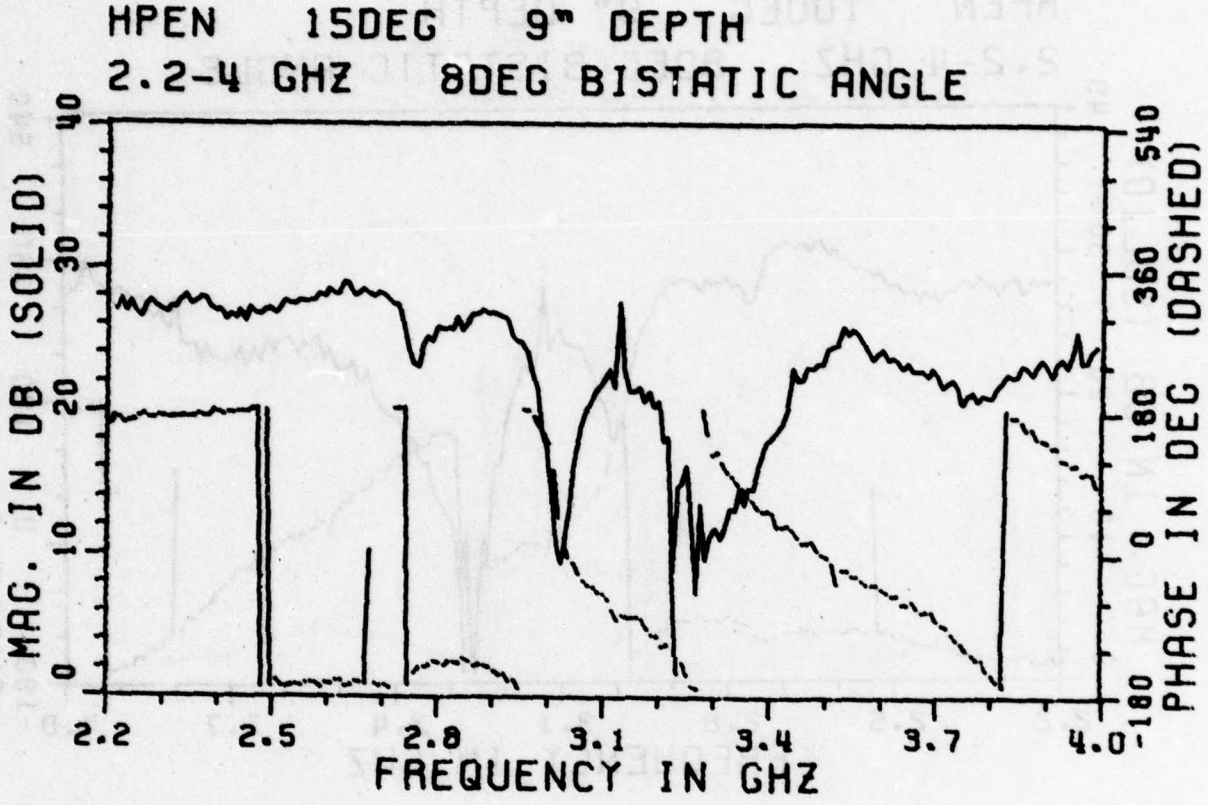


Figure 73. Measured amplitude and phase of scattered field, HPEN model, 2.2-4.0 GHz.

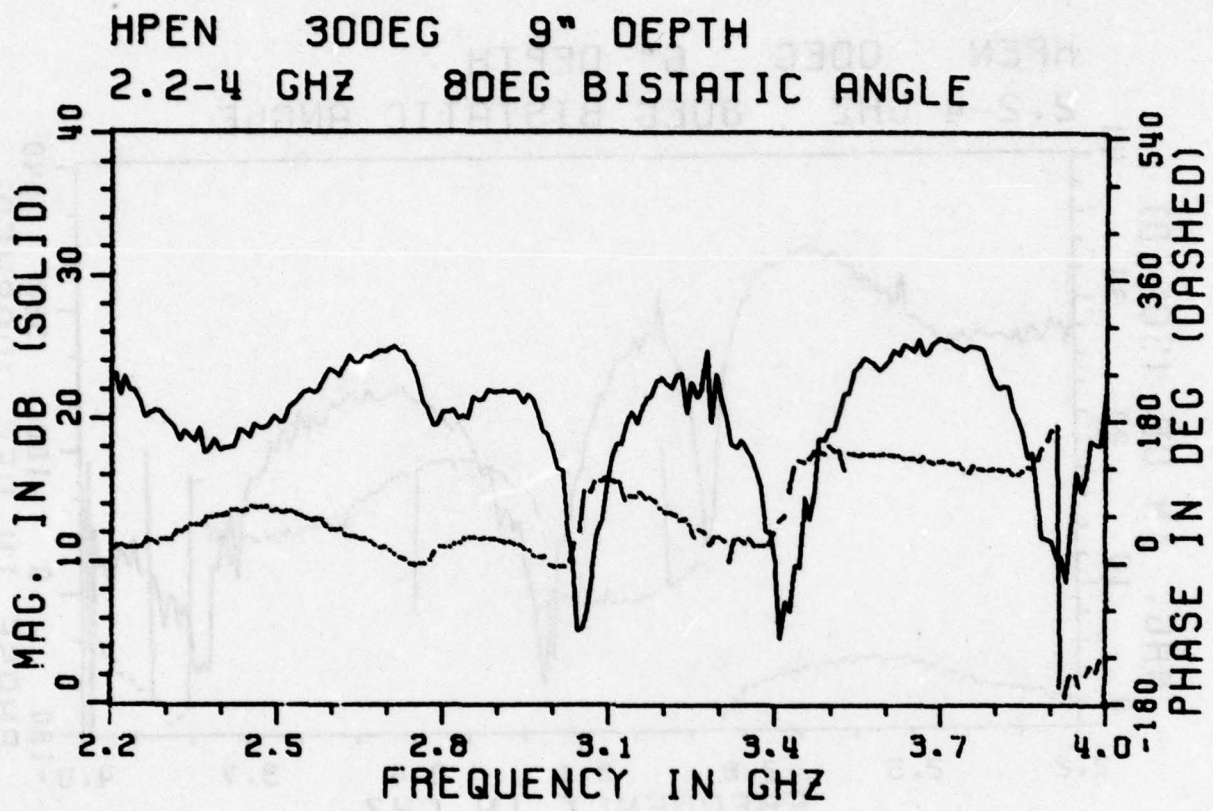


Figure 74. Measured amplitude and phase of scattered field, HPEN model, 2.2-4.0 GHz.

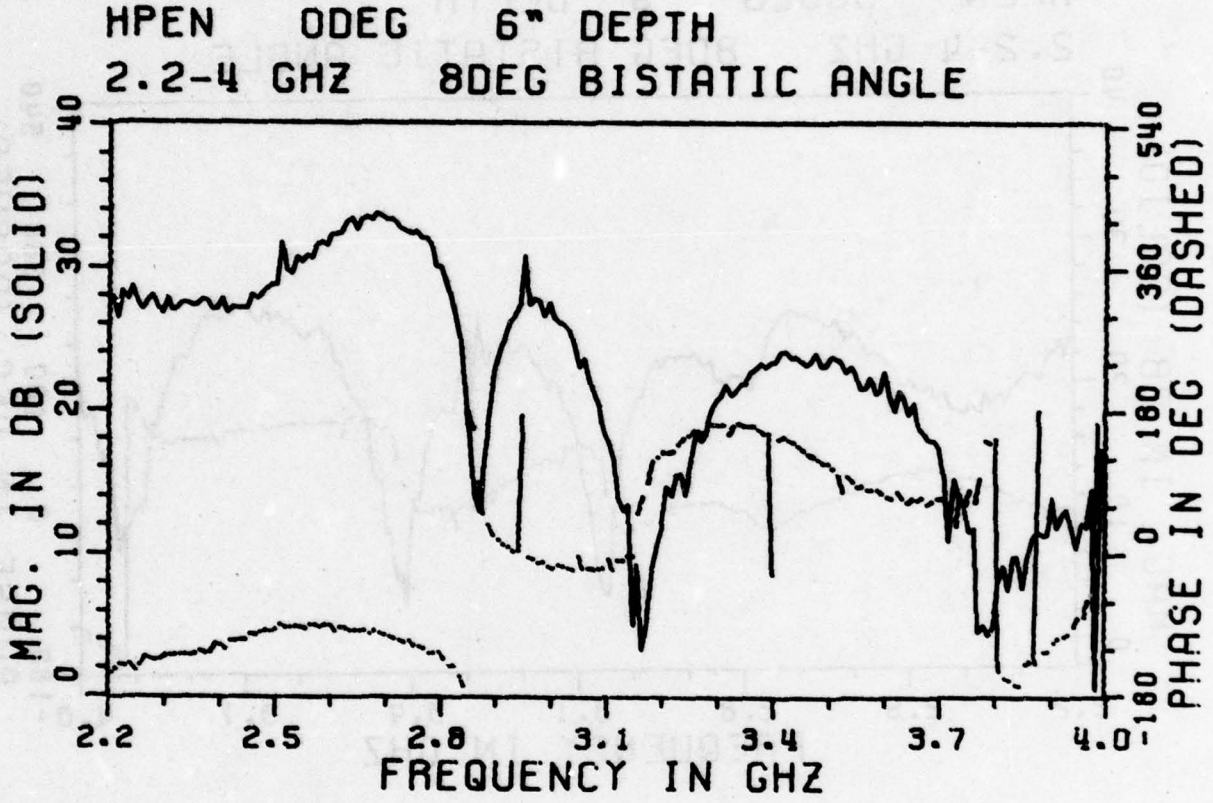


Figure 75. Measured amplitude and phase of scattered field, HPEN model, 2.2-4.0 GHz.

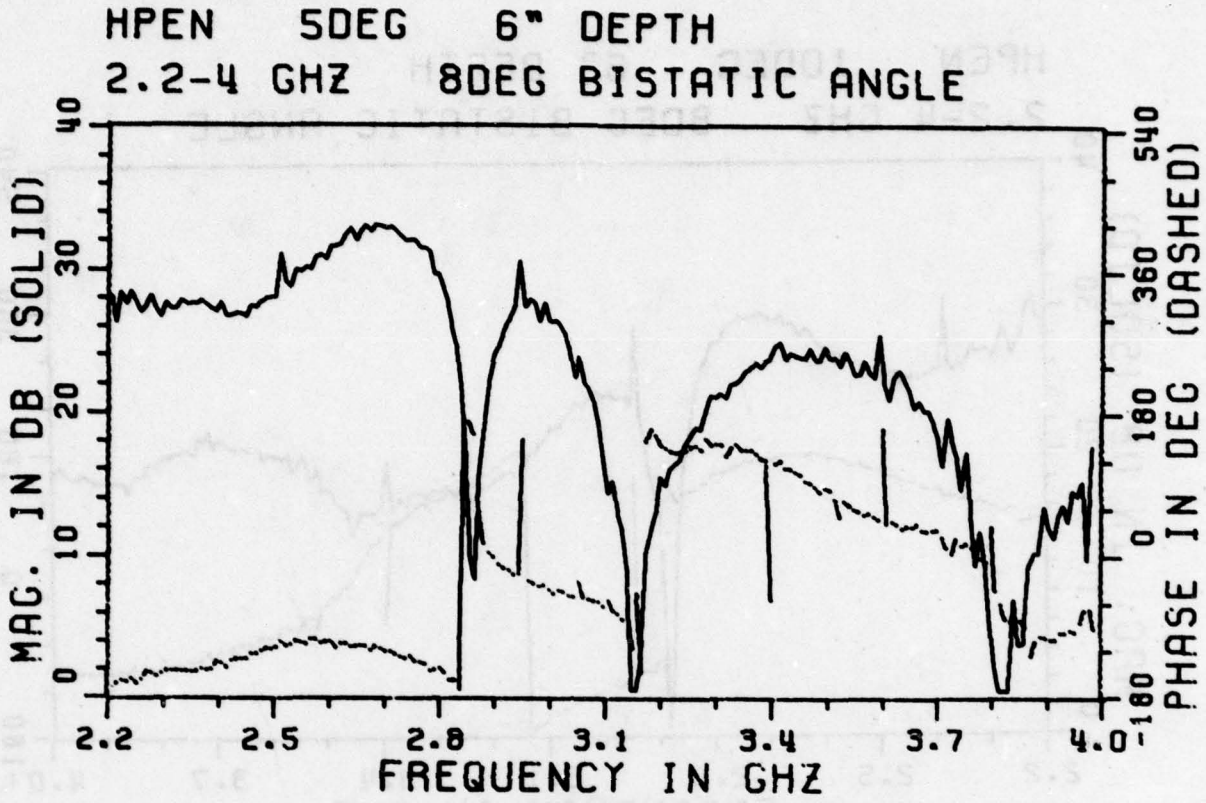


Figure 76. Measured amplitude and phase of scattered field, HPEN model, 2.2-4.0 GHz.

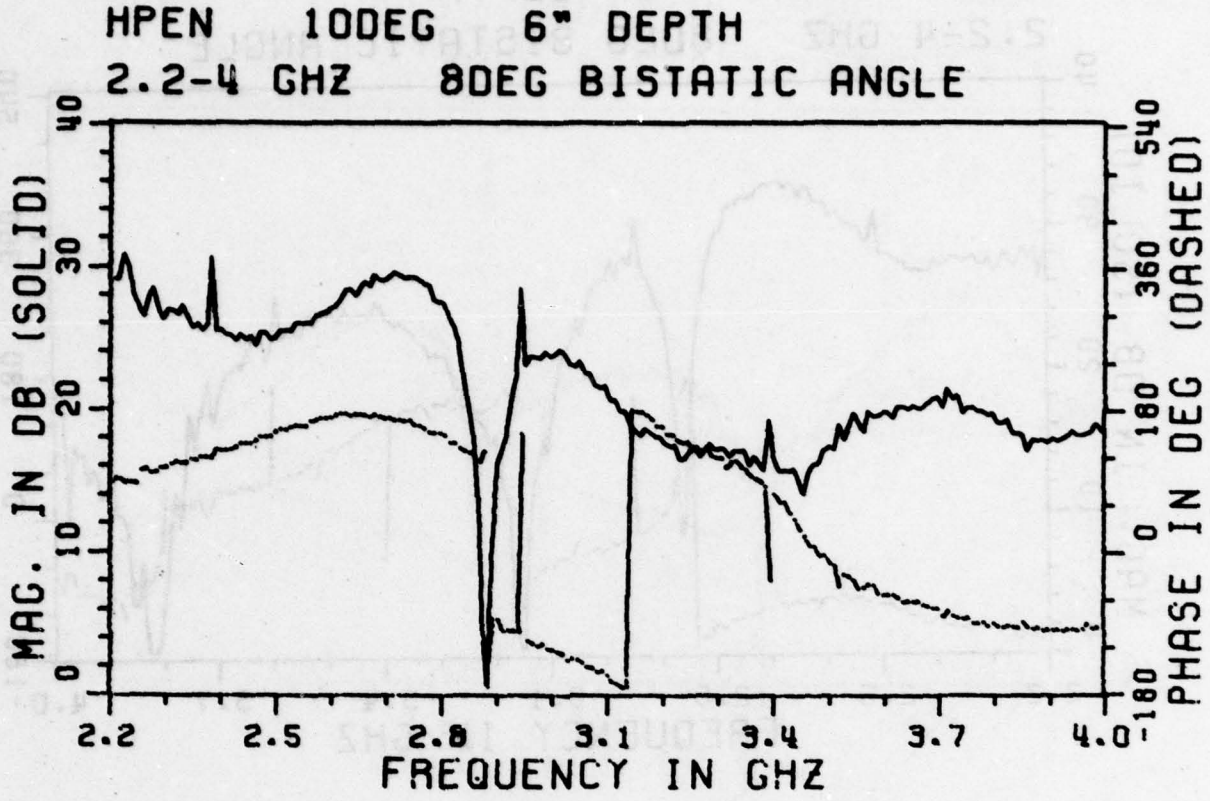


Figure 77. Measured amplitude and phase of scattered field, HPEN model, 2.2-4.0 GHz.

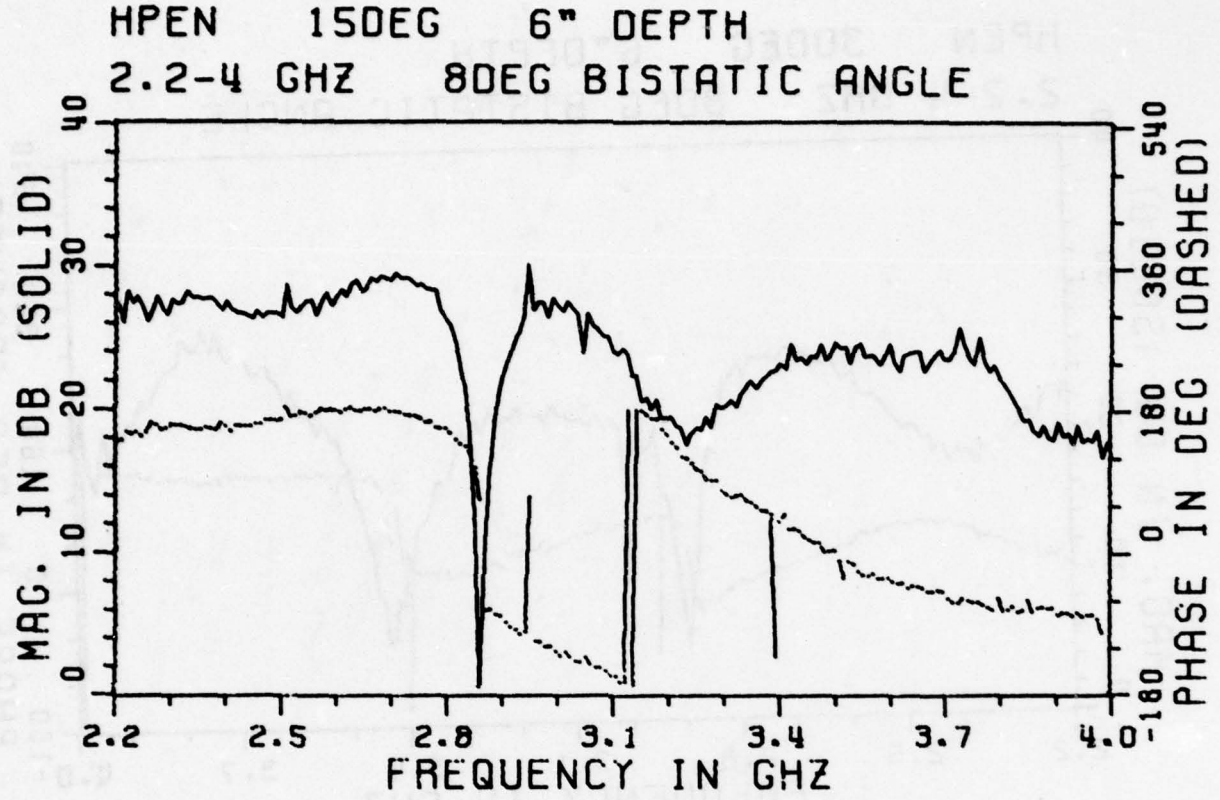


Figure 78. Measured amplitude and phase of scattered field, HPEN model, 2.2-4.0 GHz.

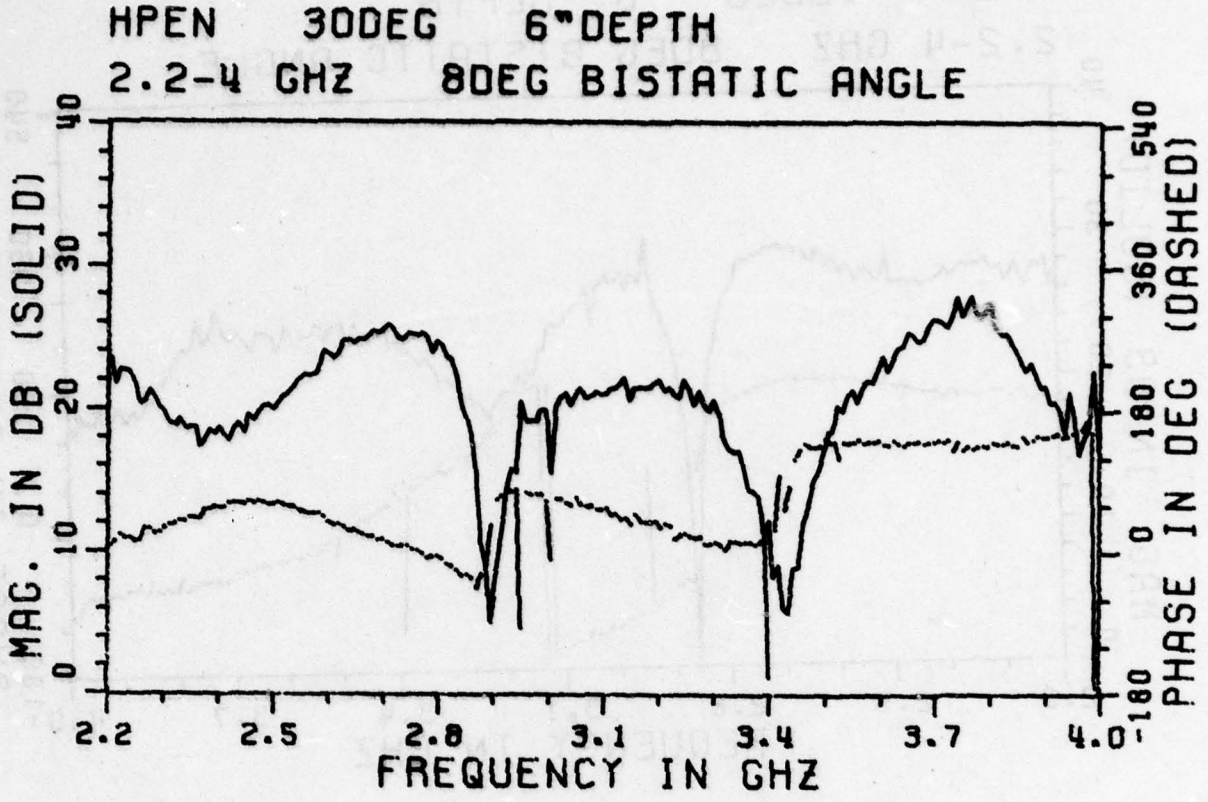


Figure 79. Measured amplitude and phase of scattered field, HPEN model, 2.2-4.0 GHz.

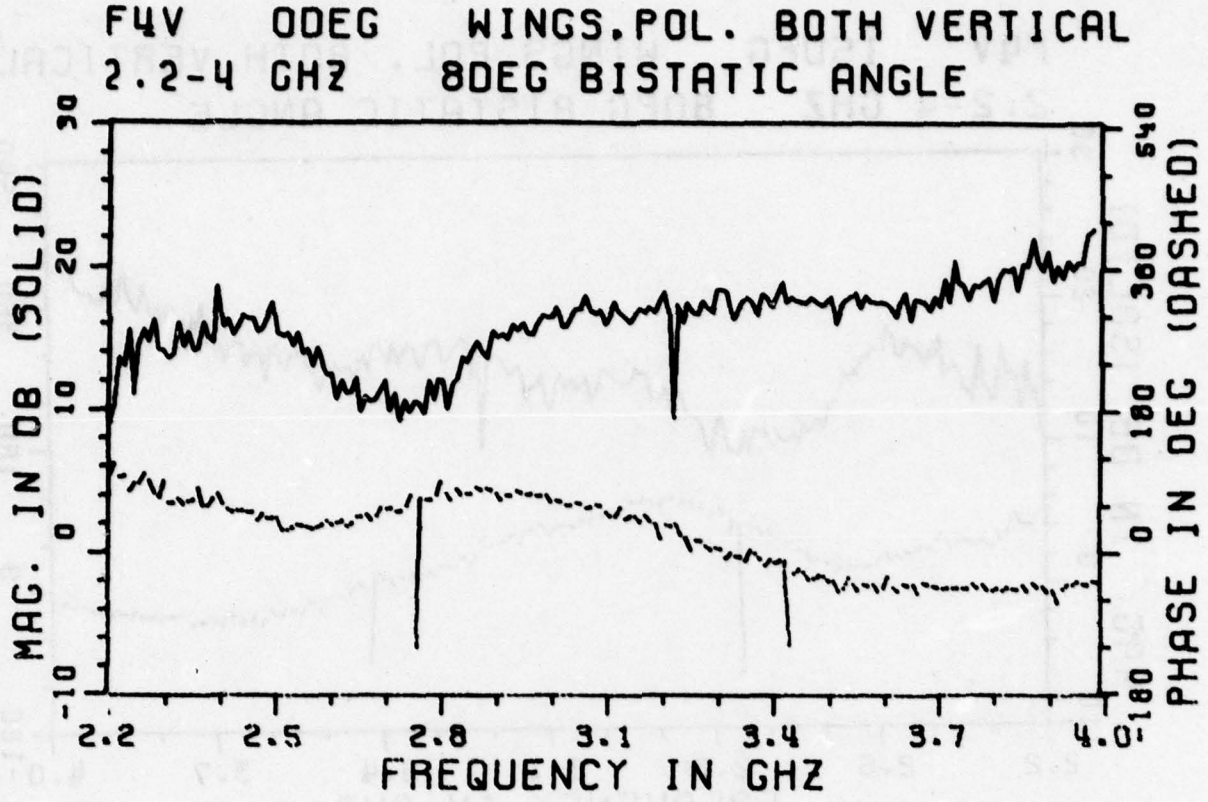


Figure 80. Measured amplitude and phase of scattered field, F4V aircraft, 2.2-4.0 GHz.

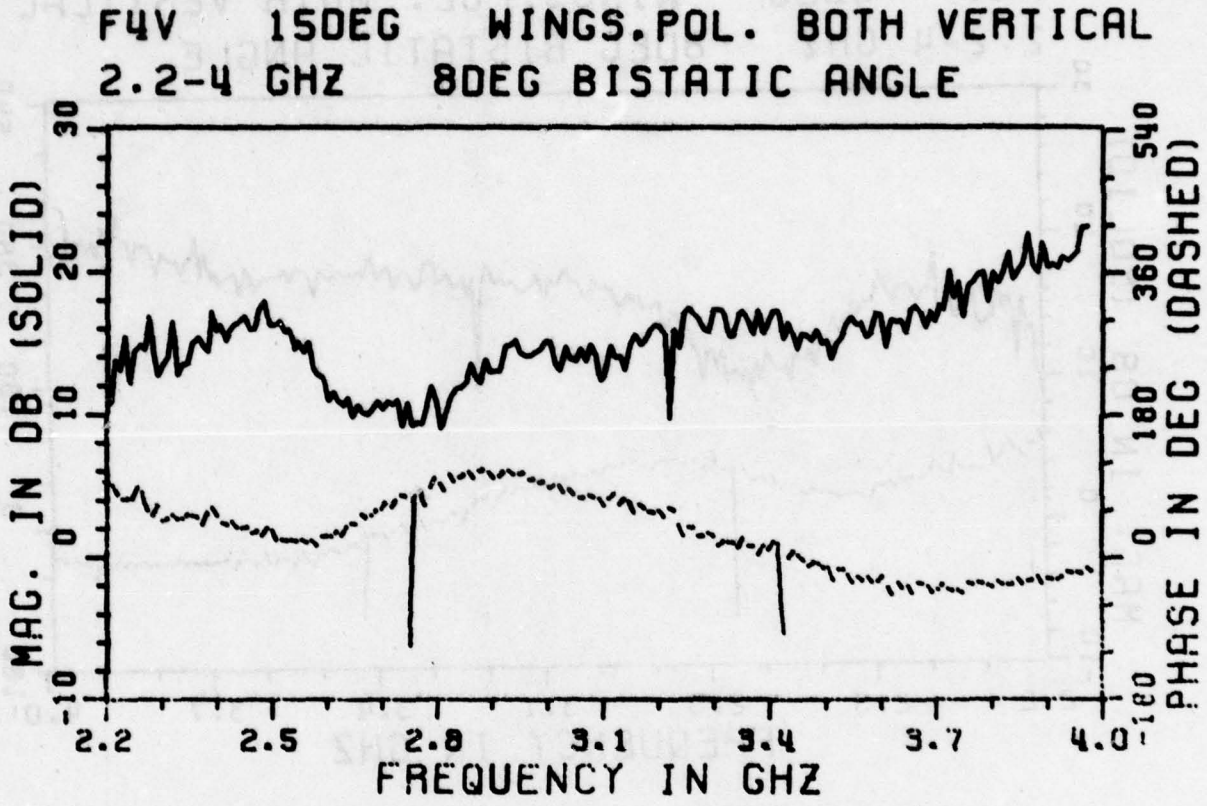


Figure 81. Measured amplitude and phase of scattered field, F4V aircraft, 2.2-4.0 GHz.

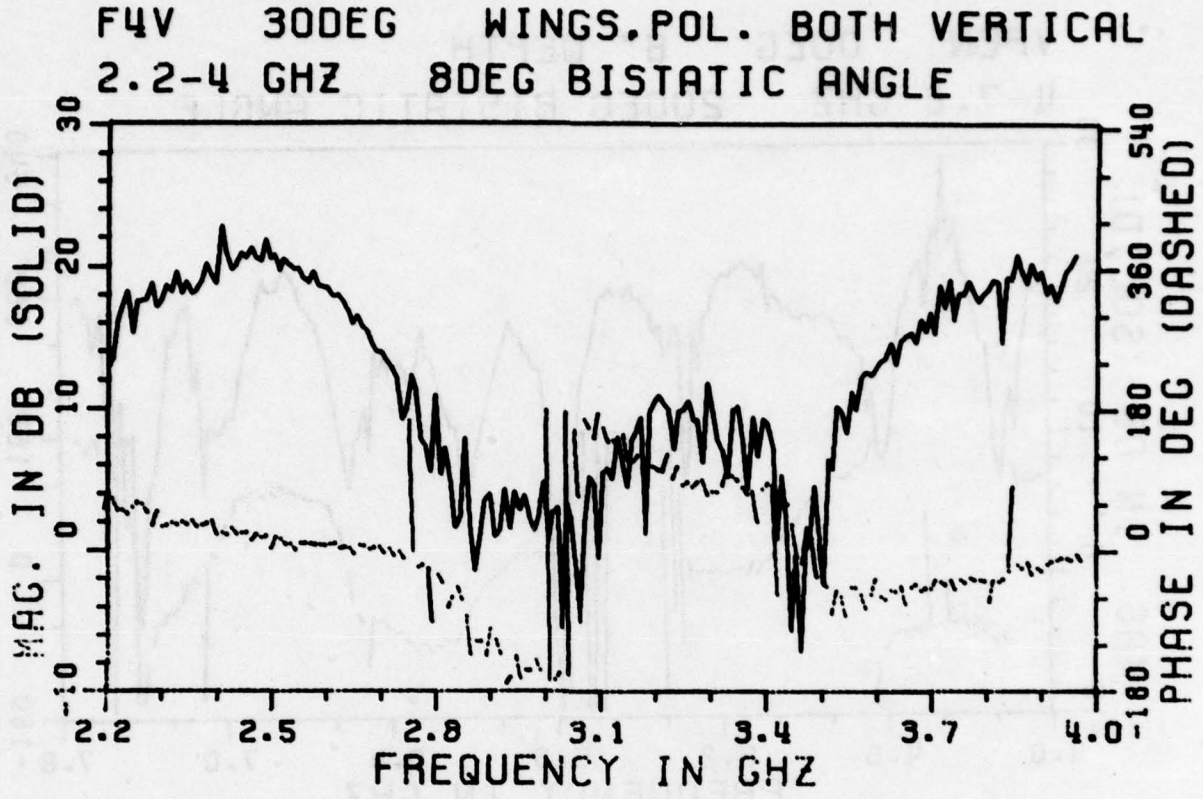


Figure 82. Measured amplitude and phase of scattered field, F4V aircraft, 2.2-4.0 GHz.

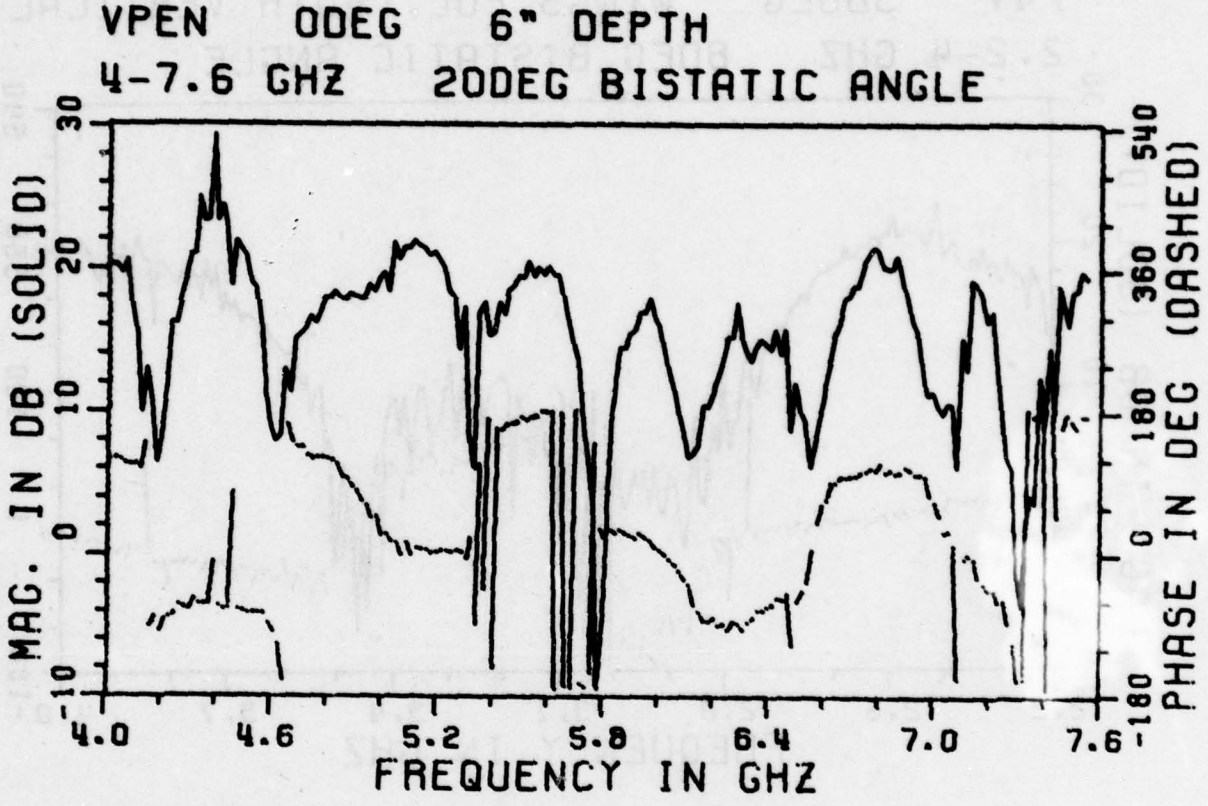


Figure 83. Measured amplitude and phase of scattered field, VPEN model, 4.0-7.6 GHz.

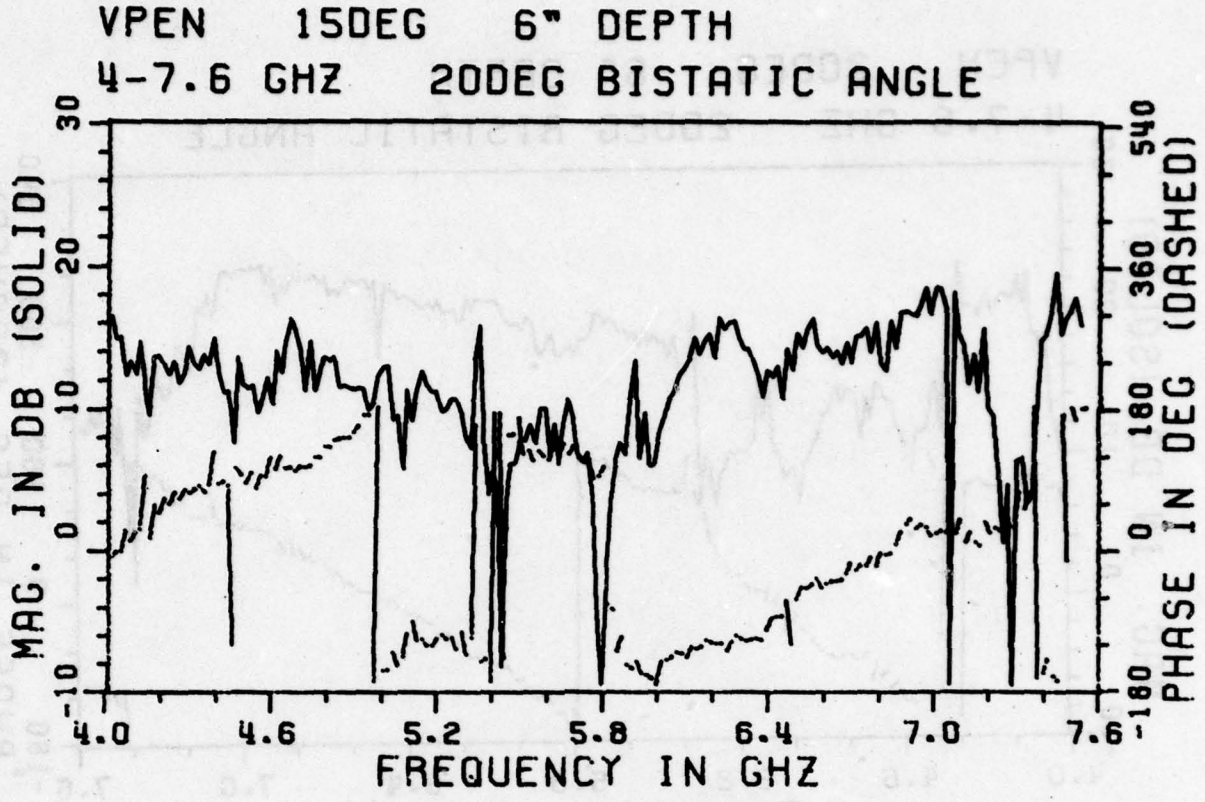


Figure 84. Measured amplitude and phase of scattered field, VPEN model, 4.0-7.6 GHz.

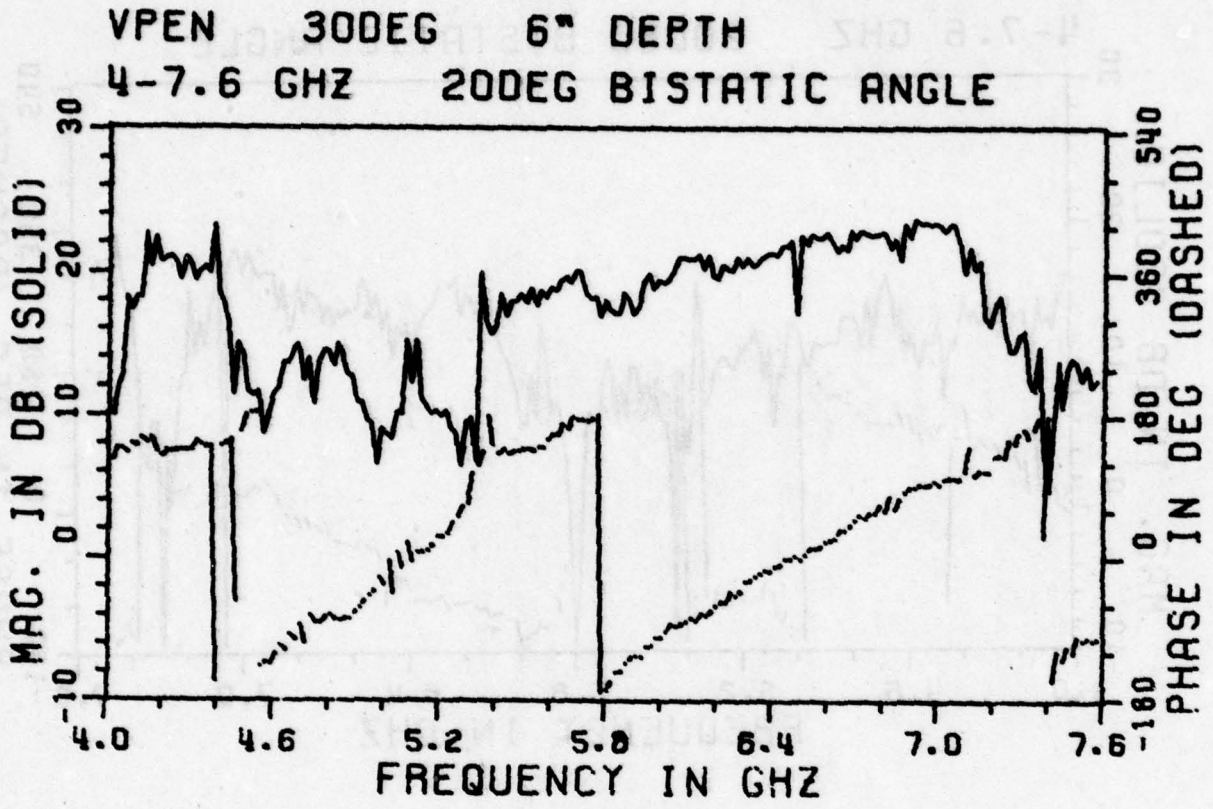


Figure 85. Measured amplitude and phase of scattered field, VPEN model, 4.0-7.6 GHz.

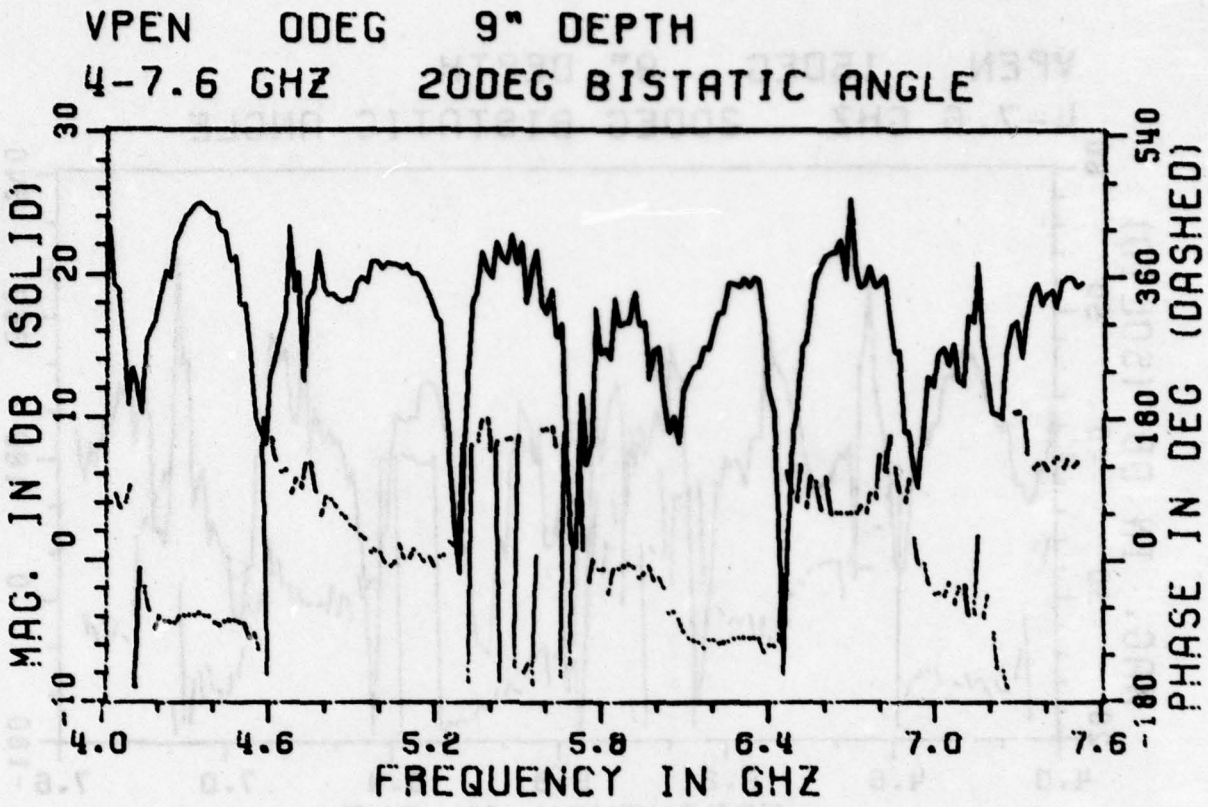


Figure 86. Measured amplitude and phase of scattered field, VPEN model, 4.0-7.6 GHz.

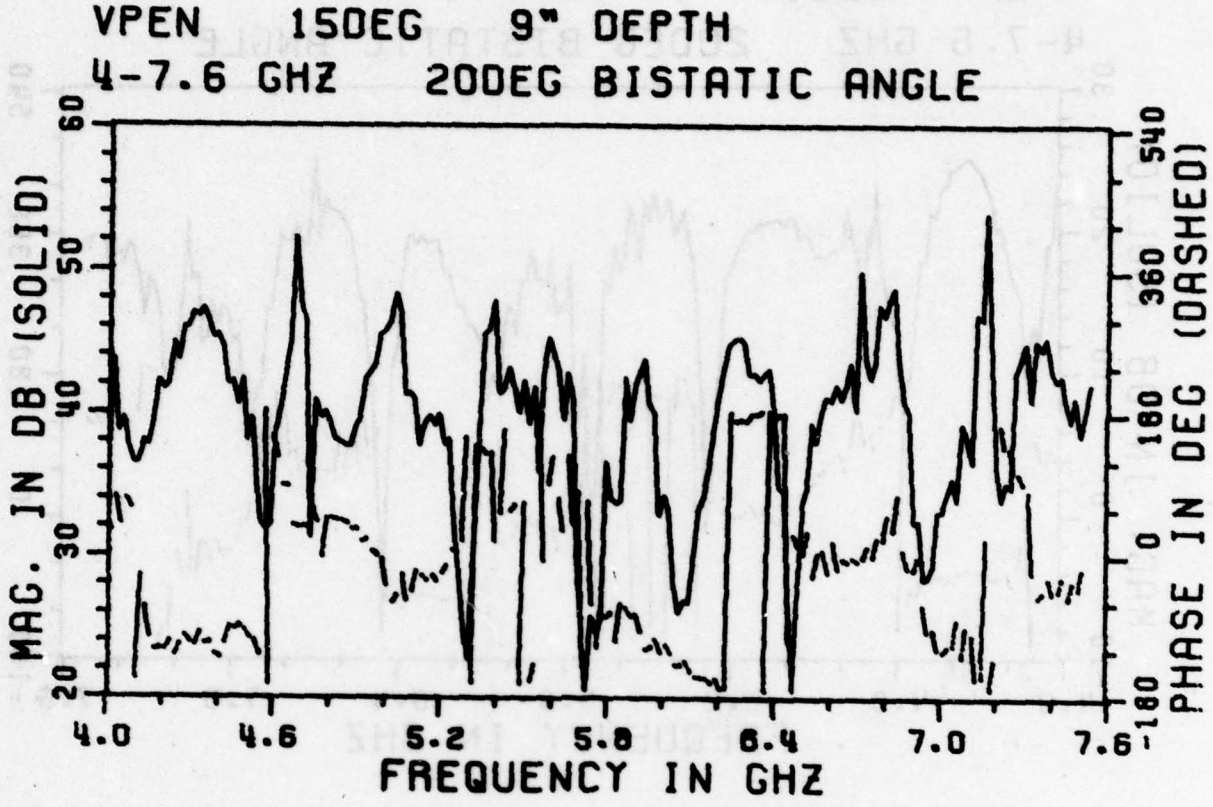


Figure 87. Measured amplitude and phase of scattered field, VPEN model, 4.0-7.6 GHz.

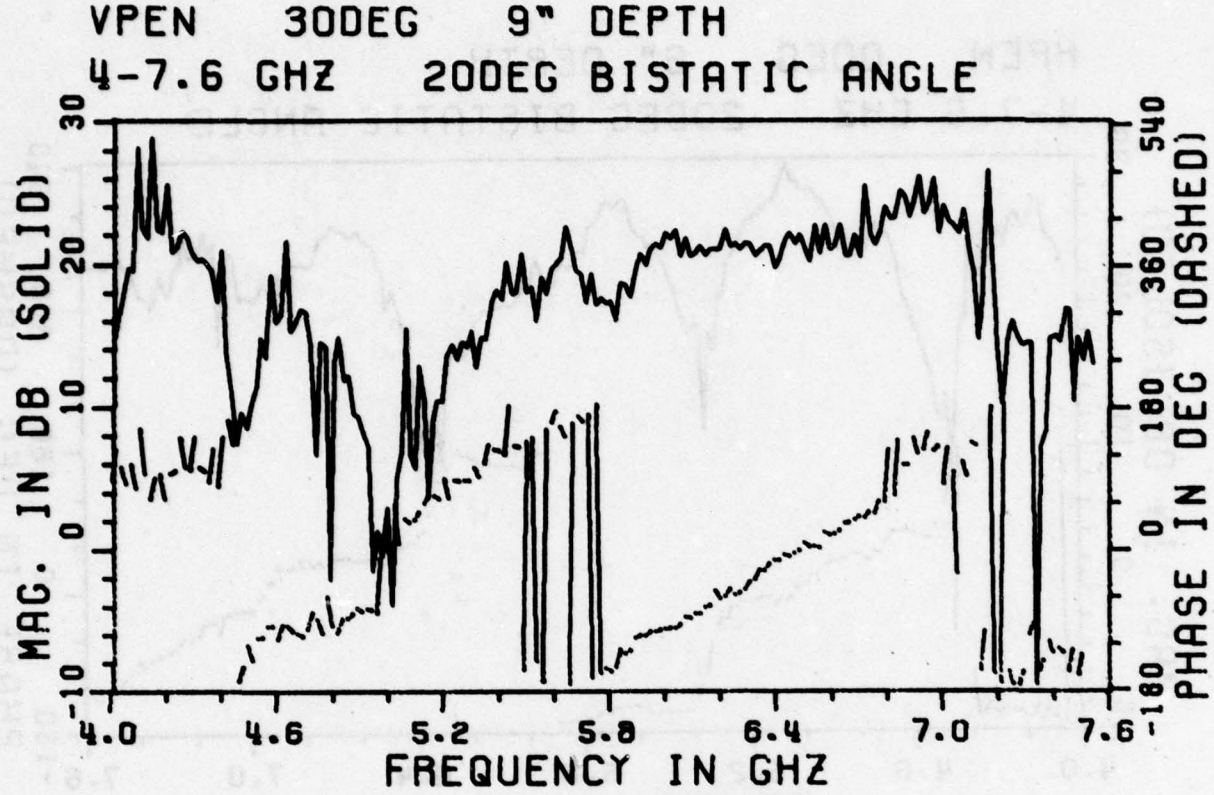


Figure 88. Measured amplitude and phase of scattered field, VPEN model, 4.0-7.6 GHz.

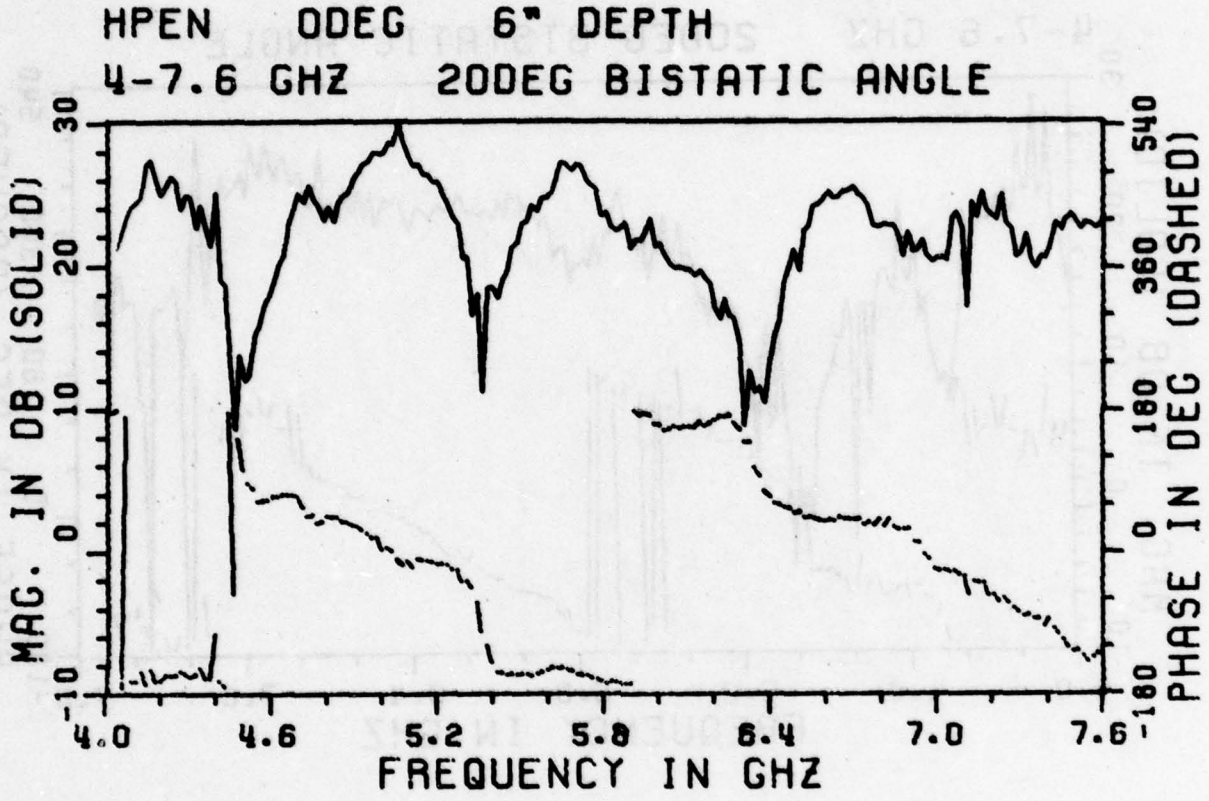


Figure 89. Measured amplitude and phase of scattered field, HPEN model, 4.0-7.6 GHz.

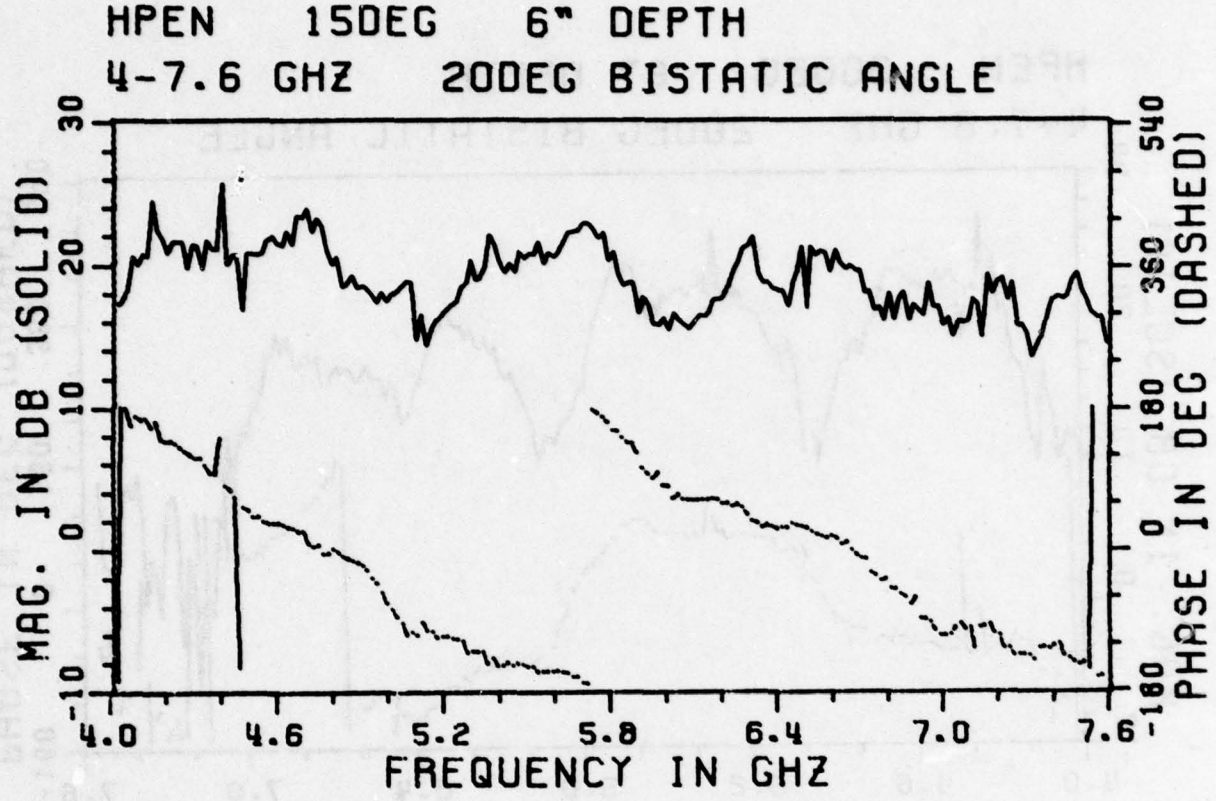


Figure 90. Measured amplitude and phase of scattered field, HPEN model, 4.0-7.6 GHz.

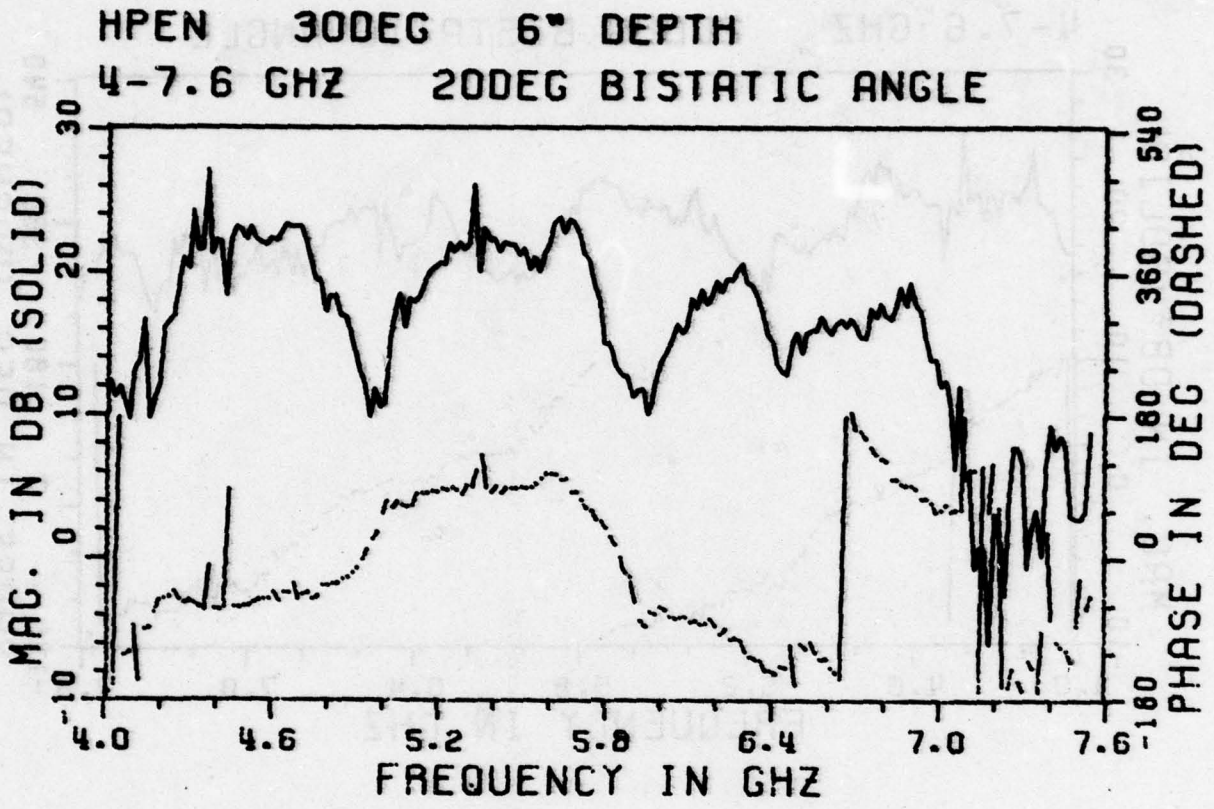


Figure 91. Measured amplitude and phase of scattered field, HPEN model, 4.0-7.6 GHz.

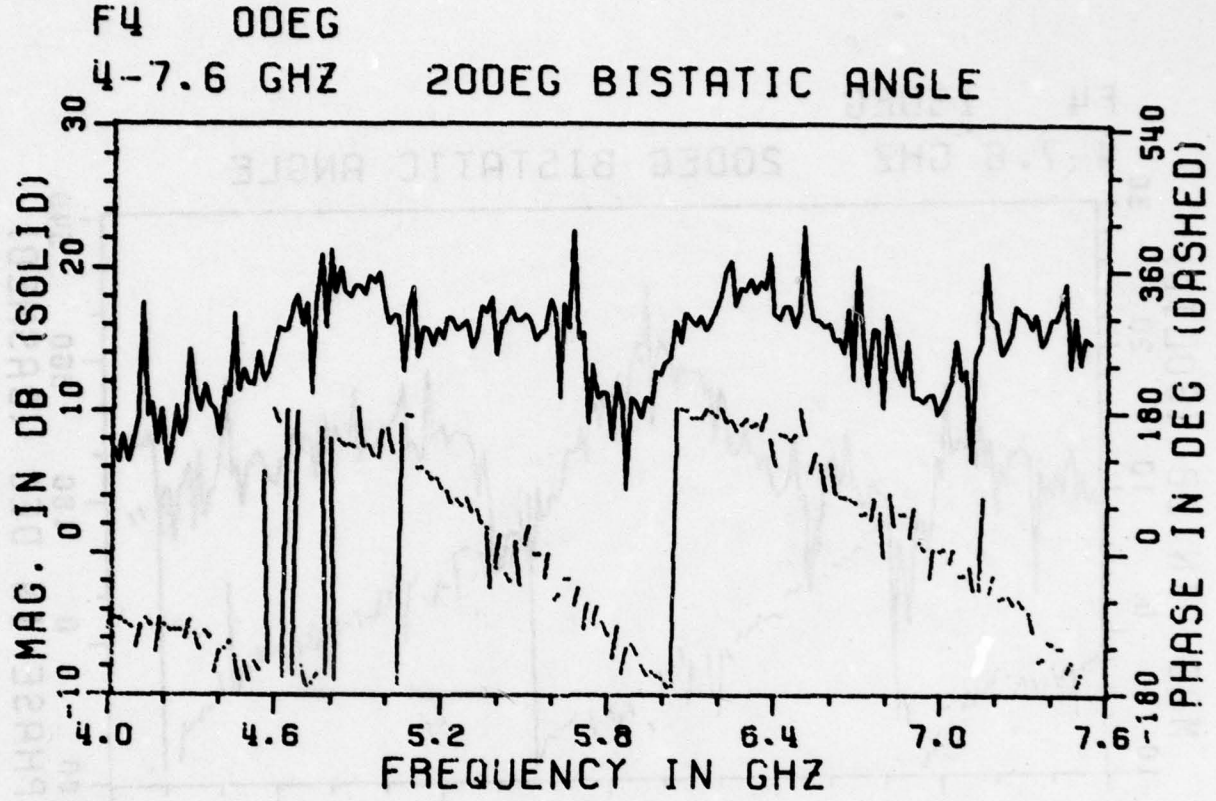


Figure 92. Measured amplitude and phase of scattered field, F-4 aircraft, 4.0-7.6 GHz.

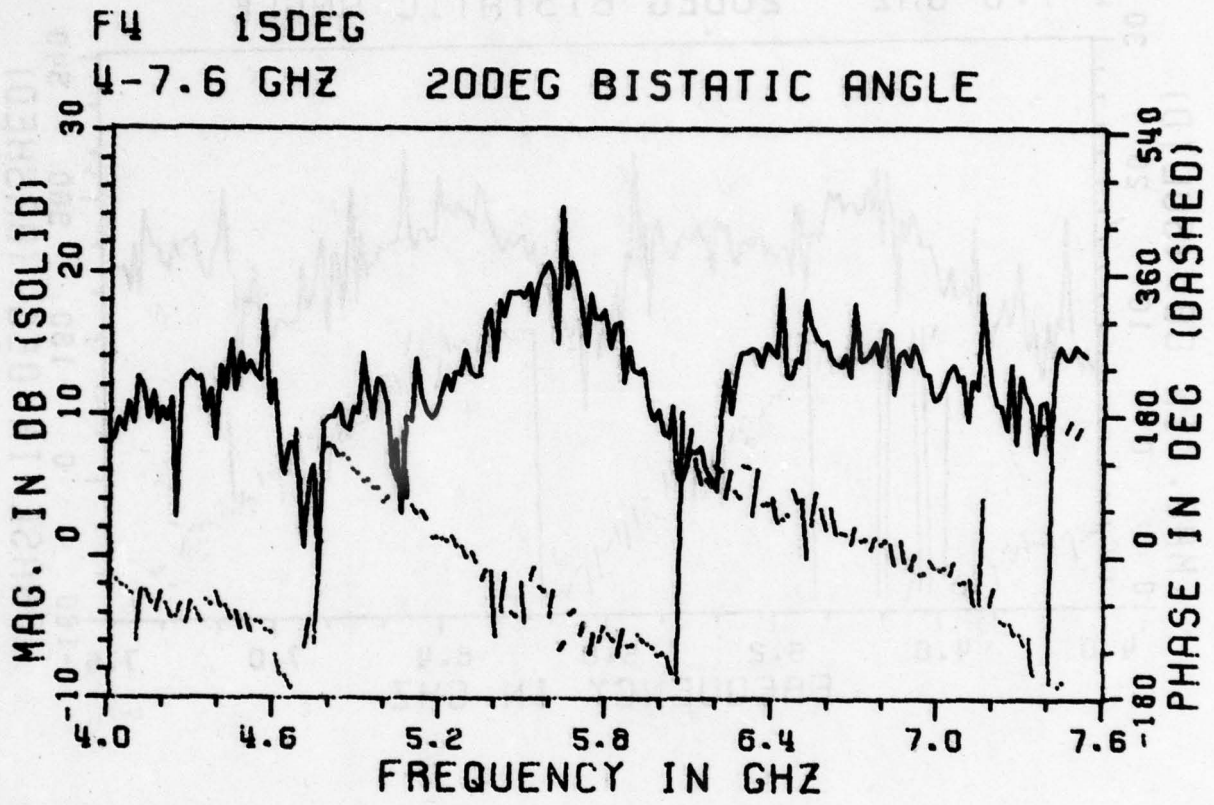


Figure 93. Measured amplitude and phase of scattered field, F-4 aircraft, 4.0-7.6 GHz.

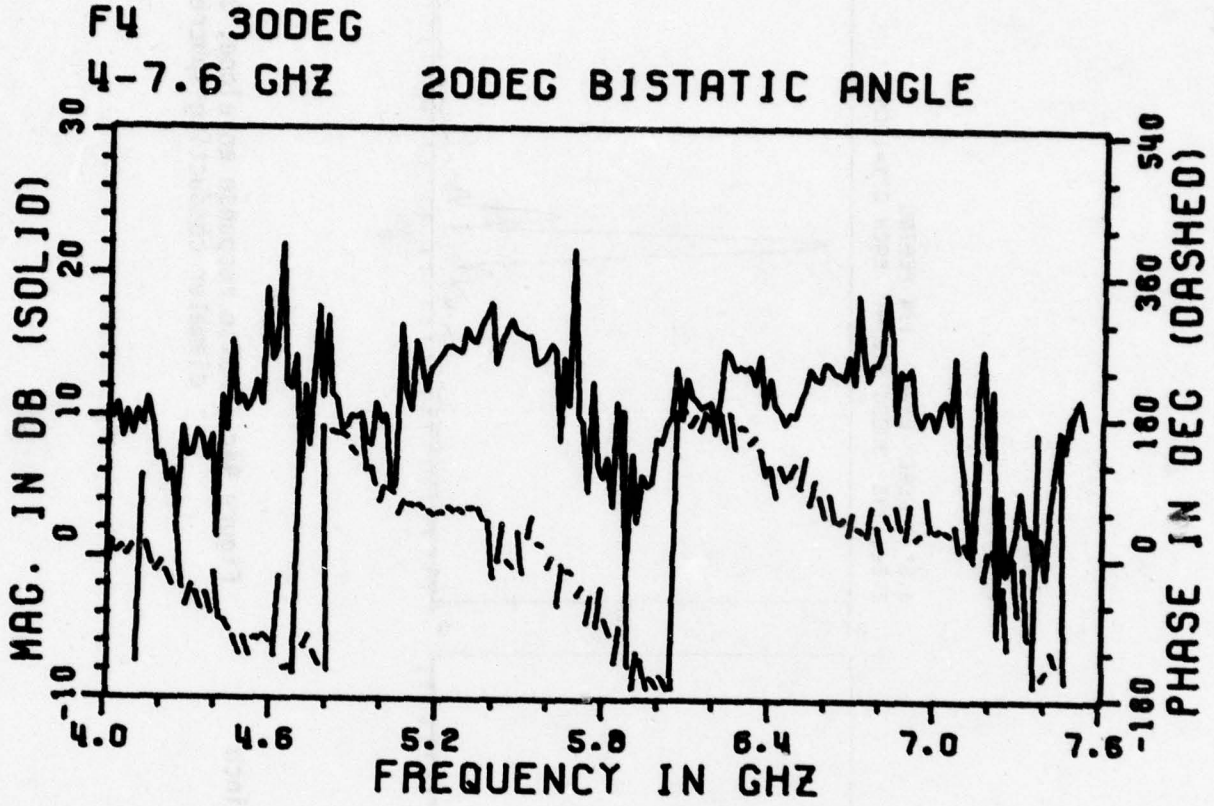


Figure 94a. Measured amplitude and phase of scattered field, F-4 aircraft, 4.0-7.6 GHz.

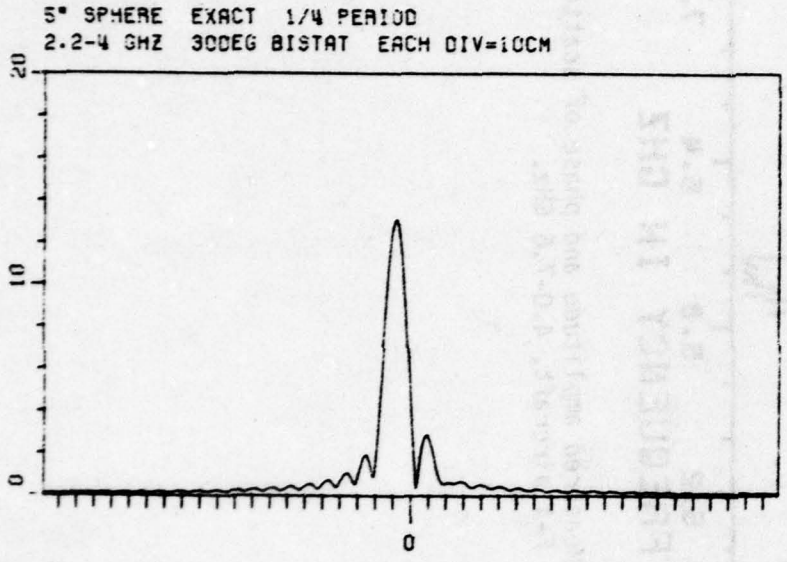


Figure 94b. Pulse response envelope, 5 inch diameter conducting sphere.

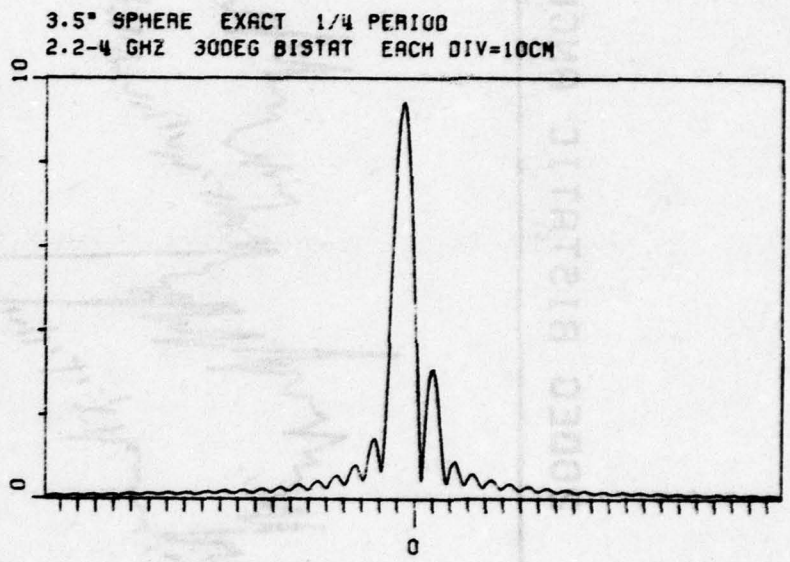


Figure 94c. Pulse response envelope, 3.5 inch diameter conducting sphere.

## V. SYNTHETIC PULSE RESPONSES

The curves given in this section of the report are synthesized short pulse time domain responses of the targets whose scattering measurements in the frequency domain were given in the previous section. To obtain these time domain curves the frequency domain data was considered to be modulated, i.e., demodulation was performed by considering the measured spectrum to be centered at zero frequency. A simple Fourier Series was then calculated yielding the curves given in Figures 95 through 168. Mathematically the pulses, p(t), are given as

$$p(t) = \frac{1}{T} \sum A(f)\, e^{j2\pi ft} \qquad (1)$$

where

$A(f)$ = complex frequency domain data at 201 evenly spaced points

$\Delta$ = spectrum width (either 4.0-2.2 GHz or 7.6-4.0 GHz)

$\delta$ = frequency increment = $\frac{\Delta}{200}$

$T$ = period = $\frac{1}{\delta}$

$f$ = frequency = $-\frac{\Delta}{2}, -\frac{\Delta}{2} + \delta, \ldots, -\delta, 0, \delta, \ldots, \frac{\Delta}{2} - \delta, \frac{\Delta}{2}$

$t$ = time = $-\frac{1}{8} T \rightarrow \frac{1}{8} T$ in 402 evenly spaced steps

$j$ = $\sqrt{-1}$ .

The pulses in the figures are considered envelopes of the pulse return in Equation (1).

The A(f) in Equation (1) were processed by a $\cos^{\alpha}$ filter [5] before this conversion to the time domain took place. If B(n) represents the frequency domain data at each of N=201 points then

$$A(n) = B(n) \cdot W(n) \qquad (2)$$

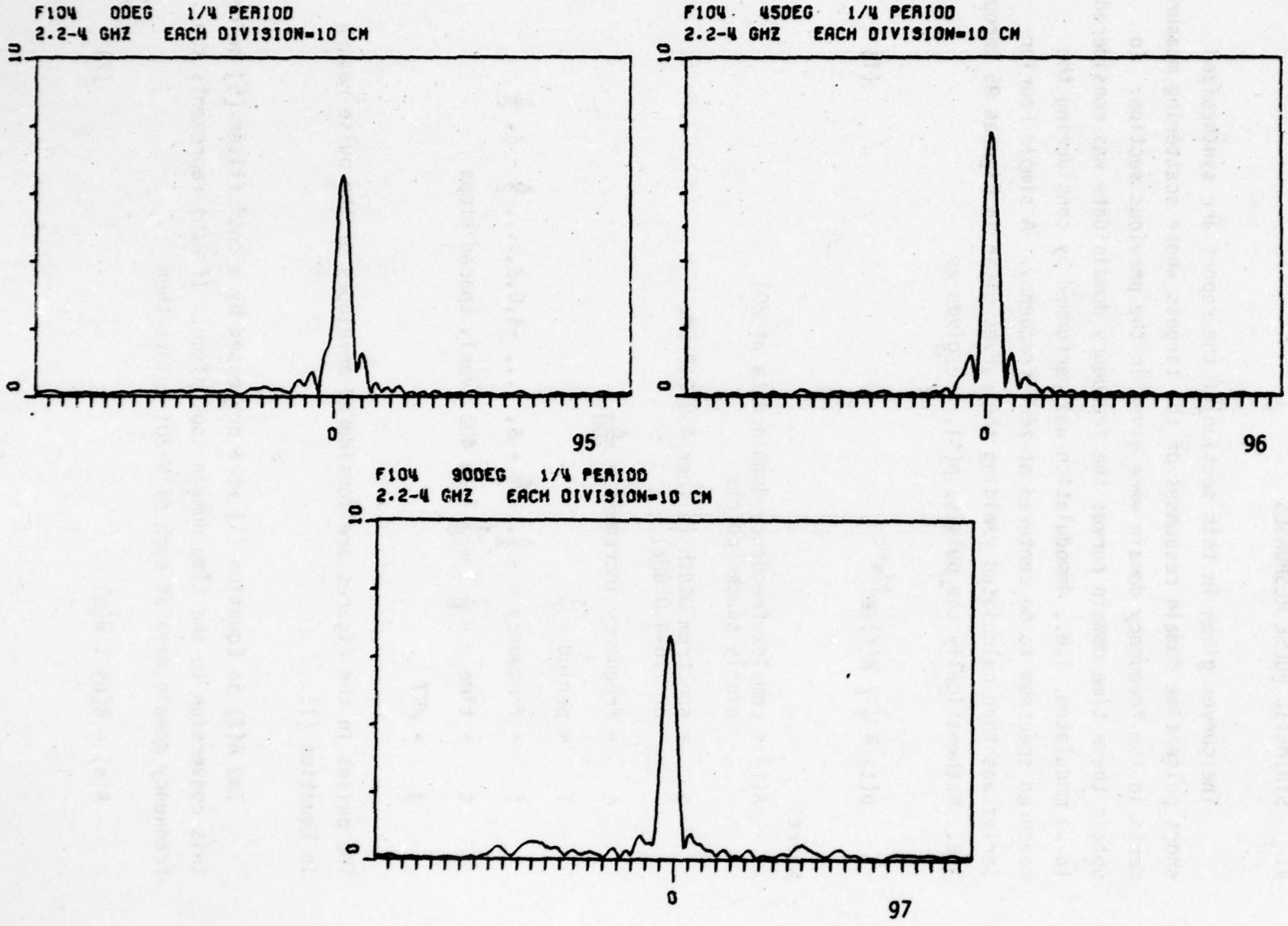


Figures 95,96,97. Pulse response envelope, F104 aircraft.

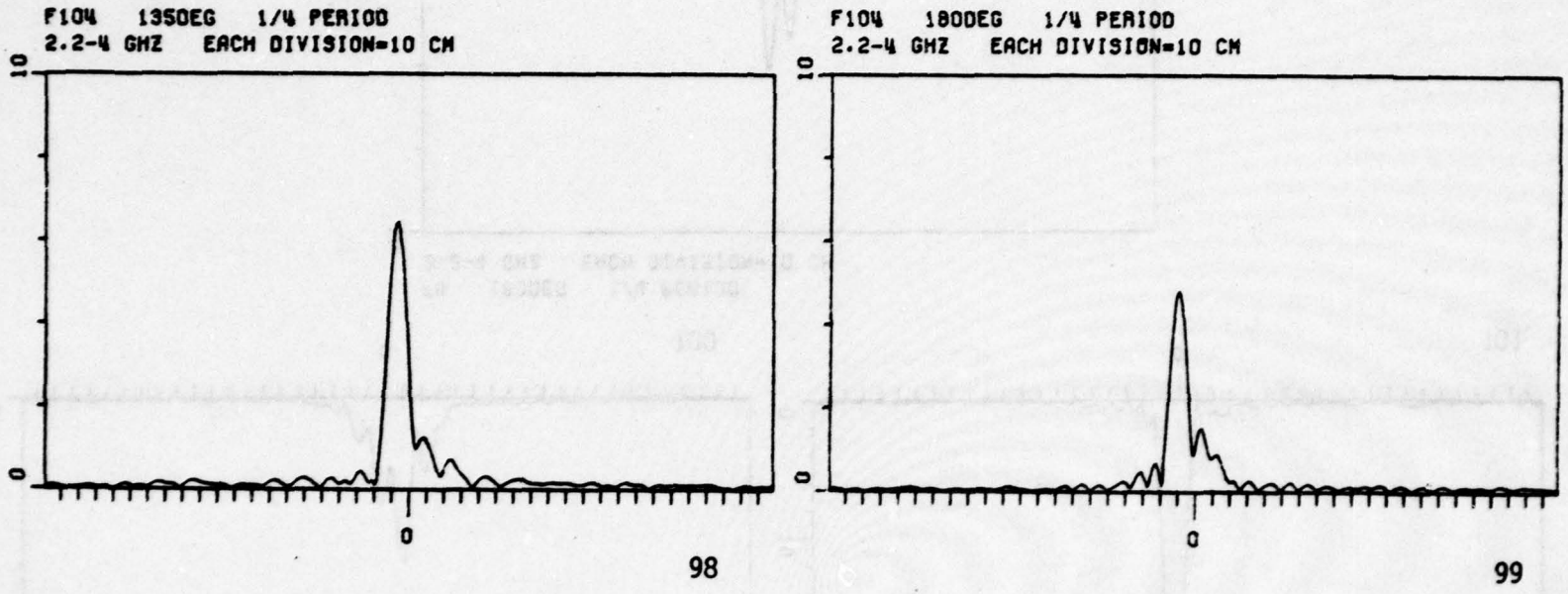


Figures 98,99. Pulse response envelope,F104 aircraft.

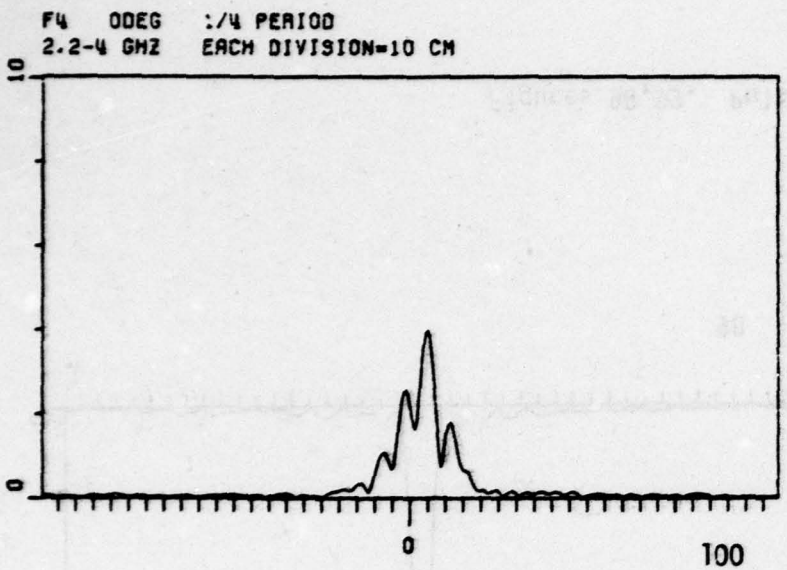


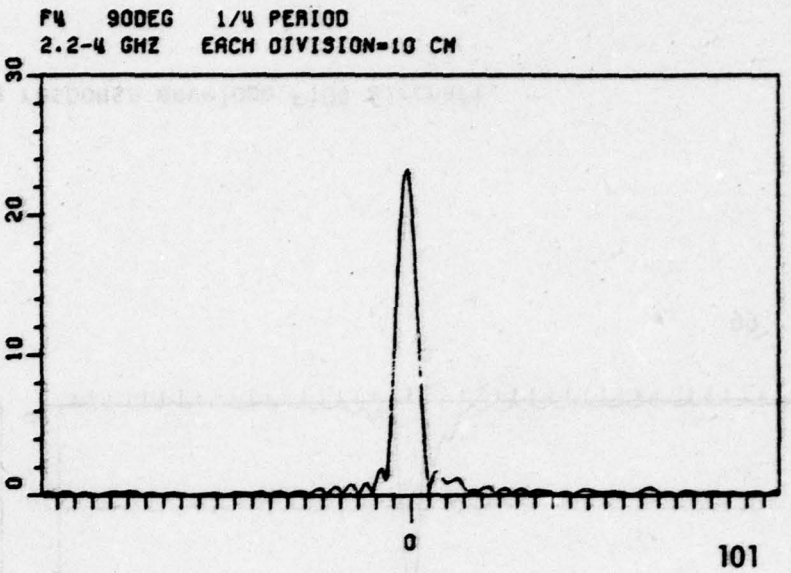


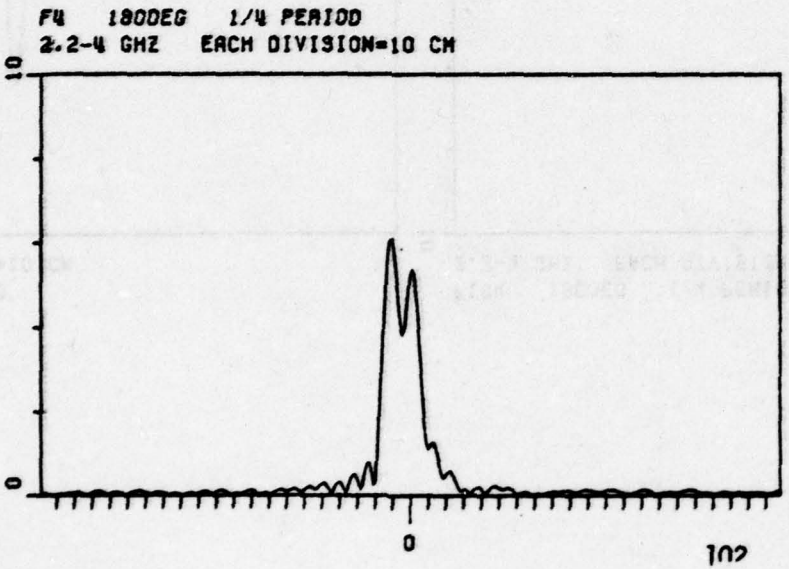


Figures 100,101,102. Pulse response envelope, F4 aircraft.

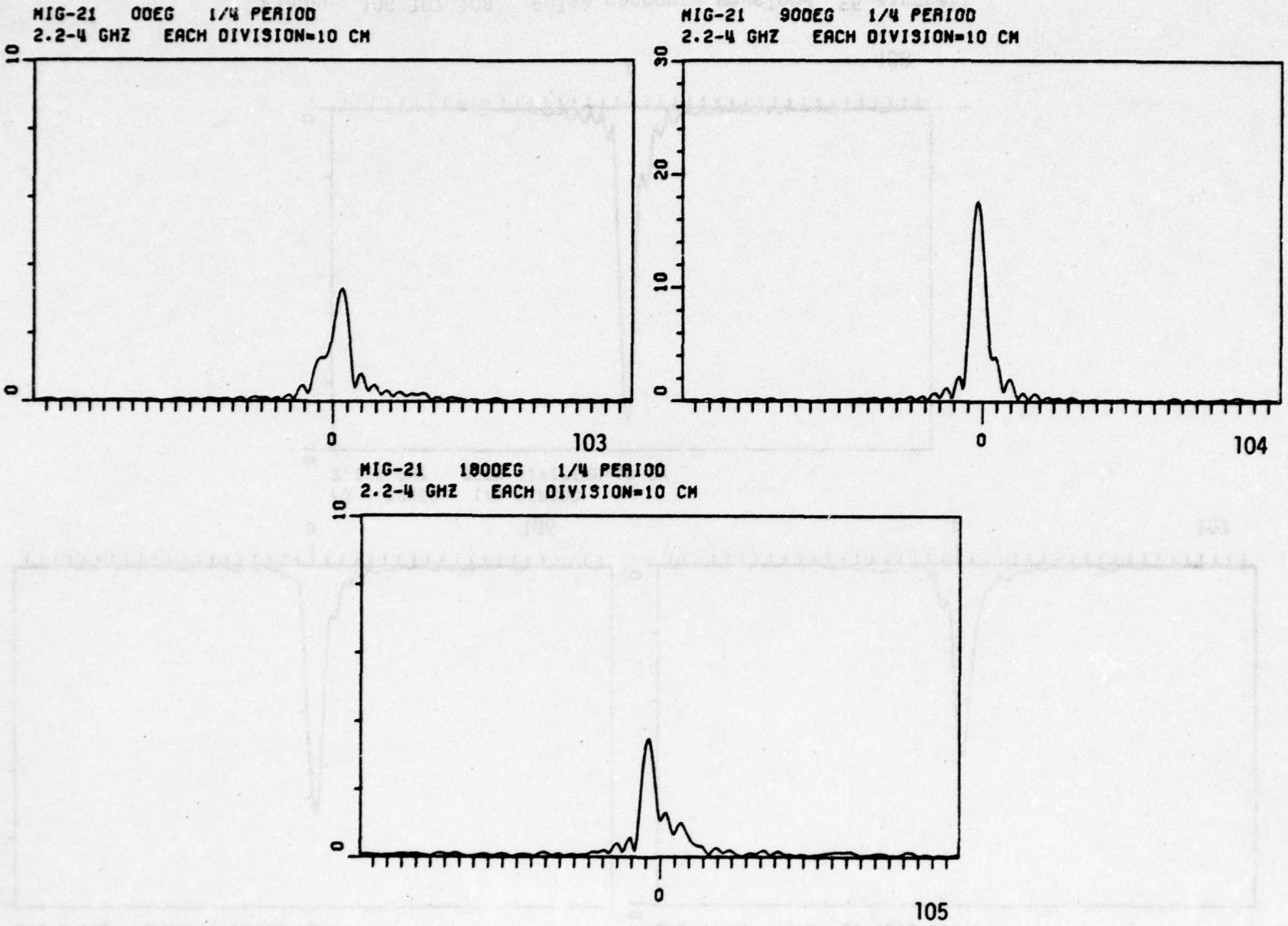


Figures 103,104,105. Pulse response envelope, MIG-21 aircraft.

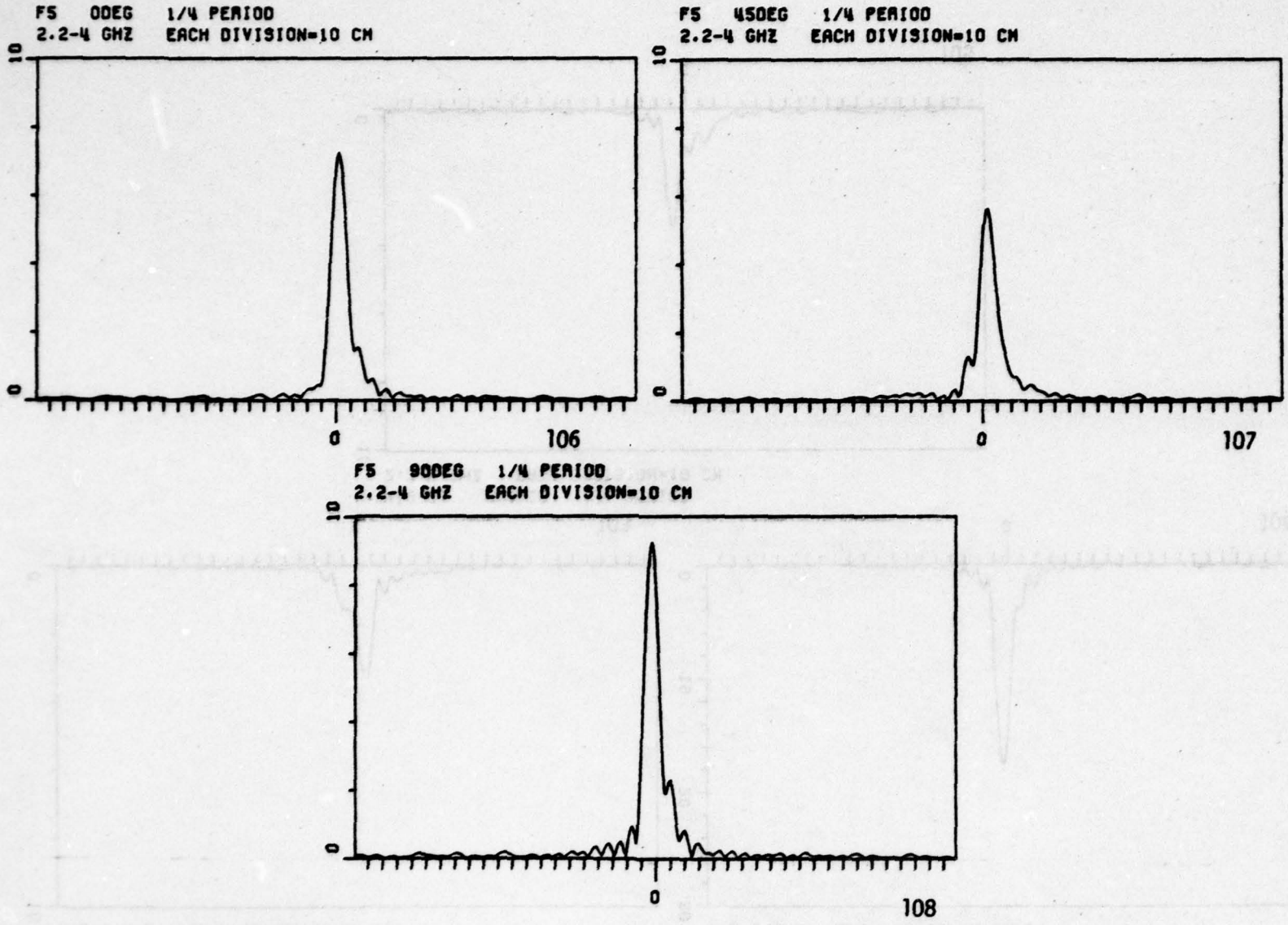


Figures 106,107,108. Pulse response envelope, F5 aircraft.

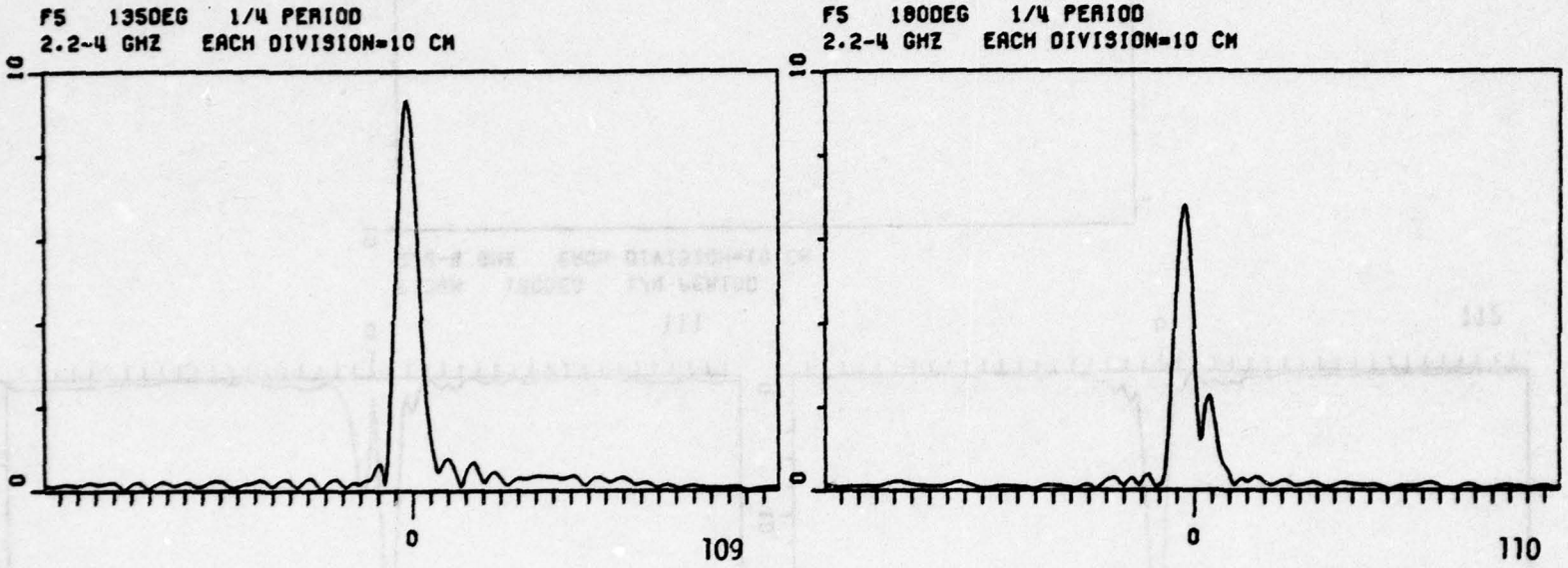


Figures 109,110. Pulse response envelope, F5 aircraft.

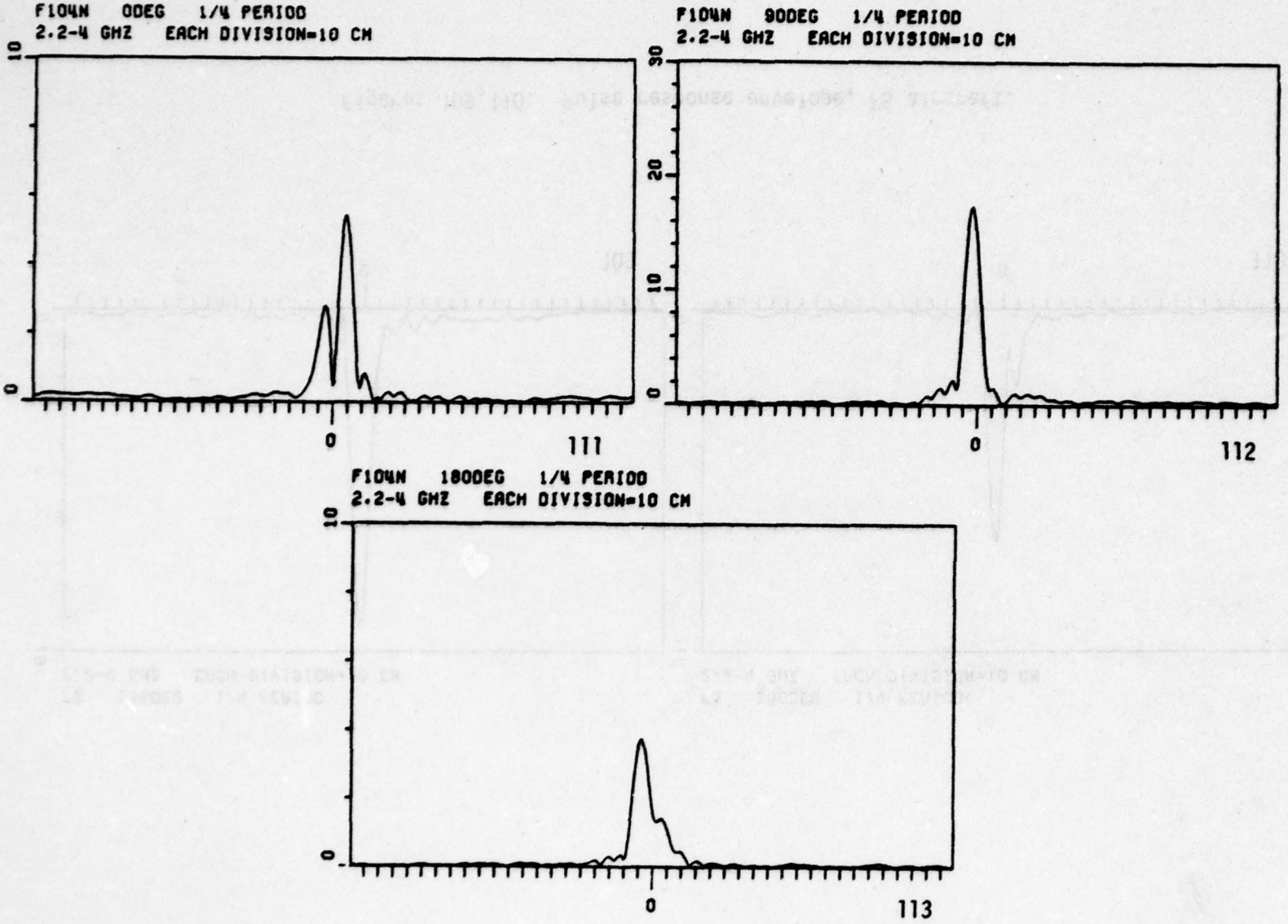


Figures 111,112,113. Pulse response envelope, F104N aircraft.

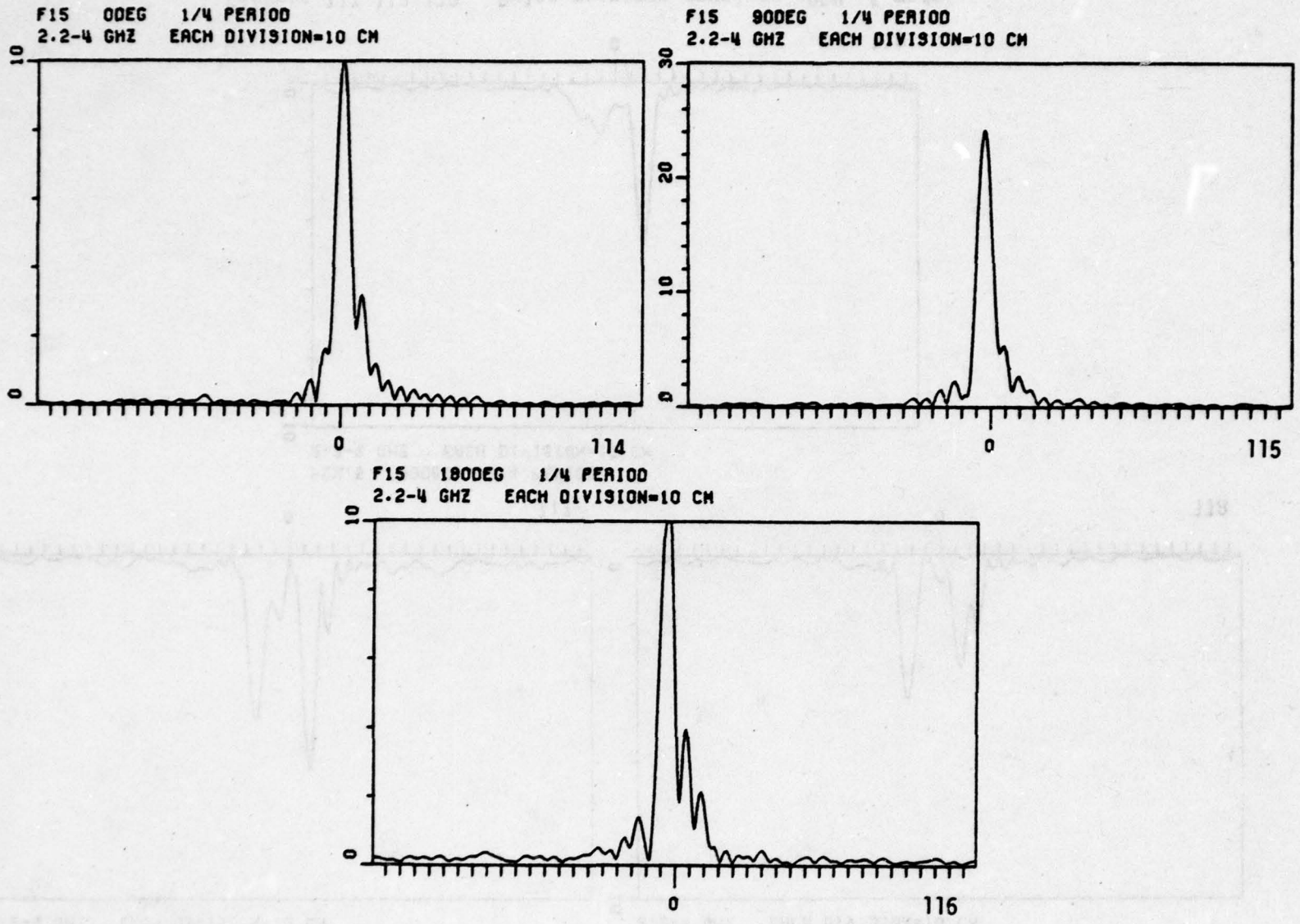


Figures 114,115,116. Pulse response envelope, F15 aircraft.

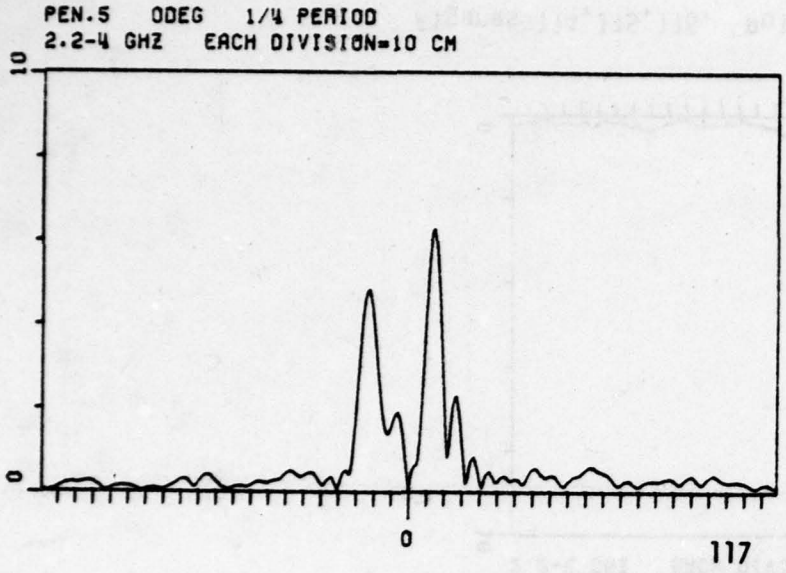


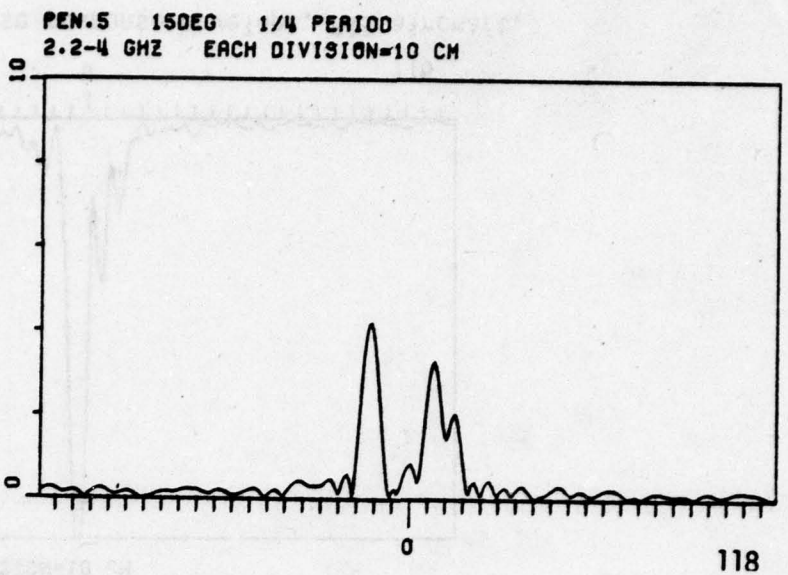


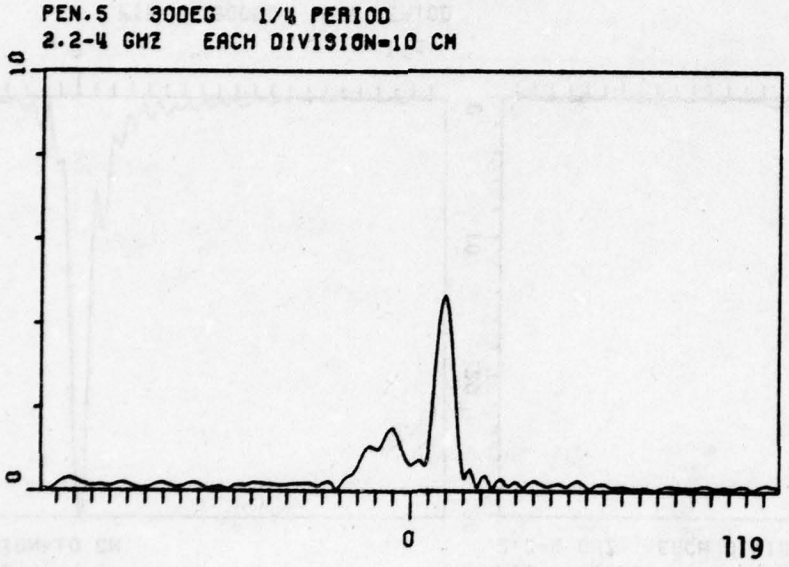


Figures 117,118,119. Pulse response envelope, PEN .5 model.

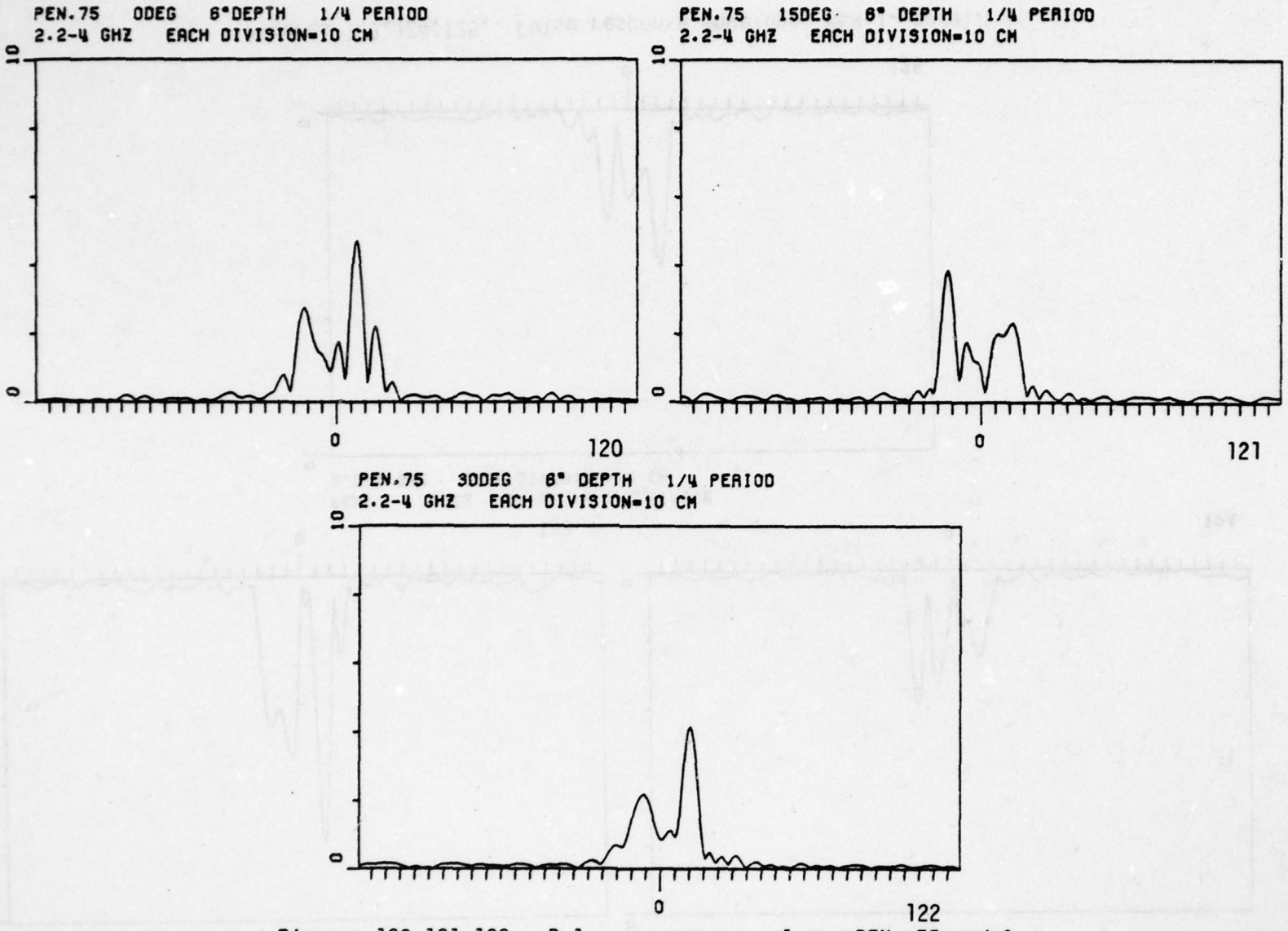


Figures 120,121,122. Pulse response envelope, PEN .75 model.

AD-A071 474 OHIO STATE UNIV COLUMBUS ELECTROSCIENCE LAB F/G 20/14
SWEPT FREQUENCY SCATTERING MEASUREMENTS OF AIRCRAFT.(U)
MAY 79 K A SHUBERT, D L MOFFATT F19628-77-C-0125
UNCLASSIFIED ESL-784677-1 RADC-TR-79-110 NL

2 OF 2
AD A071474

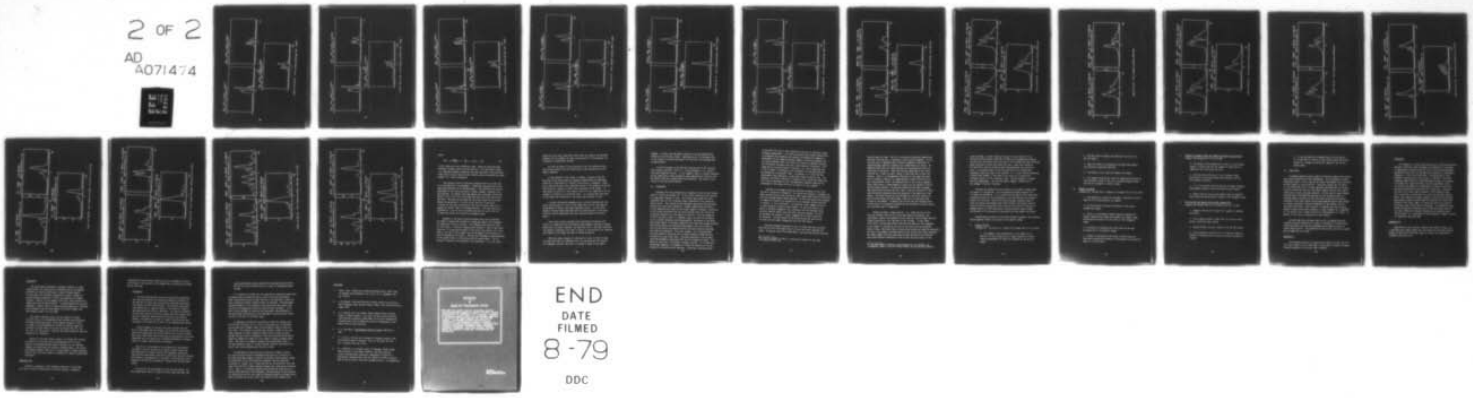

END
DATE FILMED
8-79
DDC

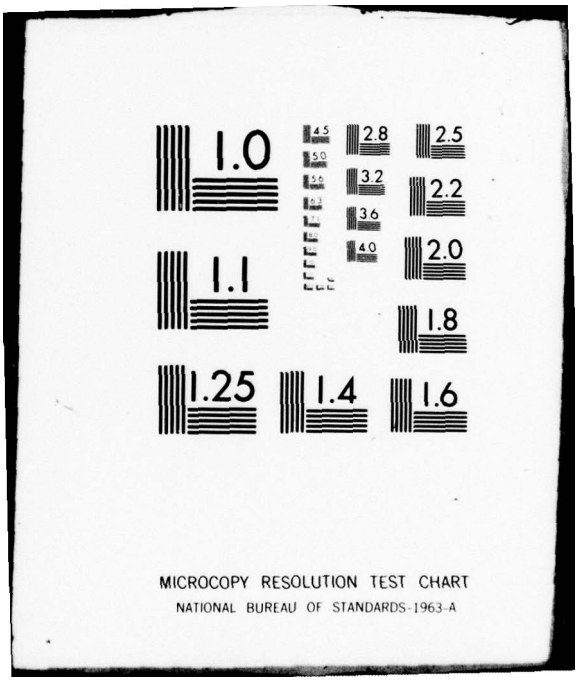
1.0
1.1
1.25
1.4
1.6
1.8
2.0
2.2
2.5
2.8
3.2
3.6
4.0
4.5
5.0
5.6
MICROCOPY RESOLUTION TEST CHART
NATIONAL BUREAU OF STANDARDS-1963-A

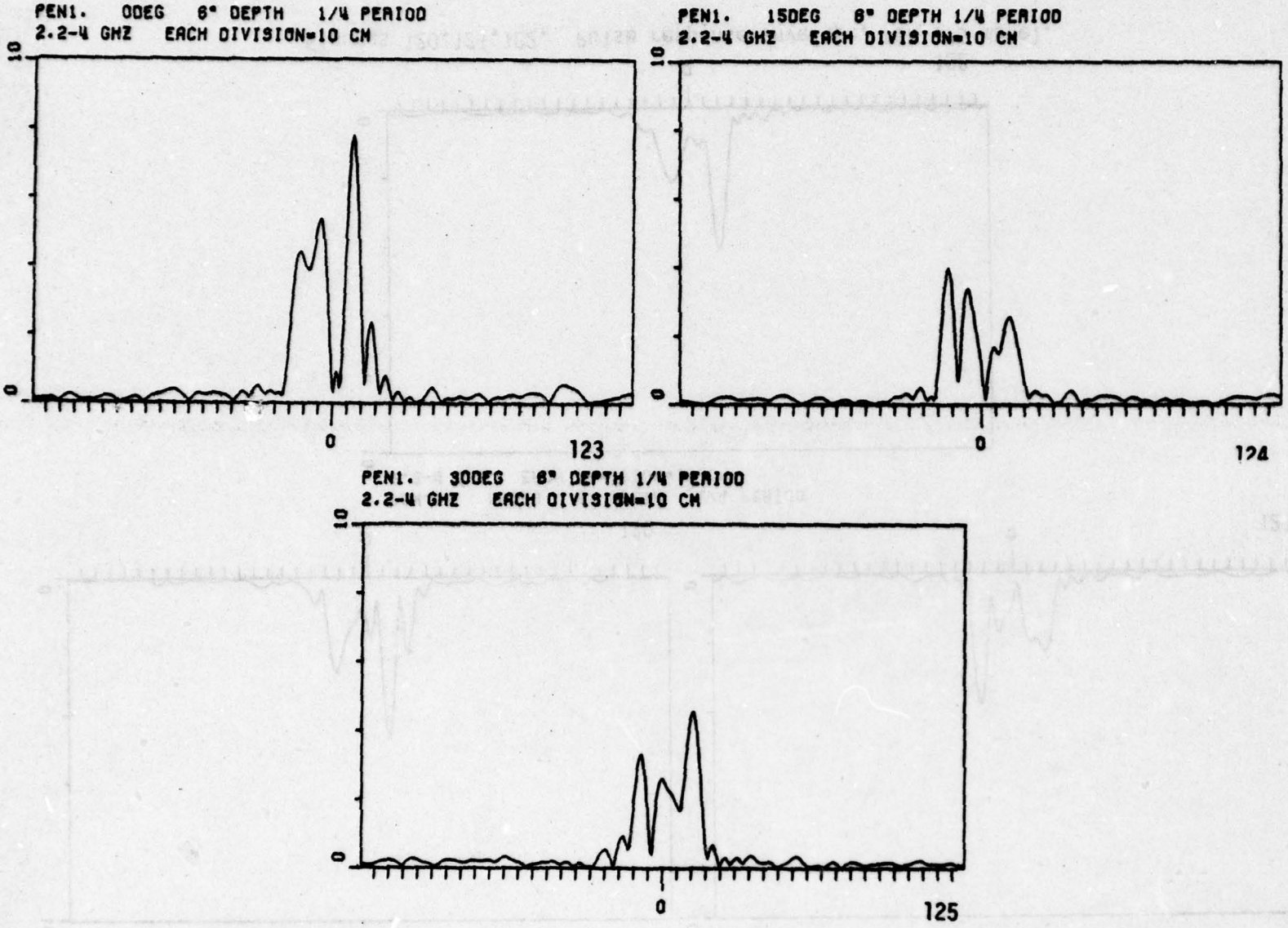


Figures 123,124,125. Pulse response envelope, PEN 1. model.

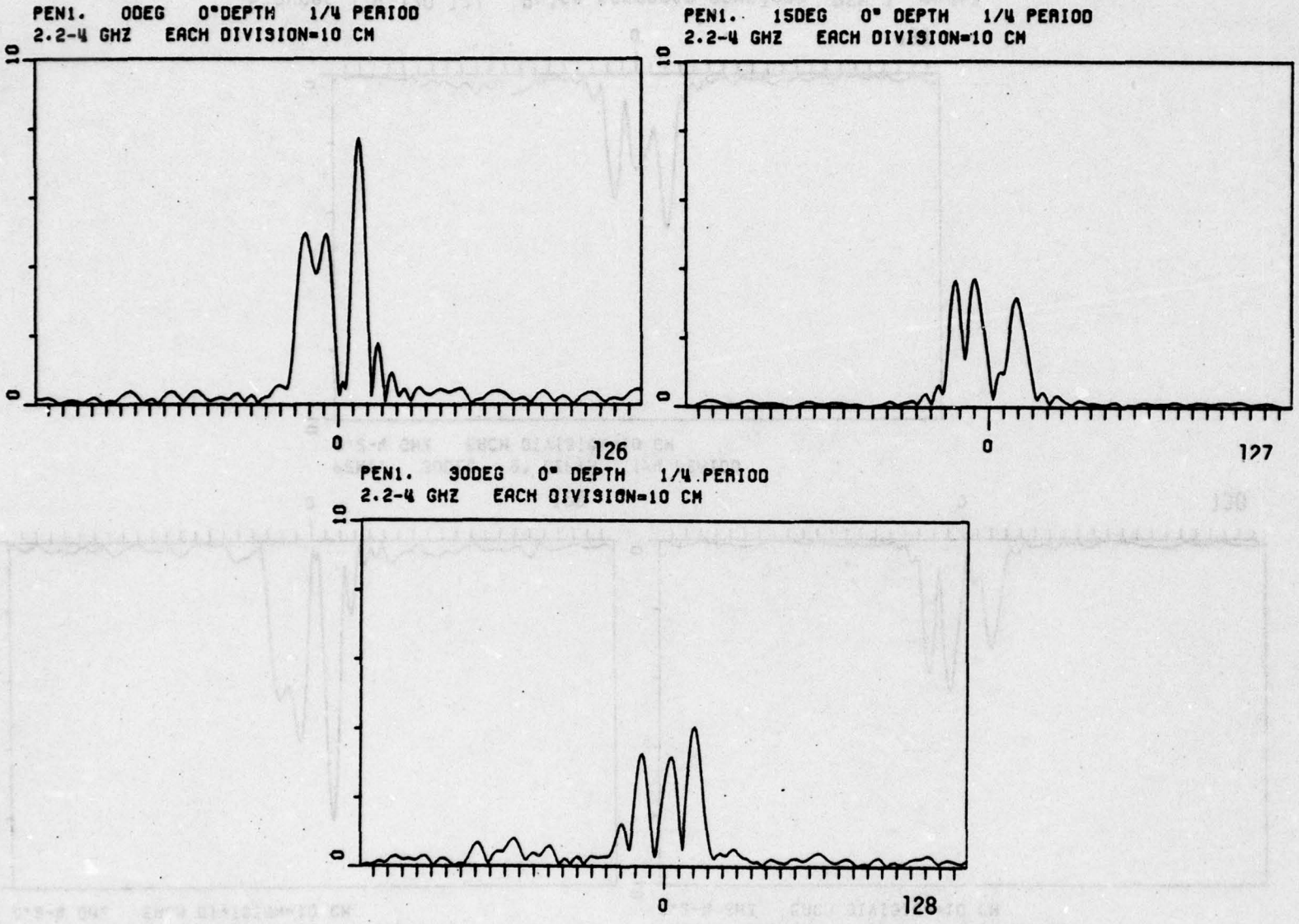


Figures 126,127,128. Pulse response envelope, PEN 1. model.

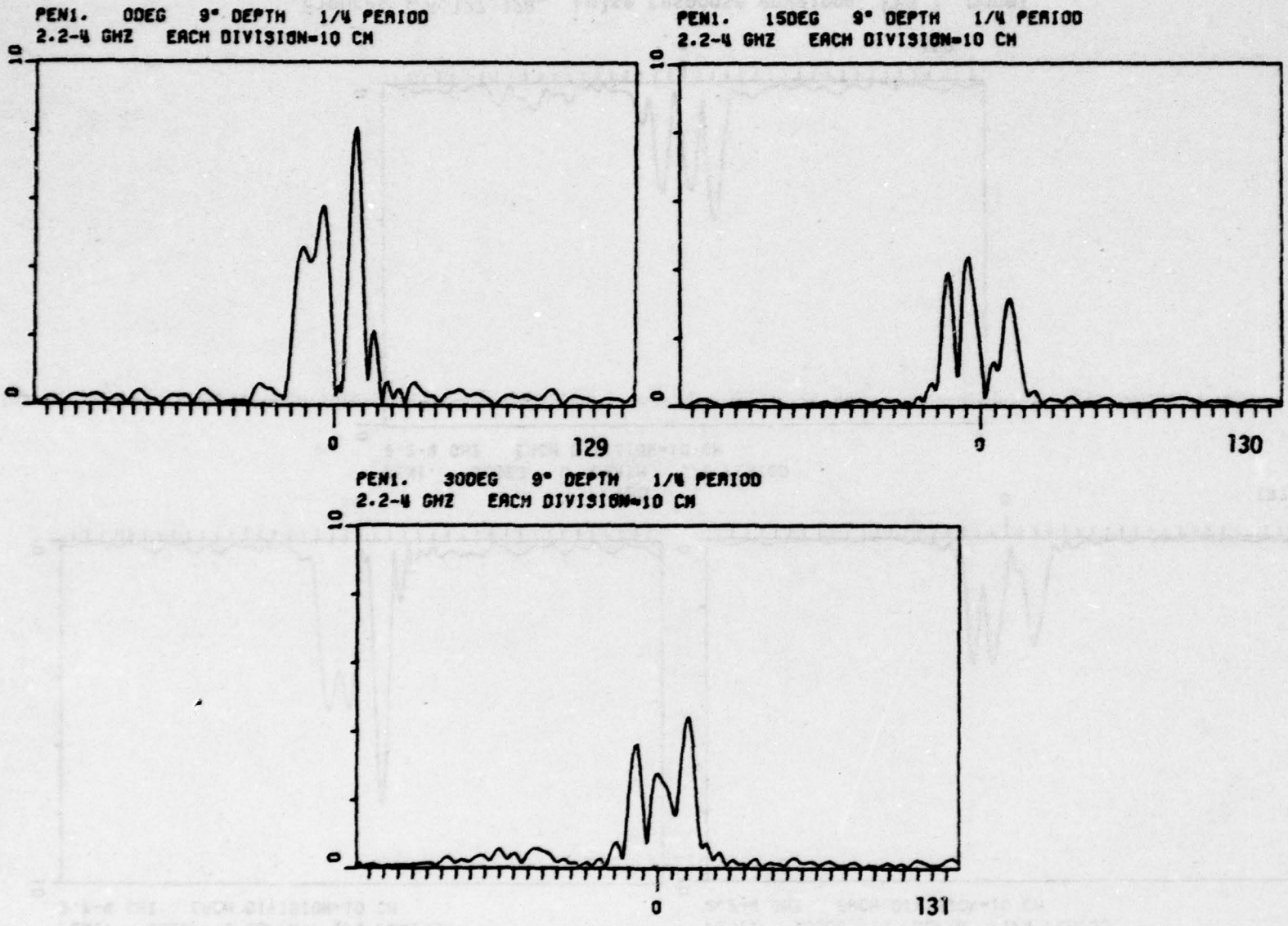


Figures 129,130,131. Pulse response envelope, PEN 1. model.

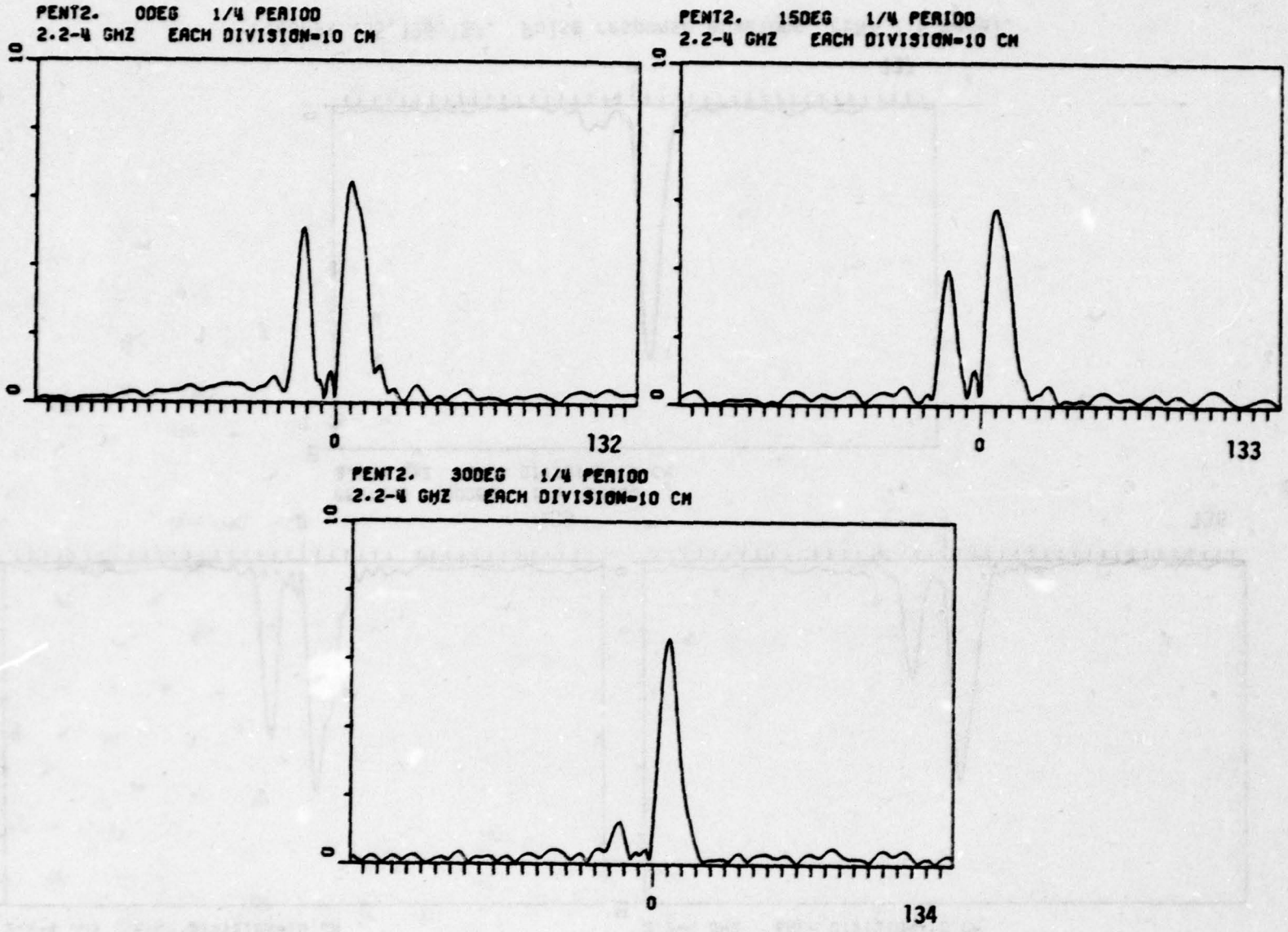


Figures 132,133,134. Pulse response envelope, PENT 2. model.

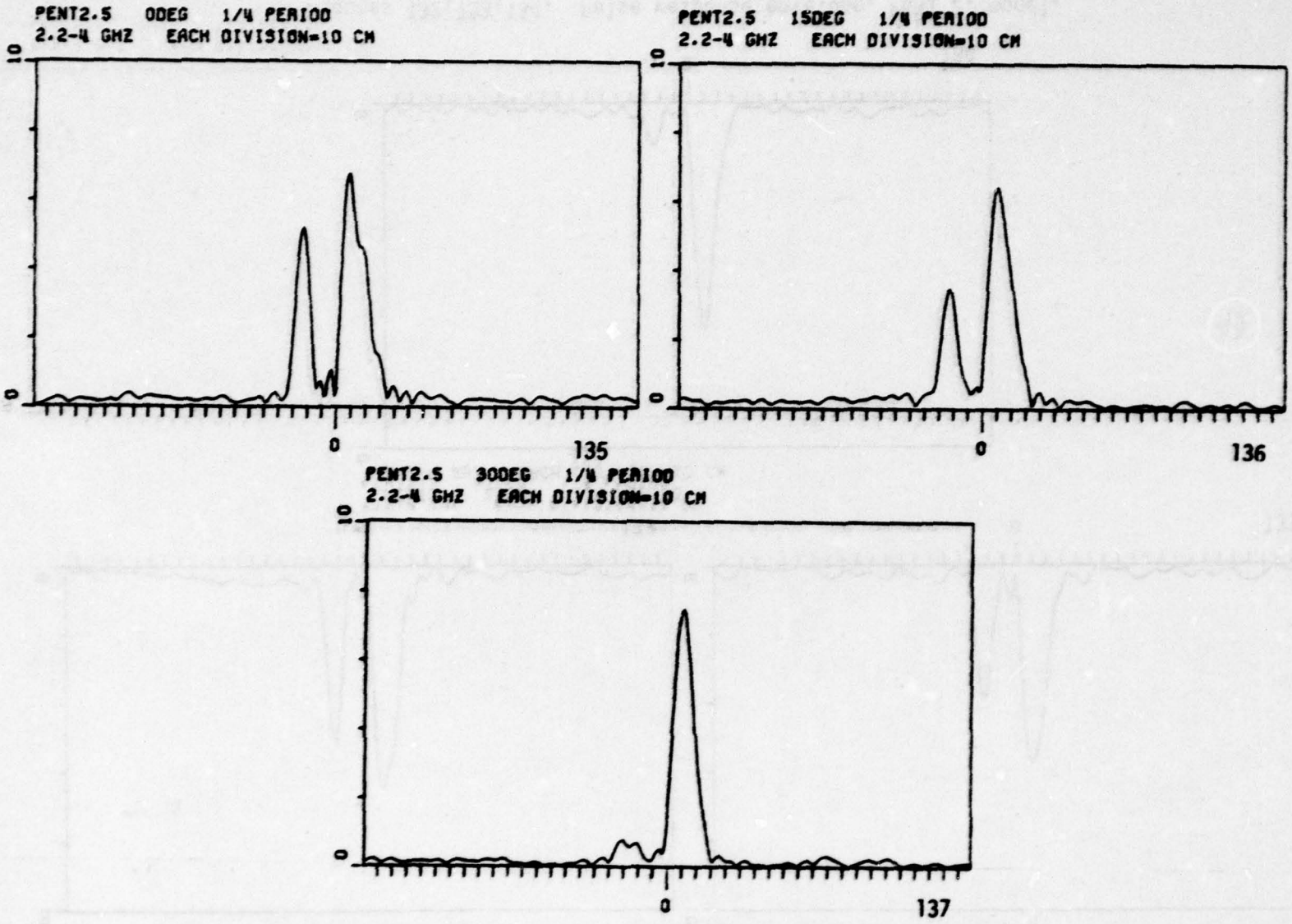


Figures 135,136,137. Pulse response envelope, PENT 2.5 model.

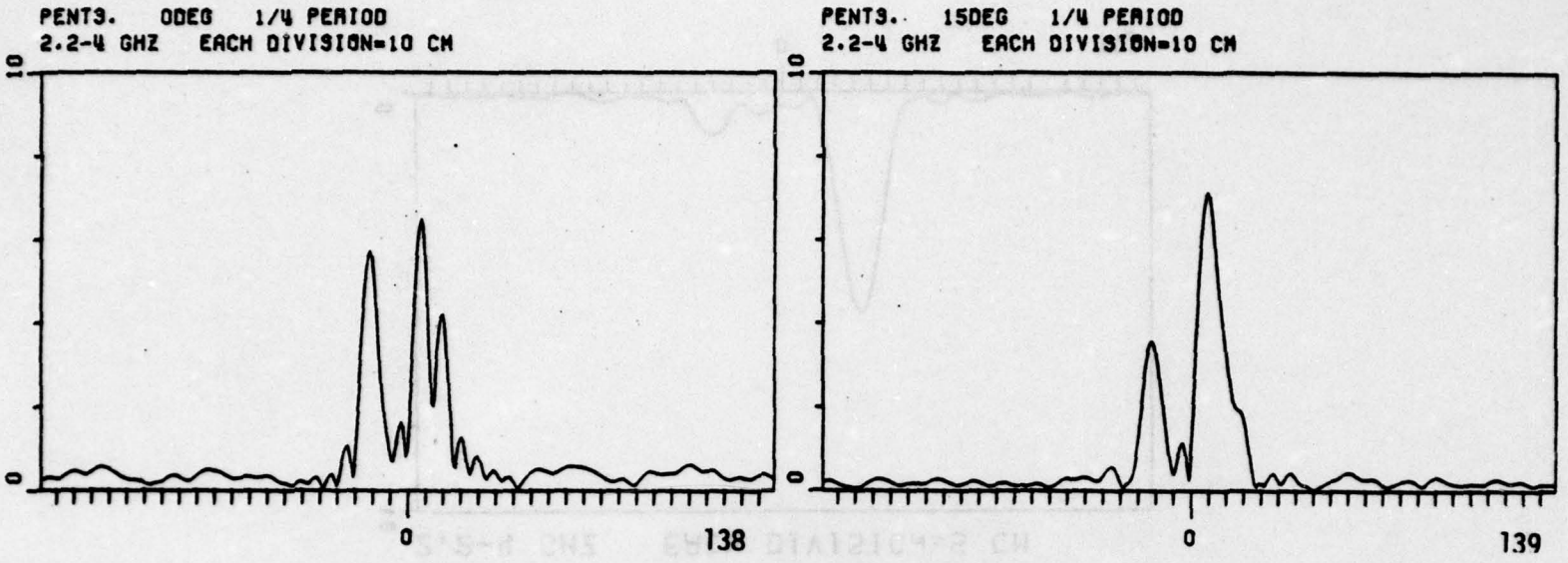





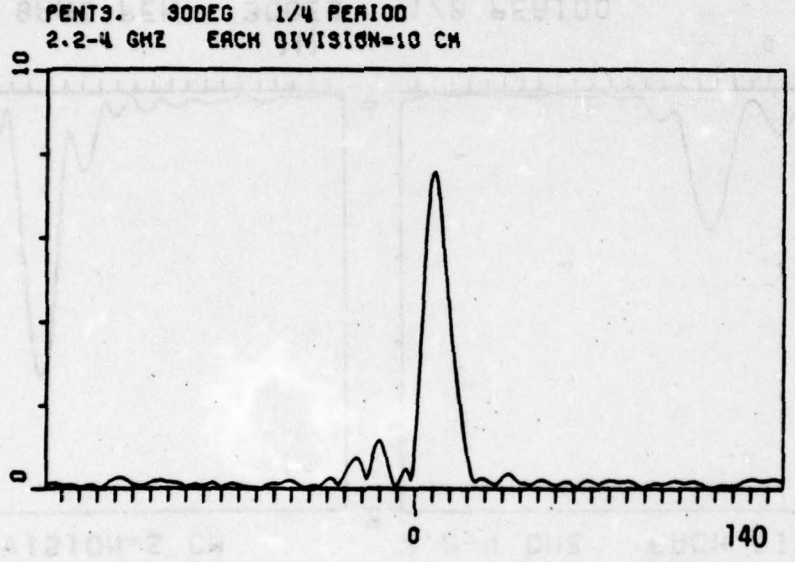


Figures 138,139,140. Pulse response envelope, PENT 3. model.

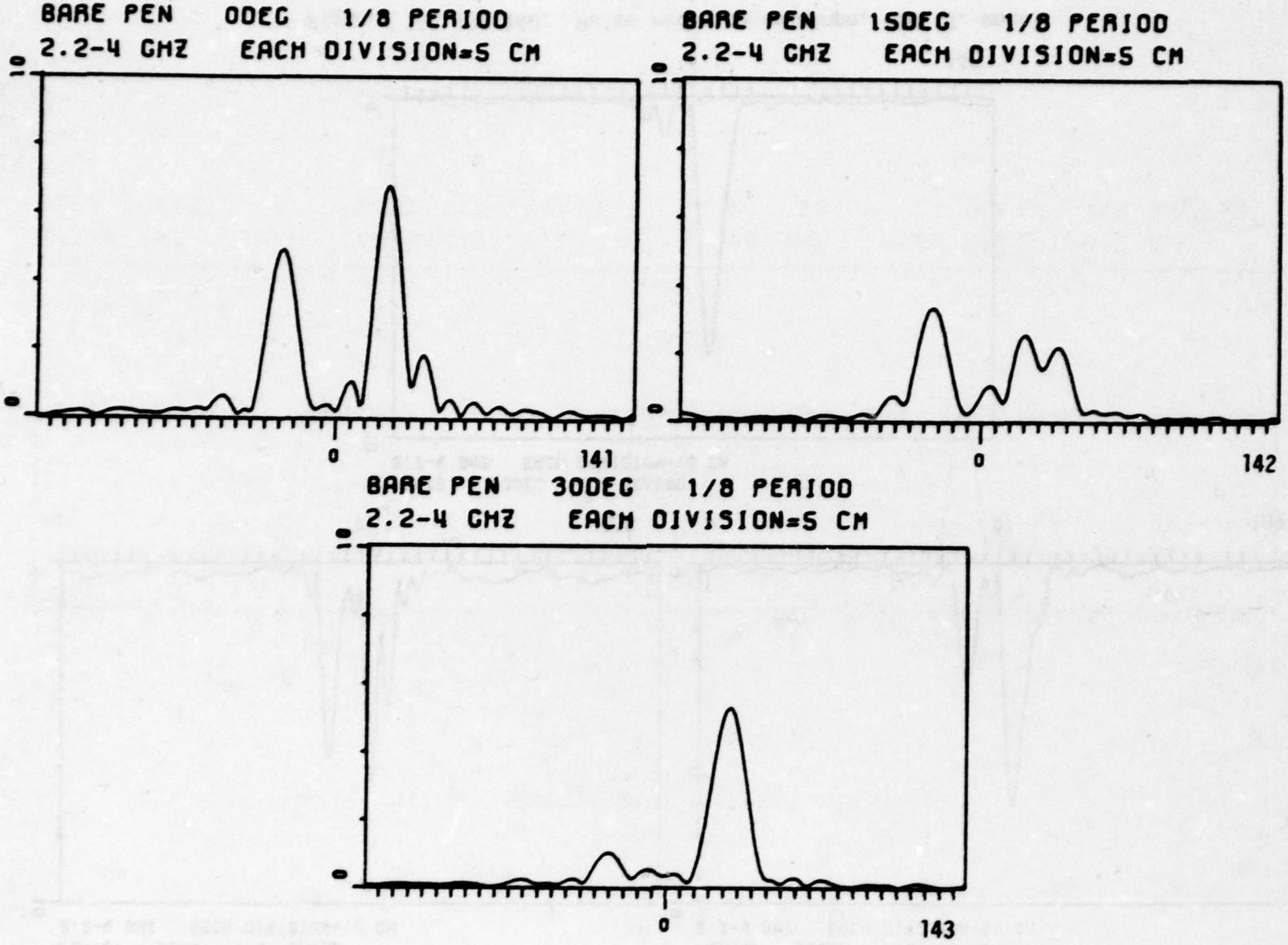


Figures 141,142,143. Pulse response envelope, Bare PEN model.

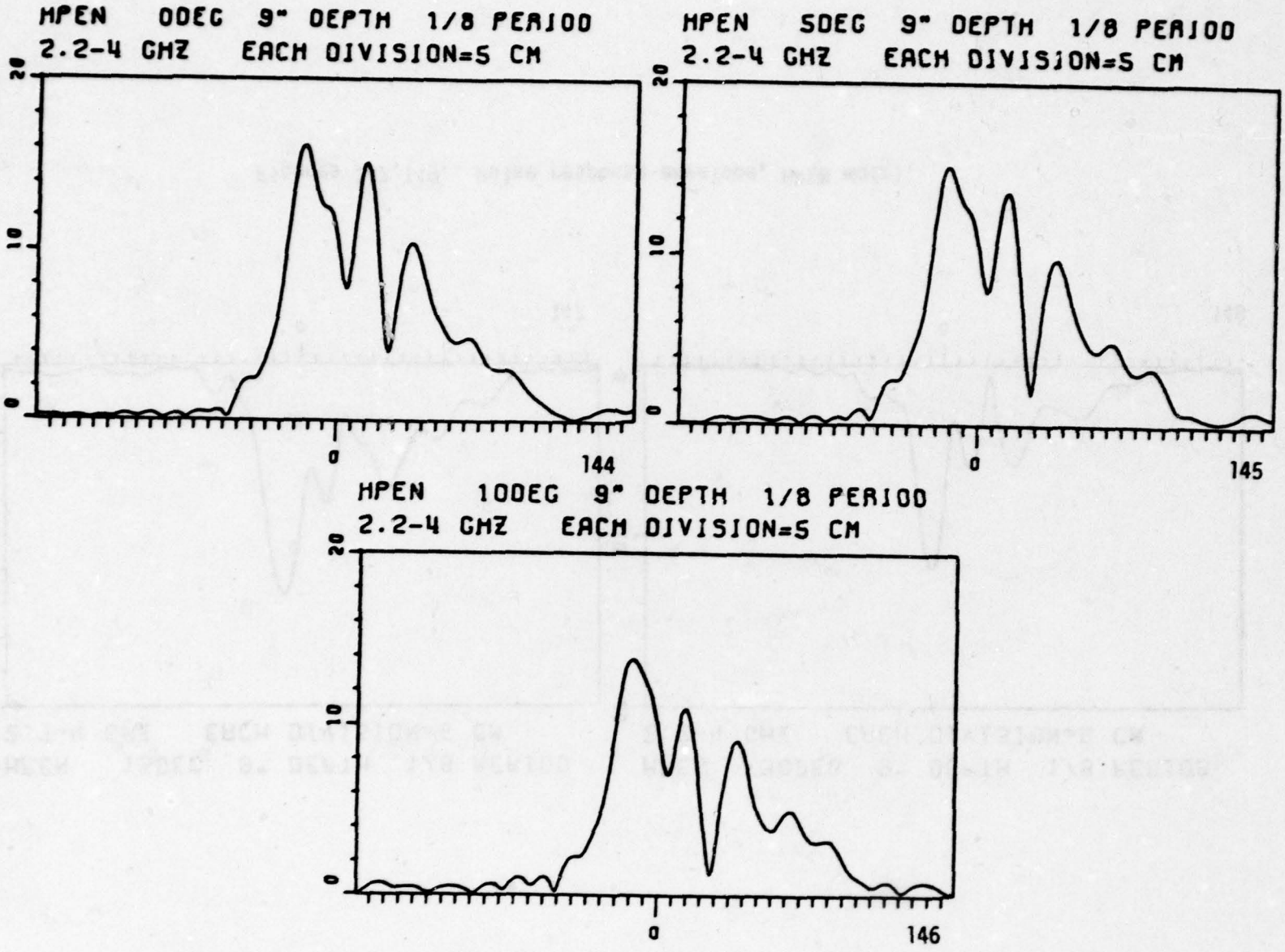


Figures 144,145,146. Pulse response envelope, HPEN model.

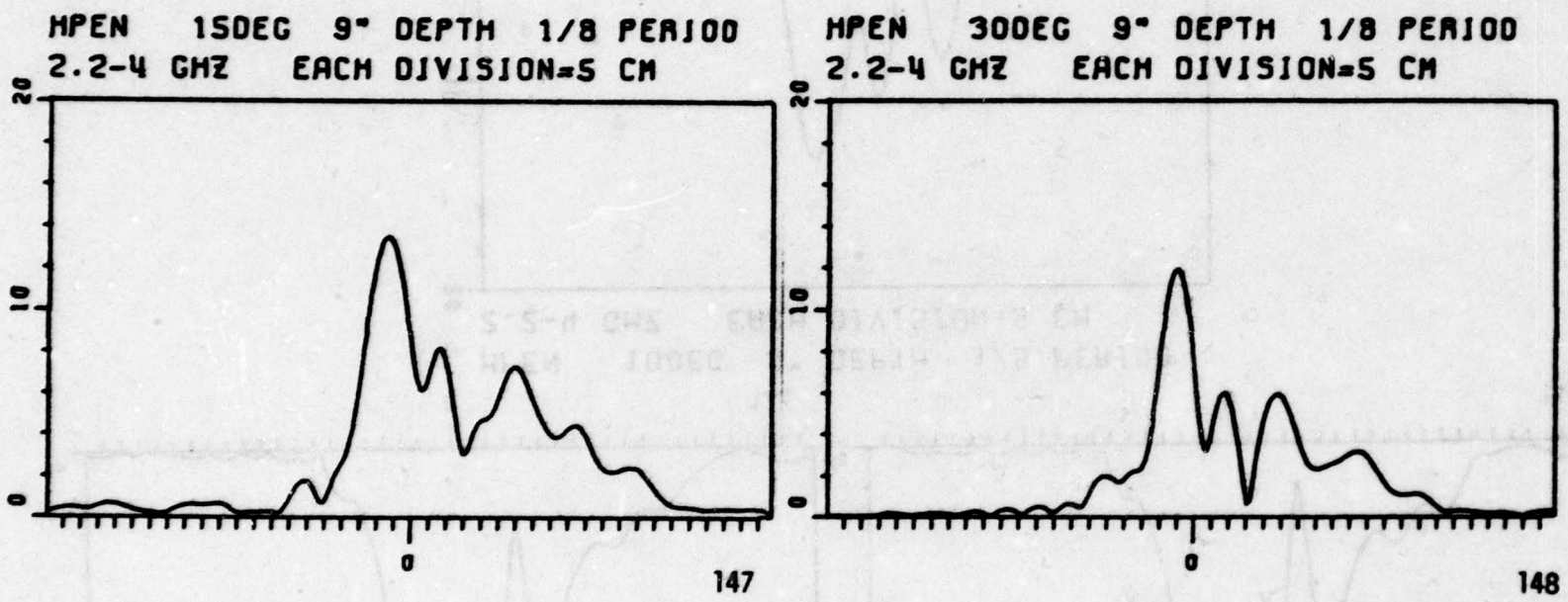


Figures 147,148. Pulse response envelope, HPEN model.

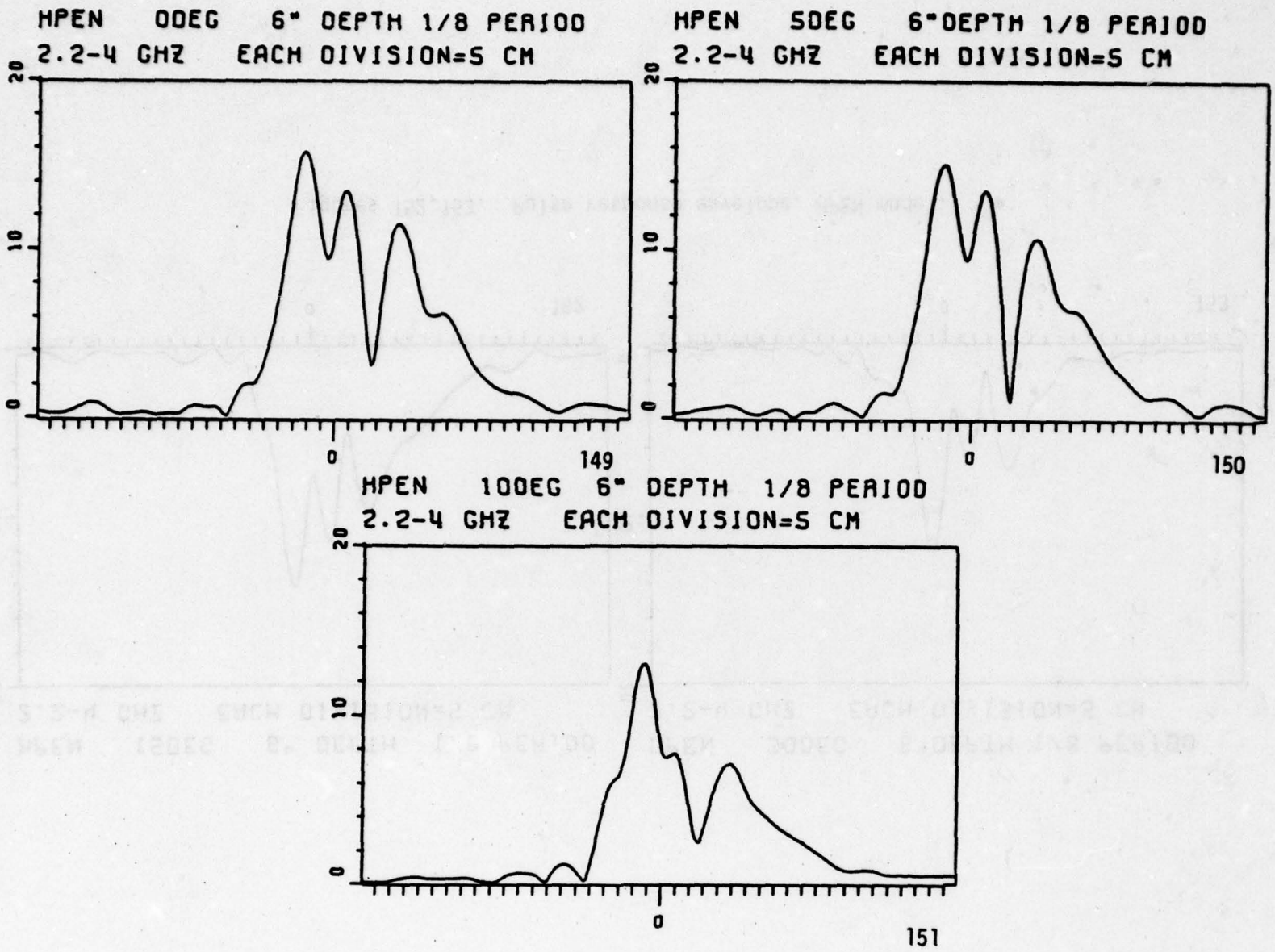


Figures 149,150,151. Pulse response envelope, HPEN model.

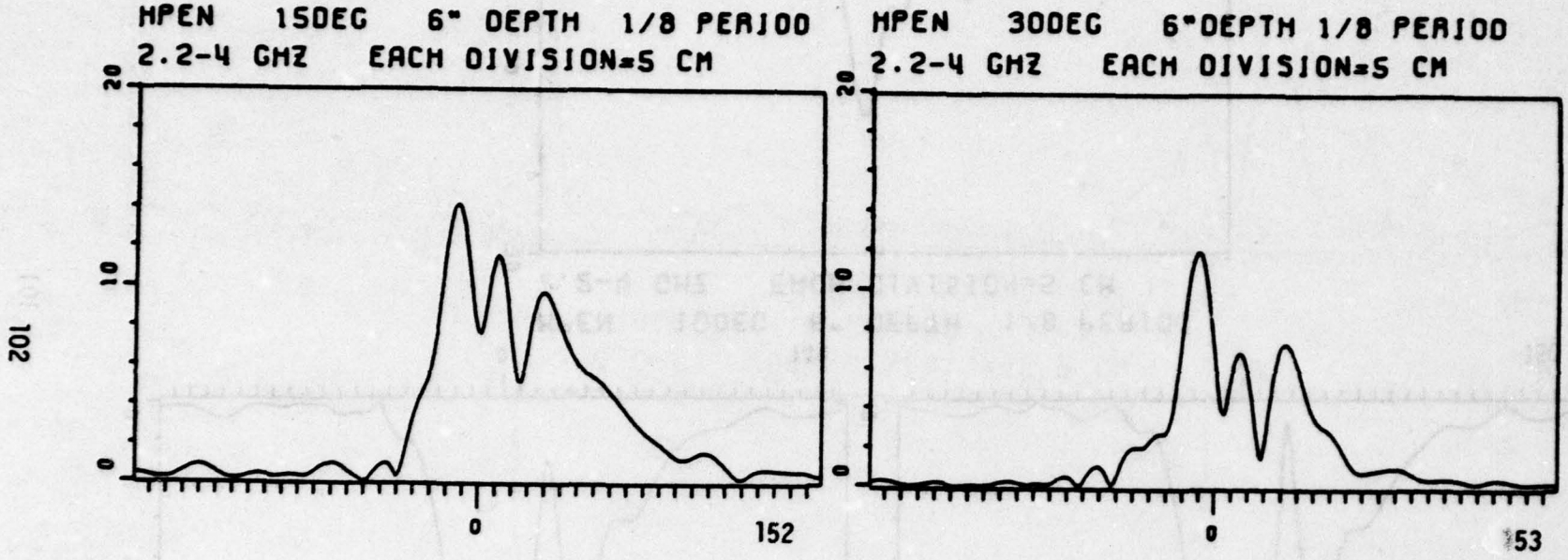


102

Figures 152,153. Pulse response envelope, HPEN model.

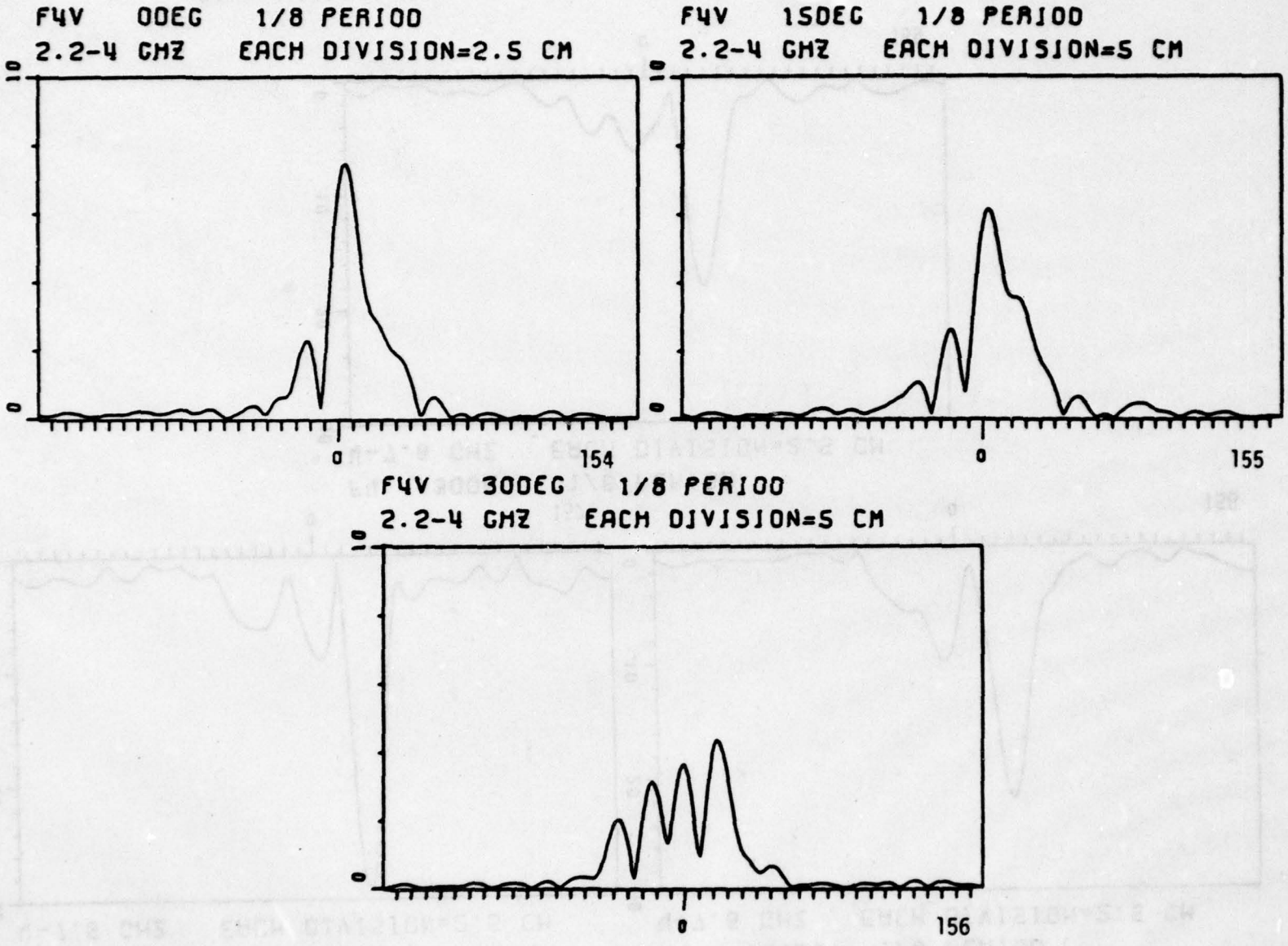


Figures 154,155,156. Pulse response envelope, F4V aircraft.

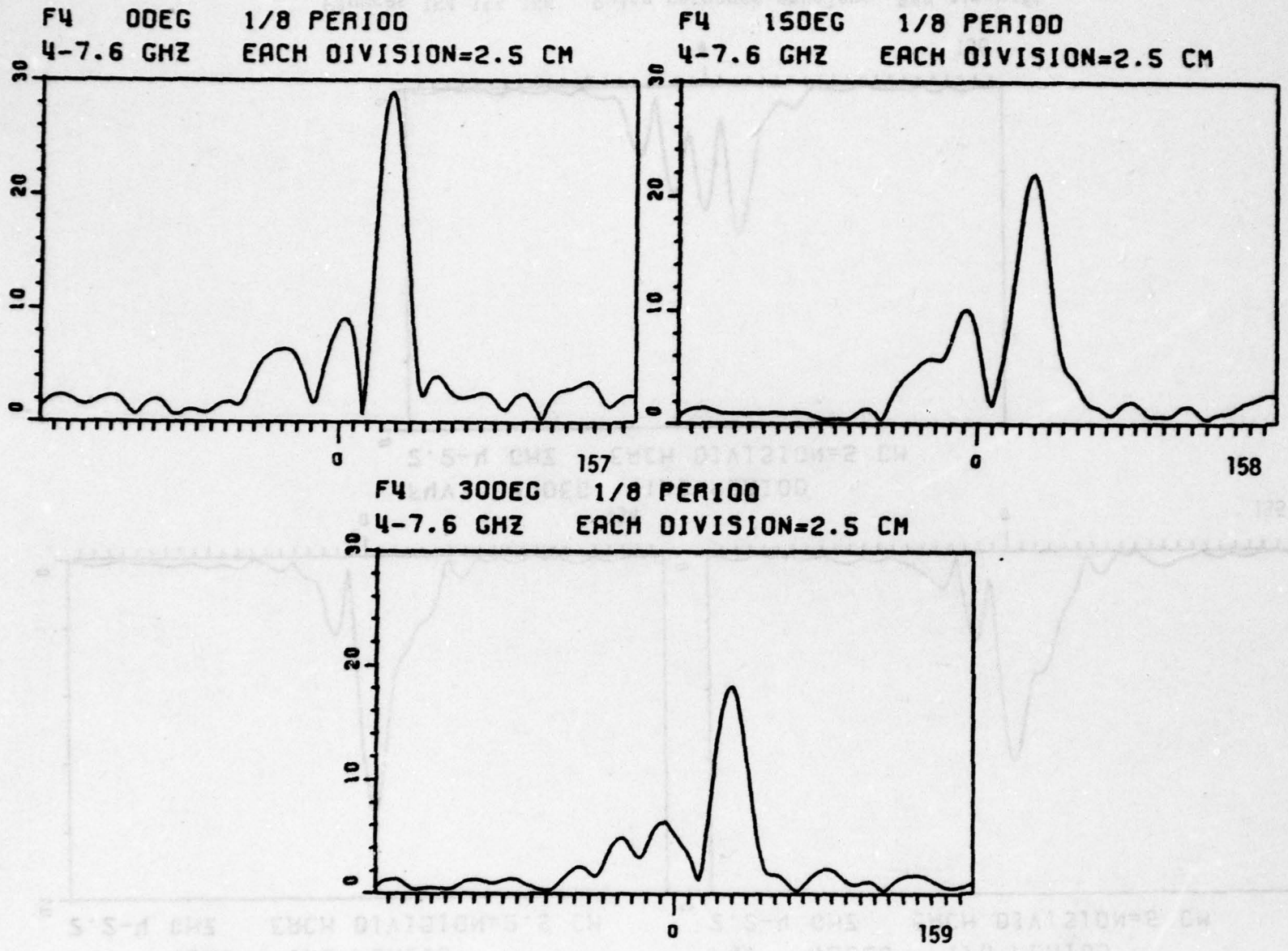


Figures 157,158,159. Pulse response envelope, F4 aircraft, 4.0-7.6 GHz.

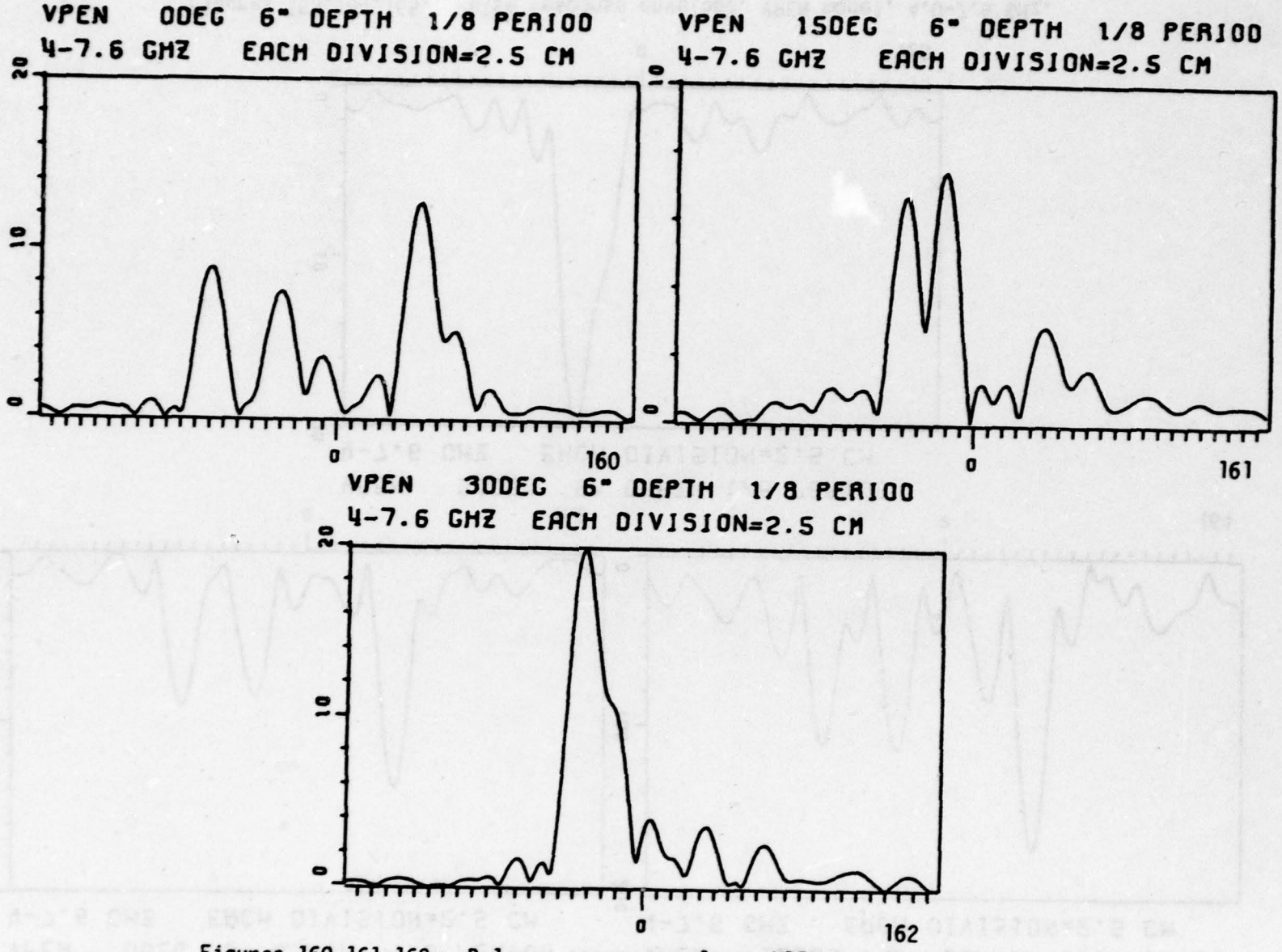


Figures 160,161,162. Pulse response envelope, VPEN model, 4.0-7.6 GHz.

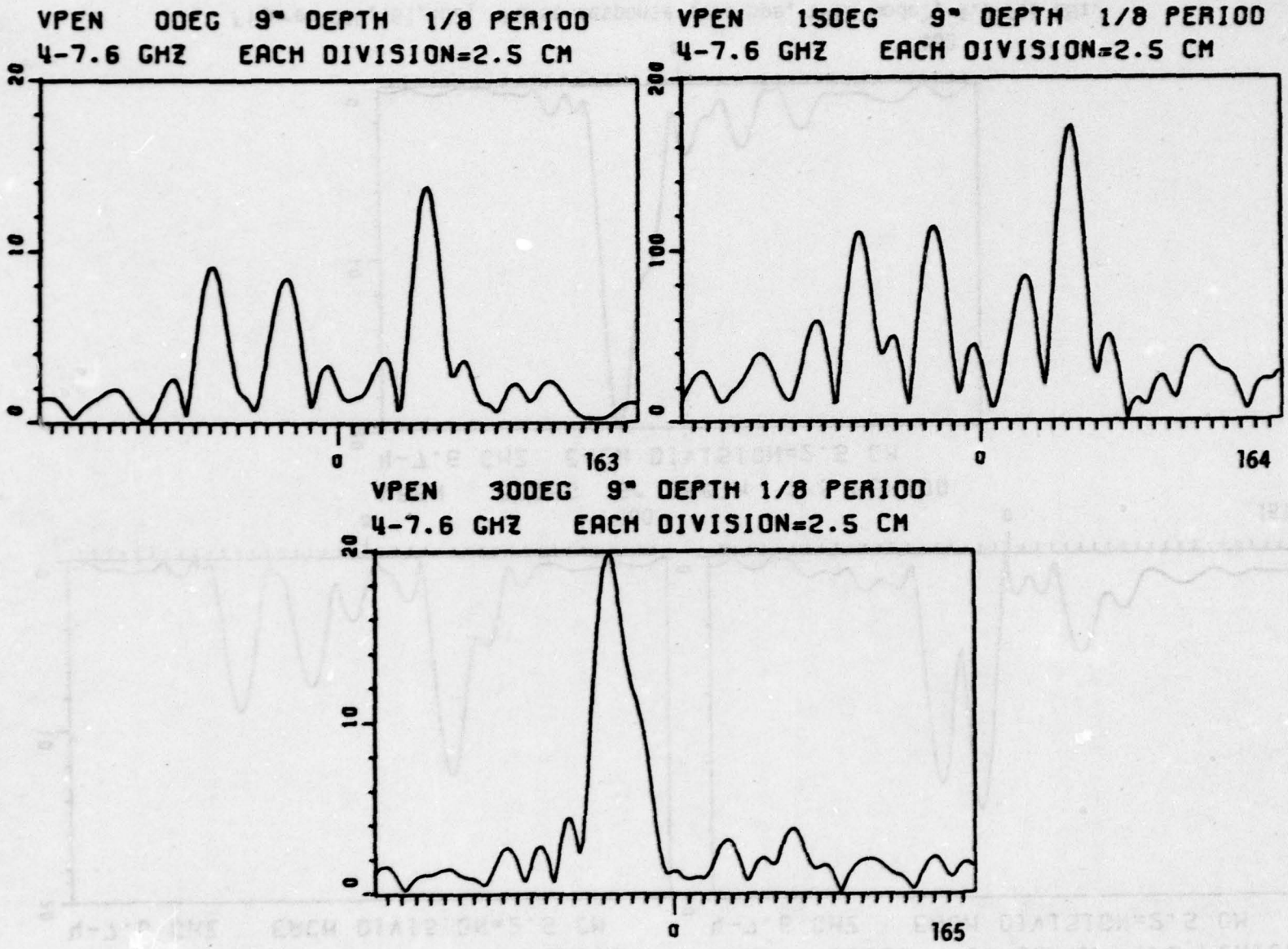


Figures 163,164,165. Pulse response envelope, VPEN model, 4.0-7.6 GHz.

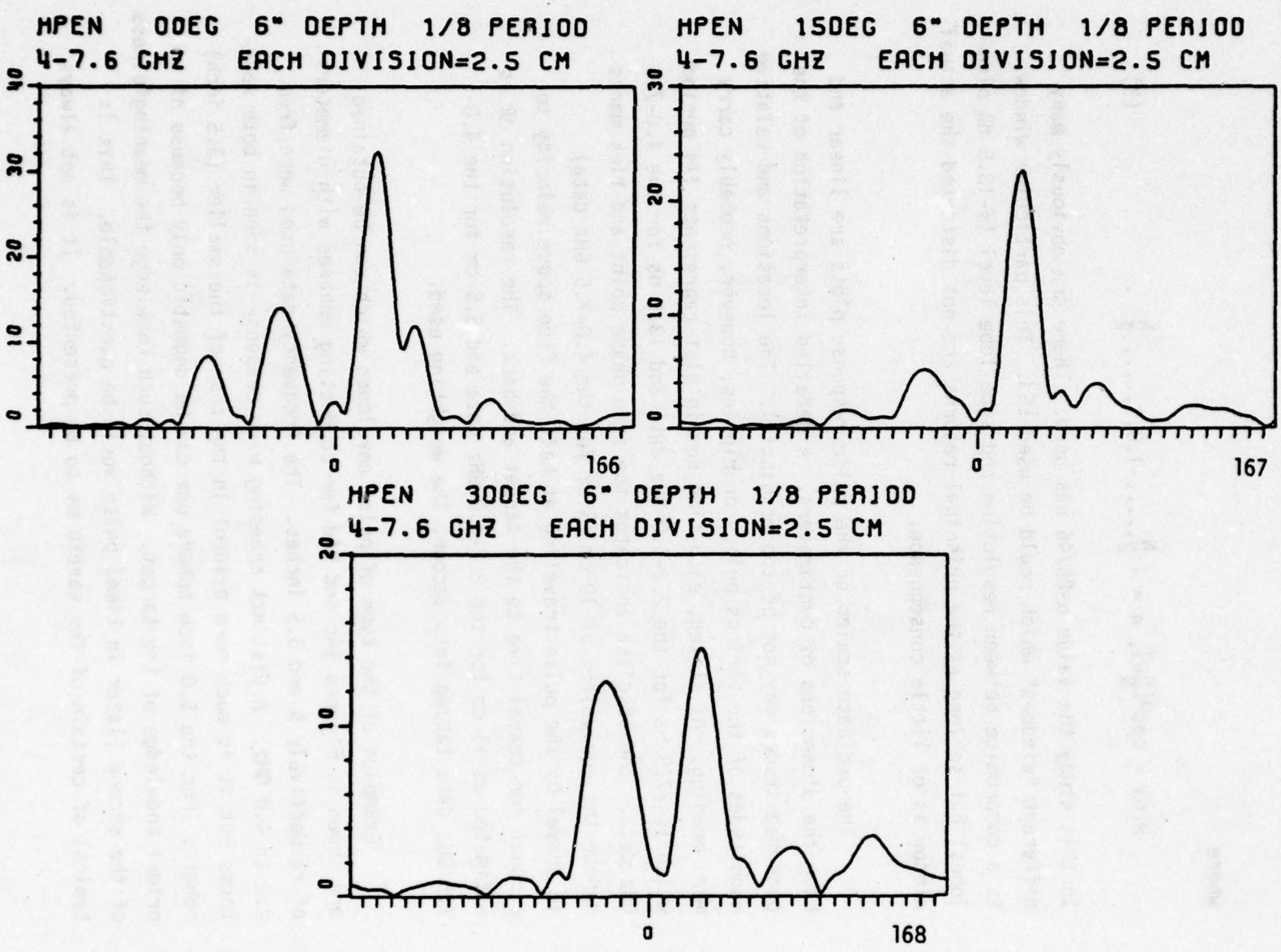


Figures 166,167,168. Pulse response envelope, HPEN model, 4.0-7.6 GHz.

where

$$W(n) = \cos^{\alpha}\left[\frac{n}{N}\pi\right], \quad n = -\frac{N}{2},\ldots,-1,0,1,\ldots,\frac{N}{2} \quad . \qquad (3)$$

In this study the value $\alpha$=25/46 was used. There are obviously many different "windows" which could be used [5]. This particular window is a compromise between resolution and side lobe level ($\mathcal{L}$-18.5 dB side lobes) but so long as the principal returns are not distorted the actual window is of little consequence.

The ordinate scales of the pulse response plots are linear and have the dimensions of centimeters. A detailed interpretation of the peak magnitudes may not be too meaningful. The locations and relative magnitudes of the various pulses or ripples, however, probably carry more meaning. As stated, each time domain plot represents 1/4 period which is 27.8 ns for the 2.2-4.0 GHz data and 13.9 ns for the 4.0-7.6 GHz data. The abscissa indicates the zero phase point and tick marks denote the equivalent of 10 cm (5 cm for the 4.0-7.6 GHz data) in travel by the pulse traveling at half the free space velocity to account for travel time to the target and back. The resolution $\Delta R$ is estimated as 11 cm for the 2.2-4.0 GHz data and 5.5 cm for the 4.0-7.6 GHz data taking into account the weighting used.

Examples of the type of pulse envelopes which can be obtained are shown in Figures 94c and 94d for conducting spheres with diameters of respectively 5 and 3.5 inches. The frequency data used were from 2.2 to 4.0 GHz. A distinct creeping wave response is seen in both waveforms but it is much more evident in the case of the smaller (3.5 inch) sphere. For the 5.0 inch sphere one can be dogmatic only because of a priori knowledge of the target. Without such knowledge the meaningfulness of the second (later in time) pulse would be questionable. This is typical of certain of the waveforms to be presented. It is not always

clear as to the level (amplitude) below which one ignores the waveform features as, for example, we ignore the precursors of the specular contributions in Figures 94c and 94d.

As with the spectral data presented in the last section we give here certain generalities one should observe when examining the time domain responses.

If the response of the target is coming, in general, from one position on the target then the response waveform should be dominated either by a single pulse or ringing in the case of a resonance. There may or may not be other minor amplitude pulses in the response indicating the presence or absence of other minor scatterers on the target. In some cases (as with the 5 inch sphere) there will be a question as to the presence or absence of a scattering point. In locating these positions on the target the resolution of the signal must be borne in mind.

A strong interference phenomena such as pulses bouncing back and forth from the ends of a thin finite length wire will be indicated by the presence of several near equal magnitude pulses. As the pulses become of disportionate magnitude then the interpretation is much more difficult and one approaches the minor scatterer question discussed above.

Two or more closely located (pulse resolution) scatterers will result in a smearing of the individual pulses together yielding a broader pulse with or without secondary (not baseline) nulls. With the resolution and targets in question, this type of result is very difficult to interpret with regard to the number and type of scattering points.

While the aspect changes are necessarily coarse in order to keep the total data base of reasonable size, one can postulate the location of a dominant scatterer and track its change in delay as the aspect

changes. In every case the phase reference is at the bottom of the midpoint of the fuselage length. Some human error is inevitable here as the targets are positioned despite the fact that the fuselages were suitably marked.

A high Q resonance associated with some portion of the structure would normally manifest itself as a ringing phenomena, i.e., several near equal magnitude pulses. If, for example, there is a high-Q resonance on the stabilizers, pulses delayed by some combination of vertical plus horizontal stabilizer lengths would be postulated. This point is discussed in the Conclusions Section.

## VI. DISCUSSION

Consider first the envelope pulse responses of the aircraft targets shown in Figures 95 through 116. In most cases essentially one isolated (in time span) response is seen. This result does support our main contention that in this frequency range a dominance of one scattering center exists. The contention that phenomena associated with horizontal and vertical stabilizers dominate is further supported by the motion of this dominant pulse delay as the target aspect is changed. The motion of this delay associated with the pulse response peak can, within the resolution achieved, be associated with the tail. With the exception of the F-15 model, which is a somewhat larger aircraft not considered in our original resonance search measurements, the motion of the delay with target aspect is entirely compatible with stabilizer-centered effects. Time did not permit the additional measurements with one or more of the aircraft partially dismantled which would have possibly confirmed the stabilizer dominance. We do not, however, see a ringing effect one would normally associate with a high-Q resonance except possibly in particular cases cited later. One might postulate a set of quasi-invariant parameters associated with the tail response as shown. This aspect of the study is discussed in another section. It is difficult, and perhaps dangerous, to attempt to isolate and identify all of the features of the pulse return envelopes. Additional resolution would

be desirable but this is only achieved at the cost of additional swept frequency measurements. As finally achieved (after delays necessitated by automating the procedure and changing instrumentation computers), measurement of 201 sampled-frequency complex scattering responses over an octave bandwidth takes less than five minutes to complete including the calibration procedure with one or more spherical scatterers. This speed and the accuracy quoted in Section II ($\pm$ 1 dB in amplitude and $\pm$ 10$^{o}$ in phase) is achievable with reasonable care and would possibly be enhanced by a dedicated* range. At present, it is felt that the measurement range represents a significant state-of-the-art tool. Admittedly, the effort required for automation plus significant down time and finally replacement of the instrumentation computer made the full advantages of the system difficult to exploit on this program.

Consider as an example the pulse envelope responses of the F-104 aircraft in Figures 55 through 59. At nose-on the response is asymmetrical about the peak and the small precursor (main peak) peaks might be associated with the fuselage-engine intake junction. At 45$^{o}$ from nose-on the response is symmetrical essentially through the first sidelobes and the junction, if present, is less discernable. At broadside a near symmetrical pulse is again obtained as would be anticipated. At 135$^{o}$ from nose-on the pulse is decidedly asymmetric with radiation from the fuselage-intake junction (and the nose?) occurring after the main response. At tail-on incidence the response is again asymmetrical but quite difficult to interpret. The peak beyond the main peak may be the junction but its time position seems incompatible with the 135$^{o}$ return.

The pulse response envelopes of the F-4 target show more variation than those of the F-104 despite the fact that only three responses are shown. At nose-on, four discernable peaks, two preceding and one following

*Our anechoic chamber is used on a share basis except for very high (2-3 day) priority runs.

the main peak are seen. The F-4 is structurally much more complicated than the F-104 and this is reflected in the nose-on responses. If the aircraft nose is neglected then a possible sequential resolution is intake-fuselage junction, wingtips and a complicated tail return. We emphasize that these are highly speculative interpretations with the resolution of the pulse. Note that the peak magnitude of the return from the F-4 is down at least a factor of two from that of the F-104 nose-on. There is a corresponding difference in the swept data with the F-4 showing a deep null at approximately 3.0 GHz while the F-104 has a much gentler trend. At broadside the F-4 has a nearly symmetric sharp return which is approximately a replica of the synthetic interrogating signal envelope. It should be noted from the swept frequency amplitude scattering data that the F-104 is the only aircraft for which some postulated resonances cannot be observed in the spectrum at some aspect. The above discussion could be made for the pulse returns of each aircraft target but there seems little point in pursuing these reviews at the moment. In general one can see that the sharpest pulse returns occur for broadside incidence and tht the MIG-21 aircraft returns are relatively small in magnitude.

Viewing the pencil target nose-on, i.e., along the axis of the cone and cylinder with the tip of the cone toward the observer, one can predict returns from sequentially the cone tip, cone-cylinder junction, intake discontinuity, tail and base of the cylinder. If the intake return were a cavity-type effect* then the time delay for this component of the signal is dictated by the base of the cavity and the waveguide modes excited. Note that these are postulated scattering radiation mechanisms and not, at the moment, the description of any actual pulse return waveform. One might suggest traveling wave-type currents excited on the structure which would manifest themselves as two or more distinct pulses in the

*At the measurement frequencies reported here (2.2 to 4.0 GHz), the rectangular intake is cut-off and any effects are discontinuity effects.

return envelope. Current reaching the base of the cylinder will be partially diffracted back along the cylinder with accompanying radiation and partially diffracted across the base of the cylinder and then diffracted again along the cylinder back toward the cone - again with radiation. For other than nose-on incidence these same mechanisms will generally exist. At broadside there is also the possibility of creeping wave components around the body of the cylinder. It is clear from the preceding footnote that changes in the width of the cavity will produce only secondary effects in this frequency range. They are generally included here for completeness. One can anticipate, however, effects due to the changes in the tail structure.

Consider the sequence of pulse returns for the pencil target shown in Figures 117 through 167. The corresponding frequency spectra are in Figures 43 through 94. It is evident from the spectra that complicated interactions which can be interpreted as both interference and resonance effects are occurring. Each of the pulse envelope responses shows at least two sharply discernable peaks whose location and spacing indicate returns from the cone-cylinder joint and the rear section of the pencil. Between nose-on and $30^{o}$ from nose-on the delay should roughly change by 10% which will be marginally discernable with the present resolution.

Concentrating primarily on the pulse envelope responses, the following certain general effects can be seen for the pencil target.

A. <u>Effects of Tail</u>

(Figures 141, 142 and 143 vs. Figures 132 through 140) 2.2 to 4.0 GHz.

1. The changes in the response with a tail added can be seen for all tail heights and all aspect angles but is most clearly discernable for larger tail heights at the nose-on aspect.

2. The most drastic changes with addition of a tail is at the $15^{o}$ aspect.

3. Some tail effects are merged with cylinder base effects with the pulse resolution obtained.

4. The effects of tail addition changes with aspect.

5. The response from the tail does not dominate the scattering from the pencil target in the 2.2 to 4.0 GHz frequency range but the tail presence is clearly evident.

B. Effects of Cavity

(Figures 141, 142 and 143 vs. Figures 117 through 131) 2.2 to 4.0 GHz.

1. The addition of a cavity to the pencil structure is clearly seen for all cavity widths at all aspects.

2. As with the tail structure the effects of the cavity changes with aspect.

3. There is no discernable effect caused by changing the plunger (shorting bar) depth which means that energy is not penetrating the interior of the cavity in this frequency range.

4. The effects of changing the cavity width can be seen but again this is an exterior change.

5. A short at the mouth of the cavity is easily seen but here merely shows the difference in diffraction by two parallel edges vs. a solid plate.

C. Effects of Plunger (short bar) Depth (horizontal polarization)
(Figures 144 through 153) 2.2 to 4.0 GHz.

1. The change in the response for 6 inch vs. 9 inch plunger depths is clearly seen and the changes in time delay are compatible with the plunger position.

2. With the pulse resolution in this frequency range many effects are possibly merged which would be distinct with greater resolution.

3. It is very evident that the addition of higher frequency measurements (greater resolution) would be most helpful.

4. Return from the cavity (and plunger) does not dominate the scattering from the pencil target in this frequency range.

D. F-4 Aircraft, Horizontal Polarization (denoted VP)
(Figures 154 through 159) 2.2 to 4.0 GHz and 4.0 to 7.6 GHz.

1. Response from the tail region still appears to dominate the return.

2. Pulse response endures longer than for vertical polarization, indicating some ringing.

3. Ringing effects are most evident at $15^{o}$ and $30^{o}$ aspects.

4. Pulse responses using the 4.0 to 7.6 GHz data show the effects of increased pulse resolution and again evidence of ringing.

5. It was not possible to combine the 2.2 to 4.0 and 4.0 to 7.6 GHz data (to achieve an even greater pulse resolution) because of a change in the bistatic angle for the two frequency spans.

## VII. CONCLUSIONS

A stepped-frequency system capable of measuring complex echo signals over octave bandwidths has been implemented. In the presence of steady background signals, vector subtraction permits measurement and calibration of echo signals as low as 0.05 $cm^2$. Using this system over the bands 2.2 to 4.0 GHz and 4.0 to 7.6 GHz, amplitude and phase data on low-angle bistatic scattering from 1/72 scale model fighter aircraft and a pencil target with a cavity have been obtained. For 201 equally spaced samples over each band, the amplitude and phase of the scattered signal at selected aspects and polarizations have been calibrated and recorded. Envelopes of the radar return using octave-bandwidth pulses short enough to resolve individual structural components of the fighter aircraft have been synthesized. These returns, if combined over the two bands tested to date, would permit synthesis of pulse response for a bandwidth of 1.8 octaves, with a range resolution of approximately 1.5 inches on models, or 8.7 feet on simulated full-scale objects.

Measured amplitude and phase data as well as synthesized pulse response have been examined for evidence of resonances in substructural scattering and/or traveling wave phenomena which might be useful in target identification. The hypotheses tested and the conclusions reached may be summarized as follows:

### Hypothesis I

The frequency spectrum of scattering by fighter aircraft over the full scale range of 25.0 to 100.0 MHz is sufficiently variable to require frequency sampling at less than 5 MHz increments.

Discussion:

If resonances or strong interferences occur in the backscattered spectrum, relatively small increments in frequency will be needed to approximate the spectrum and the use of an existing measurement system which uses the first through tenth harmonic of a fundamental frequency 3 will not be sufficient. An examination of representative scattering data from aircraft in the 30.0 to 56.0 MHz frequency range indicates 10.0 dB amplitude changes in a bandwidth of 4.0 MHz (F-4, Figure 26; MIG21, Figure 29 and MIG21, Figure 31) and 20.0 dB changes in a bandwidth of 3.0 MHz for vertically polarized transmitter and receiver (F-4, Figure 28). Therefore the need for at least 2 MHz increments in the frequency range 30.0 to 56.0 MHz is established for vertically polarized measurements. The frequency increment needed for horizontally polarized measurements cannot be established but should be less than 2 MHz because of the larger number of scattering centers and resonant structures (such as the wings and fuselage). At frequencies above 56 MHz the measured scattering data for the PEN target indicates less than 2 MHz may be needed to determine the spectrum shape. The PEN target is a crude model of the fuselage for fighter aircraft at frequencies above 56.0 MHz.

Hypothesis II

Observation of the transient response from fighter aircraft with a simulated pulse length shorter than the target and sufficient spectral content in the 35.0 to 100.0 MHz range will reveal any substructural resonances which may occur.

Discussion:

The substructure resonances of greatest interest in target identification are those which are characterized by low damping and which are easily excited over a range of target aspects. In such cases, the transient response will exhibit a number of maxima (regularly separated in time) corresponding to a damped sinusoid. Ideally, as for example a thin wire, these maxima would repeat after the incident wavefront has passed beyond the structural component. Effects similar to these have been observed in simulated pulse responses from wire grid models of aircraft targets over the frequency range 1.0 to 24.0 MHz.

The results obtained using 1/72 scale models of fighter aircraft and 2.2 to 4.0 bandwidth pulses indicate that resolution of target scattering centers is not complete because of limits in target size and bandwidth but evidence of multiple peaks are indicated in Figure 100 (F-4) as well as Figures 102, 103, 105, 111, 114, 116, 155 and 156. These do show some evidence of multiple reflections or resonances.

Results for the PEN target (Figures 117 through 140) indicate resolution of individual scattering components but it is not possible to determine whether some of the peaks in the transient response are associated with multiply reflected waves. The results do indicate, however, that use of a larger model or higher frequency data for the 1/72 scale targets is necessary to identify substructure resonances.

Hypothesis III

Structural resonances in the frequency range 25.0 to 100.0 MHz will occur as useful discriminants of aircraft targets. Resonances

associated with the vertical stabilizer and tail assembly will occur in this band. The cavities of jet engines may be excited at the upper end of this band.

Discussion:

The data obtained using vertically polarized transmitting and receiving antennas for simulated frequencies from 30.0 to 56.0 MHz do not reveal any strong high-Q resonances associated with fighter aircraft substructures. The dominant echo signal contribution over a range of aspects in the plane of flight is associated with the vertical stabilizer. For the F-4 and MIG-21 aircraft near nose-on and tail-on aspects both the spectral data and pulse responses show multiple reflections to be present. However, the potential of these for target identification does not appear to be promising at least in the frequency band tested.

Several examples of spectral and pulse response over the 56.0 to 106.0 MHz range for fighter aircraft and for horizontally polarized transmission (30.0 to 56.0 GHz as well as 56.0 to 106.0 MHz) reveal additional returns which may be attributed to structural components but are inconclusive in determining whether resonances useful for target identification are present.

Results on a crude model of a fuselage with flush-mounted rectangular cavities simulating jet engine intakes reveal that some penetration of engine cavities and subsequent reflections from shorting terminations within the cavity occur when the incident polarization is perpendicular to the major cross-sectional cavity dimension, and when this dimension is greater than one-half wavelength.

The scale of the crude model was such that the overall size would approximate that of a fighter aircraft above 60.0 MHz, and

cavity penetration would be observed for horizontal polarization, but not for vertical polarization, at least at frequencies below 120 MHz.

It is generally evident that our expectations regarding substructure resonances have not been realized at least in the form anticipated. Other interpretations must be qualified until the additional scattering data at generally higher frequency bands are obtained. The measurement system developed is fully capable of obtaining these data whose scope could not be encompassed within the time and funds available. To the best of our knowledge the spectral and time domain data obtained are new and unique contributions to the knowledge of scattering fom fighter aircraft in the 30.0 to 56.0 MHz range.

A completely satisfactory explanation of why the response from the aircraft structure fails to ring as anticipated yet is dominated by the stabilizer assembly, again as anticipated, cannot be given at this time. This question is particularly vexing in light of the simulated responses at lower frequencies where strong ringing occurred. Perhaps the most logical assumption is that the vertical and horizontal stabilizer geometries simply will not support a high-Q resonance phenomena. One would also suggest, however, that experimental tests in the same frequency range of a known resonant structure fabricated from plastic and silver-painted would also be in order.

The dominance of the stabilizer structure of fighter aircraft for vertical polarization of transmitter and receiver in the 30.0 to 56.0 MHz range does suggest a possible alternative identification scheme. An examination of the isolated pulse responses from the stabilizer structures vs. aspect, e.g., Figures 95, 96, 97, 98 and 99 for the F-104 shows that the form of these responses beyond their peak may be characteristic. That is, a difference equation may possibly be found which will satisfy these portions of the envelopes. An explanation of the procedure for testing the data for this type of difference equation and some initial results obtained are given in the final report on this contract [6].

## REFERENCES


1. John L. Kerr, "Short Axial Length Broad Band Horns," IEEE Trans. on Antennas and Propagation, Vol. AP-21, No. 5, September 1973, pp. 710-714.

2. C. M. Rhoads, "The Identification of Naval Vessels Via an Active, Multi-frequency Radar System," Masters Thesis, Ohio State University, August 1978.

3. D. L. Moffatt and C. M. Rhoads, "Radar Identification of Naval Vessels," Report 784558-1, July 1978, The Ohio State University ElectroScience Laboratory, Department of Electrical Engineering; prepared under Contract N00014-76-C-1079 for Department of the Navy, Office of Naval Research.

4. R. F. Harrington, Time-Harmonic Electric Fields, McGraw-Hill, 1961.

5. F. J. Harris, "On the Use of Windows for Harmonic Analysis with the Discrete Fourier Transform," Proc. of the IEEE, Vol. 66, No. 1, January 1978, pp. 51-83.

6. D. L. Moffatt, K. A. Shubert and E. M. Kennaugh, "Radar Target Identification," Final Report 784677-2, The Ohio State University ElectroScience Laboratory, Department of Electrical Engineering; prepared under Contract F19628-77-C-0125 for Department of the Air Force, Electronic Systems Division. In preparation.

# *MISSION*
# *of*
# *Rome Air Development Center*

*RADC plans and executes research, development, test and selected acquisition programs in support of Command, Control Communications and Intelligence ($C^3I$) activities. Technical and engineering support within areas of technical competence is provided to ESD Program Offices (POs) and other ESD elements. The principal technical mission areas are communications, electromagnetic guidance and control, surveillance of ground and aerospace objects, intelligence data collection and handling, information system technology, ionospheric propagation, solid state sciences, microwave physics and electronic reliability, maintainability and compatibility.*

Printed by
United States Air Force
Hanscom AFB, Mass. 01731